REPORT DOCUMENTATION PAGE

AFRL-SR-AR-TR-02-

0321

1. AGENCY USE ONLY *(Leave blank)*	2. REPORT DATE	3. REPORT TYPE AND DATES COVERED
		15 JANUARY 1999 TO 14 MAY 2002

4. TITLE AND SUBTITLE
Coordination and Control of Multiple Spacecraft using Convex Optimization Techniques

5. FUNDING NUMBERS
F49620-99-1-0095

6. AUTHOR(S)
Jonathan P. How

7. PERFORMING ORGANIZATION NAME(S) AND ADDRESS(ES)
Stanford University
Aeronautics & Astronautics
Stanford, CA 94305

8. PERFORMING ORGANIZATION REPORT NUMBER

9. SPONSORING/MONITORING AGENCY NAME(S) AND ADDRESS(ES)
AFOSR/NM
801 N. Randolph Street Room 732
Arlington, VA 22203-1977

10. SPONSORING/MONITORING AGENCY REPORT NUMBER
F49620-99-1-0095

11. SUPPLEMENTARY NOTES

12a. DISTRIBUTION AVAILABILITY STATEMENT
APPROVED FOR PUBLIC RELEASE, DISTRIBUTION UNLIMITED

12b. DISTRIBUTION CODE

13. ABSTRACT *(Maximum 200 words)*

Formation flying of multiple spacecraft is an enabling technology for many future space science missions. These future missions will, for example, use the highly coordinated, distributed array of vehicles for earth mapping interferometers and synthetic aperture radar. This thesis presents coordination and control algorithms designed for a fleet of spacecraft. These algorithms are embedded in a hierarchical fleet architecture that includes a high-level coordinator for the fleet maneuvers used to form, re-size, or re-target the formation configuration and low-level controllers to generate and implement the individual control inputs for each vehicle. The trajectory and control problems are posed as linear programming (LP) optimizations to solve for the minimum fuel maneuvers. The combined result of the high-level coordination and low-level controllers is a very flexible optimization framework that can be used off-line to analyze aspects of a mission design and in real-time as part of an on-board autonomous formation flying control system. This thesis also investigates several critical issues associated with the implementation of this formation flying approach. In particular, modifications to the LP algorithms are presented to: include robustness to sensor noise, include actuator constraints, ensure that the optimization solutions are always feasible, and reduce the LP solution times.

14. SUBJECT TERMS

20021011 001

15. NUMBER OF PAGES
164

16. PRICE CODE

17. SECURITY CLASSIFICATION OF REPORT	18. SECURITY CLASSIFICATION OF THIS PAGE	19. SECURITY CLASSIFICATION OF ABSTRACT	20. LIMITATION OF ABSTRACT

Coordination and Control of Multiple Spacecraft using Convex Optimization Techniques

Michael J. Tillerson and Jonathan P. How

Department of Aeronautics and Astronautics

Massachusetts Institute of Technology

June, 2002

Formation flying of multiple spacecraft is an enabling technology for many future space science missions. These future missions will, for example, use the highly coordinated, distributed array of vehicles for earth mapping interferometers and synthetic aperture radar. This thesis presents coordination and control algorithms designed for a fleet of spacecraft. These algorithms are embedded in a hierarchical fleet architecture that includes a high-level coordinator for the fleet maneuvers used to form, re-size, or re-target the formation configuration and low-level controllers to generate and implement the individual control inputs for each vehicle. The trajectory and control problems are posed as linear programming (LP) optimizations to solve for the minimum fuel maneuvers. The combined result of the high-level coordination and low-level controllers is a very flexible optimization framework that can be used off-line to analyze aspects of a mission design and in real-time as part of an on-board autonomous formation flying control system. This thesis also investigates several critical issues associated with the implementation of this formation flying approach. In particular, modifications to the LP algorithms are presented to: include robustness to sensor noise, include actuator constraints, ensure that the optimization solutions are always feasible, and reduce the LP solution times. Furthermore, the dynamics for the control problem are analyzed in terms of two key issues: 1) what dynamics model should be used to specify the desired state to maintain a passive aperture; and 2) what dynamics model should be used in the LP to represent the motion about this state. Several linearized models of the relative dynamics are considered in this analysis, including Hill's equations for circular orbits, modified linear dynamics that partially account for the J_2 effects, and Lawden's equations for eccentric orbits. The complete formation flying control approach is successfully demonstrated using a nonlinear simulation environment that includes realistic measurement noises, disturbances, and actuator nonlinearities.

Research funded under Air Force grant #F49620-99-1-0095.
Thesis submitted by M. Tillerson for the Master of Science degree, June 2002.

Contents

List of Figures

List of Tables

Chapter 1

Introduction

Formation flying of multiple spacecraft is a key technology for many future space science missions including enhanced stellar optical interferometers and virtual platforms for earth observations. Formation flying of spacecraft involves a distributed array of simple but highly coordinated satellites to form a *virtual satellite bus* that will replace the standard monoliths used today [1, 2]. Strong interest in the formation flying concept has led to several planned and proposed space missions including: ST-3 and Terrestrial Planet Finder [3], EO-1 [4], TechSat-21 [5], and Orion-Emerald [6].

As discussed in Reference [7], there are numerous advantages in replacing standard monoliths with formation flying satellites. The traditional monolithic satellite is a large, specialized spacecraft containing payloads to meet several different mission objectives. Replacing the single, large satellite with several smaller vehicles can reduce launch costs by reducing launch mass and using multiple launch vehicles to "build-up" the fleet. Using multiple spacecraft also allows mass production techniques to reduce manufacturing cost. The satellites in the fleet could be constructed with a modular base design that is the same for each vehicle. The satellites are then equipped with the unique hardware required for the particular mission. Because the payloads are distributed across the fleet, robustness is increased by eliminating single point failures. Spacecraft formation flying also allows the replacement of a vehicle within the fleet to introduce new technology or replace damaged parts. Another advantage of formation flying is the adaptability of the formation. In a standard monolith, the aperture size is

constrained by the geometry of the vehicle; however, in formation flying the aperture size can be adjusted by increasing the distance between the spacecraft. Formation flying allows adjustments in aperture size and orientation with relative ease.

In order to implement spacecraft formation flying for future science missions, many guidance, navigation, and control challenges must be addressed. For example, very tight coordination, control, and monitoring of the distributed vehicles in the cluster will be required to achieve the stringent payload pointing requirements for a radar mission such as TechSat-21 [5]. Some of the key challenges for this problem are in the design of a fleet control architecture that can perform the high-level (mission management and planning to enable resource allocation across the fleet) and low-level (on board sensing, autonomous closed-loop relative navigation, and attitude determination) tasks. The primary difficulties are that: 1) with a large fleet, the computational aspects of the sensing and control are complicated by the large information flow and amount of processing required; 2) the vehicles must work cooperatively to perform the science observations; 3) the differential disturbance environment and nonlinear actuator operations could be uncertain; and 4) the fleet must undergo both resizing and configuration change maneuvers.

The focus of this thesis is the development of control and coordination algorithms for a formation of spacecraft. A key aspect of the formation control in low earth orbit is to maneuver the vehicles in the fleet to specified positions in a fleet configuration, which is essentially a trajectory design and tracking problem. The goal is to optimize these trajectories so that the vehicles are accurately initialized in a reasonable amount of time using the least amount of fuel possible. With disturbance modeling errors, sensor noise, and actuator nonlinearities, this initialization will typically be imperfect, which will eventually cause the cluster to disperse. Disturbance forces within the fleet such as differential drag and gravity gradient effects, will also cause the formation to disperse. Fuel optimized formation-keeping control will be required to maintain the vehicles to within a specified tolerance of the desired locations for each spacecraft in the fleet.

1.1 Previous Work

The primary focus of the formation flying research to date has been to develop fuel-efficient methods of performing scientifically useful observations. Research in formation flying of spacecraft can be separated into three main categories. One is the development of linear and nonlinear dynamics models for the relative motion between a cluster of vehicles. The second area is the design of *passive apertures*, which are (typically short baseline) periodic formation configurations that provide good, distributed, Earth imaging and reduce the tendency of the vehicles to drift apart [8]. The third area is the development of control algorithms for achieving and maintaining these passive apertures.

The first area of research is the development of dynamic models for relative motion between spacecraft. The Clohessy-Wiltshire equations for relative motion between two spacecraft were originally developed for the Gemini rendezvous mission, but have since been extended to spacecraft formation motion [9]. The Clohessy-Wiltshire and Hill's equations are very similar with the difference being in the definition of the coordinate frame. These equations represent the linearized relative dynamics for the motion of a chase spacecraft relative to a target vehicle. The target spacecraft represents the reference orbit for the motion. The reference orbit is constrained to be circular. Slight differences in eccentricity, inclination, and argument of latitude between the chase spacecraft orbit and reference orbit lead to relative motion [10]. These equations of motion are generally not solvable but the force free equations do have closed-form solutions, available in [10, 11].

The relative dynamics were extended to eccentric reference orbits through the work of several people. The first derivation with singularities in the closed-form solutions was provided by Lawden in 1963 [12]. The results by Carter [13, 14] presented the closed form solutions with singularities removed. The same results for eccentric orbits were achieved by Marec [15] using incremental changes in orbital elements. Further research indicated that the differential gravity perturbation cause by the oblateness of the earth, the J_2 effect, is a major disturbance force in the relative motion of the

spacecraft. As a result, further work was performed to develop linearized equations of motion that also capture this disturbance effect [16, 17].

The second area of research is the design of passive apertures. Passive apertures take advantage of the natural dynamics of the spacecraft in the absence of disturbance forces to create a periodic relative motion. The periodic motion maintains the spacecraft formation over long periods without the use of control effort. Passive apertures can be designed using the closed-form solutions provided by the linearized orbital equations (Hill's equations for a circular reference orbit) [8, 16, 18, 19]. The relative motion of the vehicles can be initialized to result in a periodic, elliptical motion when viewed in the reference frame. Passive aperture design using Hill's equations was investigated by Miller *et al.* [8] and Yeh [20]. Miller also investigated the reduction in fuel cost achieved through the use of passive apertures. Passive aperture initialization was extended to eccentric reference orbits at zero true anomaly by Inalhan in [18, 21]. This thesis further extends the initialization to any point in the eccentric orbit. Inalhan also presents a detailed examination of the error incurred by ignoring reference orbit eccentricity. A method of establishing zero average relative drift orbits in the presence of J_2 by matching the average drift rates of the vehicles in the fleet is presented in [16].

The passive apertures create periodic motion without control inputs in the absence of disturbances. However, no two spacecraft are exactly the same, so there will be disturbances and the periodic motion will deteriorate. The passive apertures are unstable in the sense that if a vehicle is perturbed from the required state for periodic motion, the spacecraft will not naturally return to the initial state. As a result, a controller is required to maintain the desired state for the passive aperture. Nonlinear feedback control designs have been investigated in [22, 23]. Many of the nonlinear control schemes use feedback linearization, wherein control commands are used to cancel the nonlinear dynamics and replace the nonlinear dynamics with linear dynamics that typically are not the natural dynamics of an orbiting satellite. The linearized relative dynamics discussed above also provide many avenues for control development. Numerous linear quadratic regulators have been developed which force

a vehicle to track a desired state [24, 25, 26]. However, these feedback control schemes require almost constant control effort which leads to high fuel costs over the length of a mission. In order to reduce fuel costs, research focused on fuel-time optimal methods to generate control sequences over a period of time rather than just one step. An impulsive feedback scheme is presented in [27] and a genetic algorithm scheme for determining near fuel optimal trajectories is presented in [28]. The impulsive feedback scheme in [27] controls the spacecraft to track desired orbital elements. The fuel optimization is only considered through the sensitivities of changes in the orbital elements. For example, a change in argument of latitude or inclination requires less control effort when the vehicle passes through the polar or equatorial regions than elsewhere in the orbit. The genetic algorithm searches for a fuel optimal solution subject to constraints but is limited by the computational effort required, the lack of repeatability, and the dependence on a propagation technique. These control schemes also do not consider the effect of sensing noise on the performance of the controller. The genetic algorithm would require a forward propagation of an uncertain state which could lead to poor trajectory designs and controller performance. The control algorithm presented in this thesis addresses sensor noise in detail.

A method of determining fuel/time optimal control inputs and trajectories using linear programming (LP) was first introduced in [29]. This LP formulation forms the base of the control work presented in this thesis. Linear programming solves for the minimum fuel maneuver explicitly by minimizing a sum of the control inputs for the solution. The general formulation can include any form of linearized dynamics and disturbance models. The LP formulation also provides a general framework for including various types of state and actuator constraints. LP can be used for different types of maneuvers: formation maneuvers, individual station-keeping, formation-keeping, or general trajectory planning. Note that this type of control system is also a planning control system rather than a reactive control system. The thesis further develops the LP formulation and implements the control algorithm in a spacecraft formation flying control system. One major extension is the use of an error box for formation-keeping rather than continuously tracking a desired state. The error box provides a

position tolerance constraint to remain within rather than using control to drive to the exact desired state. The error box approach does not use control effort to correct for the small periodic perturbation effects, such as those resulting from the J_2 gravity perturbation. The error box reduces fuel cost by allowing some slack in the position tolerance.

In addition to the work on control of one spacecraft relative to another, several researchers have explored a variety of fleet coordination and control architectures. The fleet can be organized in several different ways. One example is a leader-follower configuration. In this architecture one spacecraft is specified as the leader and acts as the reference point for the other members of the fleet. The leader-follower architecture is relatively simple to implement, but has several disadvantages. One disadvantage is that the follower vehicles must correct for any disturbance experienced by the leader. Another approach to fleet control is the idea of a formation template. The template of the formation shape is placed on a reference point or formation center [30]. The template then specifies the desired states for all members of the fleet. Some cooperation is achieved in this method because the placement of the template can be made a function of all vehicles in the fleet rather than one specific vehicle. A hierarchical structure using formation templates is presented in [31]. The hierarchical structure splits the decision process into high-level fleet coordination and cooperation and low-level control input generation. This thesis uses a hierarchical approach to coordinate the fleet of spacecraft.

1.2 Thesis Overview

The purpose of the following work is to develop control algorithms and a control architecture for formation flying spacecraft. The control algorithms are formulated as linear programming (LP) problems. The advantages of the LP formulation were discussed briefly in the previous section and will be further addressed throughout the algorithm formulation and implementation. The objective of the LP is to minimize the control inputs over a specified time interval subject to constraints such as dynamics,

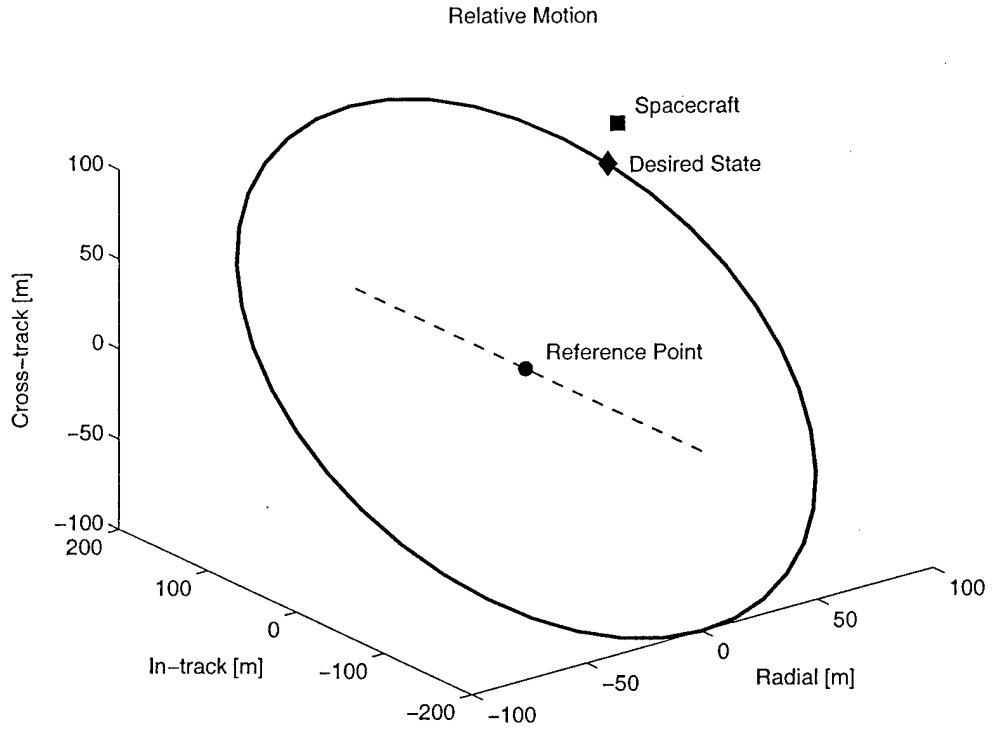

Figure 1-1: Description of the three parts of the formation flying control problem. The reference point is denoted with a circle, and the current desired relative position with a diamond. The projected desired relative motion for a passive aperture is also shown. The actual state of the spacecraft is the square.

initial conditions, terminal conditions, actuator limits, etc. The LP formulation is used within a hierarchical control architecture for a formation of spacecraft. The hierarchical architecture enables high-level coordination of the fleet and low-level control generation and execution on each vehicle.

There are three main parts to the formation flying control problem: 1) the reference point for the fleet, 2) the desired state for each vehicle, and 3) the dynamics used to represent the motion of spacecraft relative to the desired state in the controller. Figure 1-1 shows each of these aspects for a single vehicle in a typical passive aperture configuration. The reference point, shown in the figure as a $\bullet$, is used in the linearization of the relative dynamics and for the specification of the desired state for each vehicle. The reference point can be fixed on a single vehicle or determined in a coordinated method.

The desired state, represented by a ♦ in the figure, is specified relative to the reference point for each vehicle. The desired state is the state the spacecraft is controlled to achieve or the state maintained during formation-keeping. This state can be a simple in-track separation or the time-varying state required for a passive aperture. The form of relative dynamics used to represent the motion of the spacecraft relative to the reference point affects the desired state.

The third issue in the control problem is the dynamics used in the controller to model the actual motion of spacecraft, the ■ in the figure, relative to the desired state. As mentioned previously, one advantage of the LP formulation is that any form of linearized dynamics as well as disturbance models can be used in the controller formulation. Several forms of dynamics are considered for the desired state and dynamics in the controller.

This thesis addresses and presents solutions to each of these main questions in the formation flying control problem. The thesis also addresses several issues in implementing the control algorithms in a real-time control system such as: robustness to uncertainty due to sensor noise and uncertainty in dynamics and disturbance models; feasibility of LP solutions; LP computation times; and the form of dynamics to use in the controller. The result is a very flexible optimization framework that can be used off-line to analyze aspects of a mission design and in real-time as part of an on-board autonomous formation flying control system.

Chapter 2 presents the linearized relative dynamics for motion of one spacecraft relative to another. The linearized dynamics are critical to represent the motion of the spacecraft in the controller and to specify the desired state in the control problem. Three forms of the linearized dynamics are presented: Hill's equations for circular orbits, Lawden's equations for eccentric orbits, and a set of equations for circular orbits that include a linearized J_2 disturbance model. The chapter also includes a discussion of passive aperture design using the various forms of dynamics and a general aperture initialization method for eccentric reference orbits. Each form of the dynamics is considered for both the specification of the desired state and the dynamics in the controller. A discretization of the dynamics for use in the discrete

controller design is also presented.

Chapter 3 discusses the LP control algorithm formulation. The chapter is separated into a section on control generation and a section on coordination. The control section presents the LP formulation for a terminal constraint problem such as formation initialization or formation reconfiguration and for a formation-keeping control problem where a desired state is maintained within some tolerance. Methods of including additional constraints such as actuator limits and additional state constraints are also presented. The algorithms provide a method of generating fuel-optimal control inputs to achieve the desired state as well as maintaining the desired state over extended periods of time. The coordination section presents a LP method to coordinate the maneuvers of the multiple spacecraft during a formation initialization/reconfiguration. This section also contains a discussion of several methods of cooperation during formation-keeping maneuvers. The coordination is achieved through the specification of the reference point for the fleet.

Chapter 4 addresses several aspects of implementing the control algorithms discussed in Chapter 3 as part of an on-line control system. The first implementation issue is algorithm initiation. A spacecraft monitor is introduced and uses logic to decide when control action is required and subsequently initiates the LP algorithm to solve for the optimal control action. The next issue addressed is uncertainty introduced through sensor noise and state estimation. Sensor noise leads to uncertainty in the current state of the satellite which is crucial to the solution of the trajectory optimization. A brief discussion of other uncertainties, including disturbance model uncertainties and inaccuracies of the linearized dynamics used in the plant dynamics, is also provided. Modifications to the LP formulation are presented that increase robustness to each of these uncertainties. The robust LP formulation can result in feasibility problems in the LP solutions. The control algorithm is altered to include a new variable that allows the constraints to be relaxed to always ensure feasible solutions. Several methods of reducing computation time in the formulation of the LP are also presented by removing variables and constraints in the LP optimization.

The dynamics problem is also analyzed in terms of two key issues: 1) what dynam-

ics model should be used to specify the desired state to maintain a passive aperture; and 2) what dynamics model should be used in the LP to represent the motion about the desired state. The linearized models presented in Chapter 2 are considered in addressing each of these issues. Methods of including additional actuator constraints through mixed integer linear programming are also presented. The LP control formulation is modified to include actuator constraints such as minimum, nonzero actuation and constraints on actuator input sequences.

Chapter 5 describes the complete spacecraft control architecture and how the algorithms presented in the thesis are executed in a real-time spacecraft control system. The high-level coordinator and low-level controller are discussed in terms of the execution process as well as the information flows required. The high-level coordinator contains the fleet coordination algorithms for both formation maneuvers and formation-keeping. The low-level controller consists of the individual spacecraft control system including the LP control algorithms. The chapter concludes with a final simulation demonstrating the complete control system in a typical formation flying mission.

Chapter six discusses the main contribution resulting from the work performed for the thesis. The contributions range from control algorithm developments to control architecture design. The chapter also contains a discussion of future areas of work for the formation control system described in the thesis.

Chapter 2

Relative Spacecraft Dynamics

The linear programming control technique requires linearized relative dynamics between a spacecraft and a reference point. The reference point can be fixed on another vehicle in the formation, the formation center, or a virtual spacecraft. The linearized relative dynamics are used to determine the desired state for each vehicle in the fleet and describe the motion of each vehicle relative to the desired state. This chapter presents three forms of linearized relative dynamics for consideration in the formation flying control problem. Each dynamics model captures different aspects of the spacecraft motion such as orbit eccentricity and J_2 gravity perturbations. The relative dynamics derivation is shown for the more general case of eccentric orbits. Simplifications are made to arrive at Hill's equations for a circular reference orbit. The third form of dynamics is again for circular orbits but includes the differential J_2 gravity perturbation in the dynamics [17, 24]. The closed-form solutions for the force free motion in each dynamics model is also presented. Initial conditions for "drift free" motion between the spacecraft can be determined from the closed form solutions. One example of drift free motion is a passive aperture where the relative motion of the vehicle is periodic over time in the absence of disturbance forces. A general initialization method for eccentric reference orbits is presented to determine the desired state for a passive aperture at any true anomaly in the orbit. The chapter concludes with the discretization of these dynamics to the form used in the linear program controller development.

2.1 Relative Dynamics

The following presents the dynamics for the relative motion of a spacecraft with respect to a reference vehicle on an eccentric orbit. The eccentric orbit is the more general case and simplifications are made to arrive at the other forms of linearized relative dynamics. These dynamics are later used in modeling multiple spacecraft coordination problems. The following development of the equations of motion follows Reference [21], and the full details are available in References [12, 15]. The location of each spacecraft within a formation is given by

$$\vec{R}_j = \vec{R}_{fc} + \vec{\rho}_j \tag{2.1}$$

where $\vec{R}_{fc}$ and $\vec{\rho}_j$ correspond to the location of the formation center and the relative position of the j^{th} spacecraft with respect to that point. The formation center can either be fixed to an orbiting spacecraft, or just a local point that provides a convenient reference for linearization. The reference orbit in the Earth Centered Inertial (ECI) reference frame is represented by the standard orbital elements $(a, e, i, \Omega, \omega, \theta)$, which correspond to the semi-major axis, eccentricity, inclination, right ascension of the ascending node, argument of periapsis and true anomaly.

With the assumption that $|\vec{\rho}_j| \ll |\vec{R}_{fc}|$, the equations of motion of the j^{th} spacecraft under the gravitational attraction of a main body

$${}_i\ddot{\vec{R}}_j = -\frac{\mu}{|\vec{R}_j|^3}\vec{R}_j + \vec{f}_j \tag{2.2}$$

can be linearized around the formation center to give

$${}_i\ddot{\vec{\rho}}_j = -\frac{\mu}{|\vec{R}_{fc}|^3}\left(\vec{\rho}_j - \frac{3\vec{R}_{fc}\cdot\vec{\rho}_j}{|\vec{R}_{fc}|^2}\vec{R}_{fc}\right) + \vec{f}_j \tag{2.3}$$

where the accelerations associated with other attraction fields, disturbances or control inputs are included in $\vec{f}_j$. The derivatives in the ECI reference frame are identified by the preceding subscript i. A natural basis for inertial measurements and scientific

observations is the orbiting *(non-inertial)* reference frame Σ_c, fixed to the formation center (see Figure 2-1). Using kinematics, the relative acceleration observed in the inertial reference frame ${}_i\ddot{\vec{\rho}}_j$ can be related to the measurements in the orbiting reference frame

$$ {}_i\ddot{\vec{\rho}}_j = {}_c\ddot{\vec{\rho}}_j + 2{}_i\dot{\vec{\Theta}} \times {}_c\dot{\vec{\rho}}_j + {}_i\dot{\vec{\Theta}} \times ({}_i\dot{\vec{\Theta}} \times \vec{\rho}_j) + ({}_i\ddot{\vec{\Theta}} \times \vec{\rho}_j) \tag{2.4} $$

where ${}_i\dot{\vec{\Theta}}$ and ${}_i\ddot{\vec{\Theta}}$ correspond to the angular velocity and acceleration of this orbiting reference frame. The fundamental vectors $(\vec{\rho}_j, \vec{R}_{fc}, {}_i\dot{\vec{\Theta}})$ in Equations 2.3 and 2.4 can be expressed in Σ_c as

$$ \vec{\rho}_j = x_j\hat{k}_x + y_j\hat{k}_y + z_j\hat{k}_z \tag{2.5} $$

$$ \vec{R}_{fc} = R_{fc}\hat{k}_x \tag{2.6} $$

$$ {}_i\dot{\vec{\Theta}} = \dot{\theta}\hat{k}_z \tag{2.7} $$

where the unit vector $\hat{k}_x$ points radially outward from Earth's center (anti-nadir pointing) and $\hat{k}_y$ is in the in-track direction along increasing true anomaly. This right-handed reference frame is completed with $\hat{k}_z$, pointing in the cross-track direction. All of the proceeding vectors and their time rate of changes are expressed in the orbiting reference frame Σ_c. Combining Equations 2.3 and 2.4 to obtain an expression for ${}_c\ddot{\vec{\rho}}_j$, and using Equations 2.5–2.7, it is clear that the linearized relative dynamics with respect to an eccentric orbit can be expressed via a unique set of elements and their time rate of change. This set consists of the relative states $[x_j, y_j, z_j]$ of each satellite, the radius R_{fc} and the angular velocity $\dot{\theta}$ of the formation center. Using fundamental orbital mechanics describing planetary motion [32, 33], the radius and angular velocity of the formation center can be written as

$$ |\vec{R}_{fc}| = \frac{a(1-e^2)}{1+e\cos\theta}, \text{ and } \dot{\theta} = \frac{n(1+e\cos\theta)^2}{(1-e^2)^{3/2}} \tag{2.8} $$

where $n = \sqrt{\mu/a^3}$ is the natural frequency of the reference orbit. These expressions can be substituted into the equation for ${}_c\ddot{\vec{\rho}}_j$ to obtain the relative motion of the j^{th}

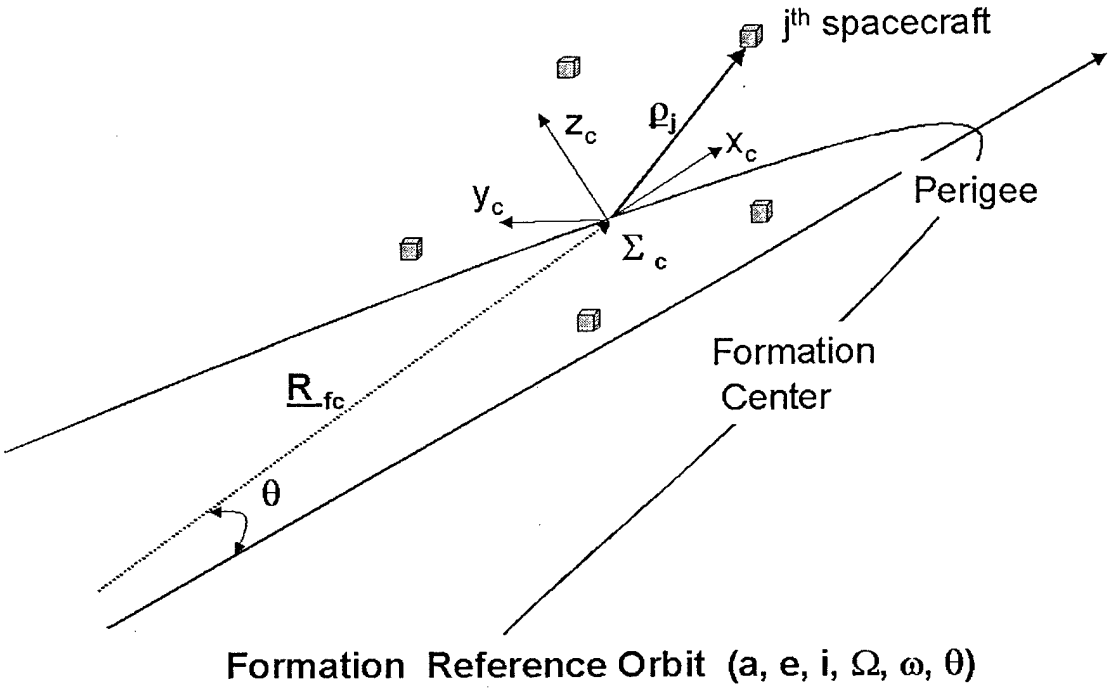

Figure 2-1: Relative Motion in Formation Reference Frame

spacecraft in the orbiting formation reference frame

$$\frac{d}{dt}\begin{bmatrix}\dot{x}\\ \dot{y}\\ \dot{z}\end{bmatrix}_j = -2\begin{bmatrix}0 & -\dot{\theta} & 0\\ \dot{\theta} & 0 & 0\\ 0 & 0 & 0\end{bmatrix}\begin{bmatrix}\dot{x}\\ \dot{y}\\ \dot{z}\end{bmatrix}_j - \begin{bmatrix}-\dot{\theta}^2 & 0 & 0\\ 0 & -\dot{\theta}^2 & 0\\ 0 & 0 & 0\end{bmatrix}\begin{bmatrix}x\\ y\\ z\end{bmatrix}_j - \begin{bmatrix}0 & -\ddot{\theta} & 0\\ \ddot{\theta} & 0 & 0\\ 0 & 0 & 0\end{bmatrix}\begin{bmatrix}x\\ y\\ z\end{bmatrix}_j + n^2\left(\frac{1+e\cos\theta}{1-e^2}\right)^3\begin{bmatrix}2x\\ -y\\ -z\end{bmatrix}_j + \begin{bmatrix}f_x\\ f_y\\ f_z\end{bmatrix}_j \quad (2.9)$$

The terms on the right-hand side of this equation correspond to the Coriolis acceleration, centripetal acceleration, accelerating rotation of the reference frame, and the virtual gravity gradient terms with respect to the formation reference. The right-hand side also includes the combination of other external and control accelerations in $\vec{f}_j$.

These terms can be explicitly presented for each spacecraft as

$$\begin{bmatrix} f_x \\ f_y \\ f_z \end{bmatrix}_j = \begin{bmatrix} u_x \\ u_y \\ u_z \end{bmatrix}_j + \begin{bmatrix} w_x \\ w_y \\ w_z \end{bmatrix}_j \tag{2.10}$$

where $u = [u_x(t)\ u_y(t)\ u_z(t)]^T : \mathbb{R} \rightarrow \mathbb{R}^3$ represents the control inputs and $w = [w_x(t)\ w_y(t)\ w_z(t)]^T : \mathbb{R} \rightarrow \mathbb{R}^3$ represents the combination of other external accelerations, such as disturbances.

The Equation 2.9 can be expressed in state space format with the introduction of the control inputs as $[u_x\ u_y\ u_z]^T$ and disturbances $[w_x\ w_y\ w_z]^T$

$$\frac{d}{dt}\begin{bmatrix} \dot{x} \\ x \\ \dot{y} \\ y \\ \dot{z} \\ z \end{bmatrix} = \begin{bmatrix} 0 & \dot{\theta}^2[1+\frac{2}{(1+e\cos\theta)}] & 2\dot{\theta} & \ddot{\theta} & 0 & 0 \\ 1 & 0 & 0 & 0 & 0 & 0 \\ -2\dot{\theta} & -\ddot{\theta} & 0 & \dot{\theta}^2[1-\frac{1}{(1+e\cos\theta)}] & 0 & 0 \\ 0 & 0 & 1 & 0 & 0 & 0 \\ 0 & 0 & 0 & 0 & 0 & -[\frac{\dot{\theta}^2}{(1+e\cos\theta)}] \\ 0 & 0 & 0 & 0 & 1 & 0 \end{bmatrix} \begin{bmatrix} \dot{x} \\ x \\ \dot{y} \\ y \\ \dot{z} \\ z \end{bmatrix}$$
$$+ \begin{bmatrix} 1 & 0 & 0 \\ 0 & 0 & 0 \\ 0 & 1 & 0 \\ 0 & 0 & 0 \\ 0 & 0 & 1 \\ 0 & 0 & 0 \end{bmatrix} \begin{bmatrix} u_x \\ u_y \\ u_z \end{bmatrix} + \begin{bmatrix} 1 & 0 & 0 \\ 0 & 0 & 0 \\ 0 & 1 & 0 \\ 0 & 0 & 0 \\ 0 & 0 & 1 \\ 0 & 0 & 0 \end{bmatrix} \begin{bmatrix} w_x \\ w_y \\ w_z \end{bmatrix} \tag{2.11}$$

which can be compactly represented as a general linear time varying state space description

$$\dot{x}(t) = A(t)x(t) + B(t)u(t) + B_d(t)w(t) \tag{2.12}$$

Care must be taken when interpreting and using the equations of motion and the relative states in a nonlinear analysis. The difficulty results from the linearization process, which maps the curvilinear space to a rectangular one via a small curvature

approximation. In this case, a relative separation in the in-track direction in the linearized equations actually corresponds to an incremental phase difference in true anomaly, θ. For the formations considered in this thesis, the separations between spacecraft are small, less than one kilometer, and the linearization error is negligible.

2.1.1 Relative Dynamics Eccentric Orbit

Although Equation 2.11 is expressed in the time domain, monotonically increasing true anomaly (θ) of the reference orbit provides a natural basis for parameterizing the fleet time and motion. This observation is based on the fact that the angular velocity and the radius describing the orbital motion are functions of the true anomaly [32]. Using θ as the free variable, the equations of motion can be transformed using the relationships

$$(\dot{\cdot}) = (\cdot)'\dot{\theta}, \text{ and } (\ddot{\cdot}) = (\cdot)''\dot{\theta}^2 + \dot{\theta}\dot{\theta}'(\cdot)' \tag{2.13}$$

With these transformations, the set of linear time-varying (LTV) equations describing the relative motion in an eccentric orbit can be written as

$$\frac{d}{d\theta}\begin{bmatrix} x' \\ x \\ y' \\ y \\ z' \\ z \end{bmatrix} = \begin{bmatrix} \frac{2e\sin\theta}{1+e\cos\theta} & \frac{3+e\cos\theta}{1+e\cos\theta} & 2 & \frac{-2e\sin\theta}{1+e\cos\theta} & 0 & 0 \\ 1 & 0 & 0 & 0 & 0 & 0 \\ -2 & \frac{2e\sin\theta}{1+e\cos\theta} & \frac{2e\sin\theta}{1+e\cos\theta} & \frac{e\cos\theta}{1+e\cos\theta} & 0 & 0 \\ 0 & 0 & 1 & 0 & 0 & 0 \\ 0 & 0 & 0 & 0 & \frac{2e\sin\theta}{1+e\cos\theta} & \frac{-1}{1+e\cos\theta} \\ 0 & 0 & 0 & 0 & 1 & 0 \end{bmatrix} \begin{bmatrix} x' \\ x \\ y' \\ y \\ z' \\ z \end{bmatrix}$$
$$+ \frac{(1-e^2)^3}{(1+e\cos\theta)^4 n^2} \left(\begin{bmatrix} 1 & 0 & 0 \\ 0 & 0 & 0 \\ 0 & 1 & 0 \\ 0 & 0 & 0 \\ 0 & 0 & 1 \\ 0 & 0 & 0 \end{bmatrix} \begin{bmatrix} u_x \\ u_y \\ u_z \end{bmatrix} + \begin{bmatrix} 1 & 0 & 0 \\ 0 & 0 & 0 \\ 0 & 1 & 0 \\ 0 & 0 & 0 \\ 0 & 0 & 1 \\ 0 & 0 & 0 \end{bmatrix} \begin{bmatrix} w_x \\ w_y \\ w_z \end{bmatrix} \right) \tag{2.14}$$

As shown, the in-plane (x, y) and out-of-plane (z) motions are decoupled (except where the disturbance models can create coupling) and can be expressed separately.

The homogenous solutions to the linear time-varying equations are available in literature for various reference frames and variables. The first derivation was provide by Lawden in 1963 [12] and similar results are available from Marec [15]. Carter [13, 14] removed the singularities in previous solutions and provides the basis of the solutions presented here. The solutions can be written in the time domain, but writing the equations as functions of the true anomaly, θ, provides a more natural description. The form presented in this paper uses the following change of variables for position, $\vec{\rho}$, and velocity, $\vec{\rho}'$ [13]

$$\vec{\rho}_* = (1 + e\cos\theta)\vec{\rho}; \quad \vec{\rho}_*' = (1 + e\cos\theta)\vec{\rho}' - e\sin\theta\vec{\rho} \tag{2.15}$$

where $\vec{\rho} = (x, y, z)$ corresponds to the previous definition of the positions and $\vec{\rho}_* = (x_*, y_*, z_*)$ represents the transformed positions. There is also a change in the reference frame. In this case, $\hat{k}_{x*}$ is radially pointing away from the earth, $\hat{k}_{y*}$ is perpendicular to $\hat{k}_{x*}$, in the direction opposed to the motion, $\hat{k}_{z*}$ remains out of plane and completes the $\hat{k}_{y*}$–$\hat{k}_{x*}$–$\hat{k}_{z*}$ right hand coordinate frame. The homogenous solutions are

$$\begin{aligned} x_*(\theta) &= r\sin\theta\left[b_1 e + 2b_2 e^2 H(\theta)\right] - \cos\theta\left[\frac{b_2 e}{r} + b_3\right] \\ y_*(\theta) &= -r^2\left[b_1 + 2b_2 e H(\theta)\right] - b_3\left[1 + r\right]\sin\theta + b_4 \\ z_*(\theta) &= b_5\cos\theta + b_6\sin\theta \end{aligned} \tag{2.16}$$

and

$$\begin{aligned} x_*'(\theta) &= \left[r'\sin\theta + r\cos\theta\right]\left[b_1 e + 2b_2 e^2 H(\theta)\right] + r\sin\theta\left[2b_2 e^2 H'(\theta)\right] \\ &\quad + \sin\theta\left[\frac{b_2 e}{r} + b_3 r\right] + \cos\theta r'\left[\frac{b_2 e}{r^2} - b_3\right] \\ y_*'(\theta) &= -2rr'\left[b_1 + 2b_2 e H(\theta)\right] - r^2\left[2b_2 e H'(\theta)\right] - b_3 r'\sin\theta \\ &\quad - b_3\left[1 + r\right]\cos\theta \\ z_*'(\theta) &= -b_5\sin\theta + b_6\cos\theta \end{aligned} \tag{2.17}$$

The b_i's are integration constants calculated from the corresponding initial conditions. The additional parameters in the solutions are $r = 1 + e\cos\theta$ and

$$\begin{aligned} H(\theta) &= \int_{\theta_0}^{\theta} \frac{\cos\theta}{(1+e\cos\theta)^3} d\theta \\ &= -\left(1-e^2\right)^{-5/2}\left[\frac{3eE}{2} - \left(1+e^2\right)\sin E + \frac{e}{2}\sin E\cos E + d_H\right] \quad (2.18) \\ \cos E &= \frac{e+\cos\theta}{1+e\cos\theta} \quad (2.19) \end{aligned}$$

where E is the orbit eccentric anomaly and d_H is calculated from $H(\theta_0) = 0$. The homogeneous solutions are used in determining the required state for maintaining a passive aperture in the absence of disturbance forces.

2.1.2 Relative Dynamics Circular Orbit (Hill's)

For a circular reference orbit, $e = 0$, substituting $\dot{\theta} = n$ and $\ddot{\theta} = 0$ into Equation 2.11 results in the well known Clohessy-Wiltshire or Hill's equations

$$\begin{aligned} \frac{d}{dt}\begin{bmatrix} \dot{x} \\ x \\ \dot{y} \\ y \\ \dot{z} \\ z \end{bmatrix} &= \begin{bmatrix} 0 & 3n^2 & 2n & 0 & 0 & 0 \\ 1 & 0 & 0 & 0 & 0 & 0 \\ -2n & 0 & 0 & 0 & 0 & 0 \\ 0 & 0 & 1 & 0 & 0 & 0 \\ 0 & 0 & 0 & 0 & 0 & -n^2 \\ 0 & 0 & 0 & 0 & 1 & 0 \end{bmatrix}\begin{bmatrix} \dot{x} \\ x \\ \dot{y} \\ y \\ \dot{z} \\ z \end{bmatrix} \\ &+ \begin{bmatrix} 1 & 0 & 0 \\ 0 & 0 & 0 \\ 0 & 1 & 0 \\ 0 & 0 & 0 \\ 0 & 0 & 1 \\ 0 & 0 & 0 \end{bmatrix}\begin{bmatrix} u_x \\ u_y \\ u_z \end{bmatrix} + \begin{bmatrix} 1 & 0 & 0 \\ 0 & 0 & 0 \\ 0 & 1 & 0 \\ 0 & 0 & 0 \\ 0 & 0 & 1 \\ 0 & 0 & 0 \end{bmatrix}\begin{bmatrix} w_x \\ w_y \\ w_z \end{bmatrix} \end{aligned} \quad (2.20)$$

The x-coordinate is in the radial direction, the y-coordinate is in the in-track direction and the z-component is in the cross-track direction. These equations are linear time invariant and the dynamics are decoupled in the in-plane and out-of-plane as with the eccentric dynamics. The closed-form solutions to Hill's equations can be written as

$$\begin{aligned} x(t) &= \frac{\dot{x}_0}{n}\sin nt - \left(\frac{2\dot{y}_0}{n} + 3x_0\right)\cos nt + \left(\frac{2\dot{y}_0}{n} + 4x_0\right) \\ y(t) &= \frac{2\dot{x}_0}{n}\cos nt + \left(\frac{4\dot{y}_0}{n} + 6x_0\right)\sin nt + \left(y_0 - \frac{2\dot{x}_0}{n}\right) - (3\dot{y}_0 + 6nx_0)t \\ z(t) &= z_0\cos nt + \frac{\dot{z}_0}{n}\sin nt \end{aligned} \tag{2.21}$$

Note the in-track oscillation is a quarter period ahead of the radial oscillation with double the amplitude. The in-plane motion is caused by slight differences in eccentricity between the two orbits. The cross-track motion is a simple oscillation corresponding to a slight inclination difference or difference in argument of latitude between the spacecraft and reference orbit [10].

2.1.3 Relative Dynamics Circular Orbit, Linearized J_2

The last form of dynamics is very similar to Hill's, but has been modified to include the linearized effects of the J_2 gravitational perturbations. The dynamics presented here are actually a combination of the work of References [17, 24]. The in-plane dynamics are from Reference [17], while the out-of-plane dynamics are from Reference [24]. This combination appears to give the best fit to the nonlinear orbital simulations.

The linearized dynamics including J_2 effects are

$$\frac{d}{dt}\begin{bmatrix}\dot{x}\\ x\\ \dot{y}\\ y\\ \dot{z}\\ z\end{bmatrix} = \begin{bmatrix} 0 & (5c^2-2)n^2 & 2nc & 0 & 0 & 0 \\ 1 & 0 & 0 & 0 & 0 & 0 \\ -2nc & 0 & 0 & 0 & 0 & 0 \\ 0 & 0 & 1 & 0 & 0 & 0 \\ 0 & 0 & 0 & 0 & 0 & -(3c^2-2)n^2 \\ 0 & 0 & 0 & 0 & 1 & 0 \end{bmatrix}\begin{bmatrix}\dot{x}\\ x\\ \dot{y}\\ y\\ \dot{z}\\ z\end{bmatrix} + \begin{bmatrix} 1 & 0 & 0 \\ 0 & 0 & 0 \\ 0 & 1 & 0 \\ 0 & 0 & 0 \\ 0 & 0 & 1 \\ 0 & 0 & 0 \end{bmatrix}\begin{bmatrix}u_x\\ u_y\\ u_z\end{bmatrix} + \begin{bmatrix} 1 & 0 & 0 \\ 0 & 0 & 0 \\ 0 & 1 & 0 \\ 0 & 0 & 0 \\ 0 & 0 & 1 \\ 0 & 0 & 0 \end{bmatrix}\begin{bmatrix}w_x\\ w_y\\ w_z\end{bmatrix} + d_c\begin{bmatrix}0\\0\\0\\0\\1\\0\end{bmatrix} \tag{2.22}$$

where

$$\begin{aligned} s &= \frac{3}{8}J_2\left(\frac{R_{\text{earth}}}{a_{\text{ref}}}\right)^2(1+3\cos(2i_{\text{ref}})) \\ c &= \sqrt{s+1} \\ d_c &= 2Anca_{\text{ref}}\cos\alpha_c\sin\theta_{\text{ref}} \\ A &= \frac{3}{2}J_2 n\left(\frac{R_{\text{earth}}}{a_{\text{ref}}}\right)^2\sin^2(i_{\text{ref}})c_2 \\ c_2 &= \frac{\rho}{a_{\text{ref}}} \end{aligned} \tag{2.23}$$

and n is the mean motion, a_{ref} is the semi-major axis, i_{ref} is the inclination, and θ_{ref} is the true anomaly of the reference orbit. α_c is the cross-track formation phasing angle and ρ is the formation radius [24]. The u's correspond to control inputs, the w's are disturbance forces. and d_c is the cross-track disturbance force due to J_2. The cross-track J_2 disturbance is modeled as a disturbance input in the LP problem.

The cross-track disturbance is the result of differential gravity effects due to the oblateness of the earth. The formation phasing angle, α_c, in the cross-track distur-

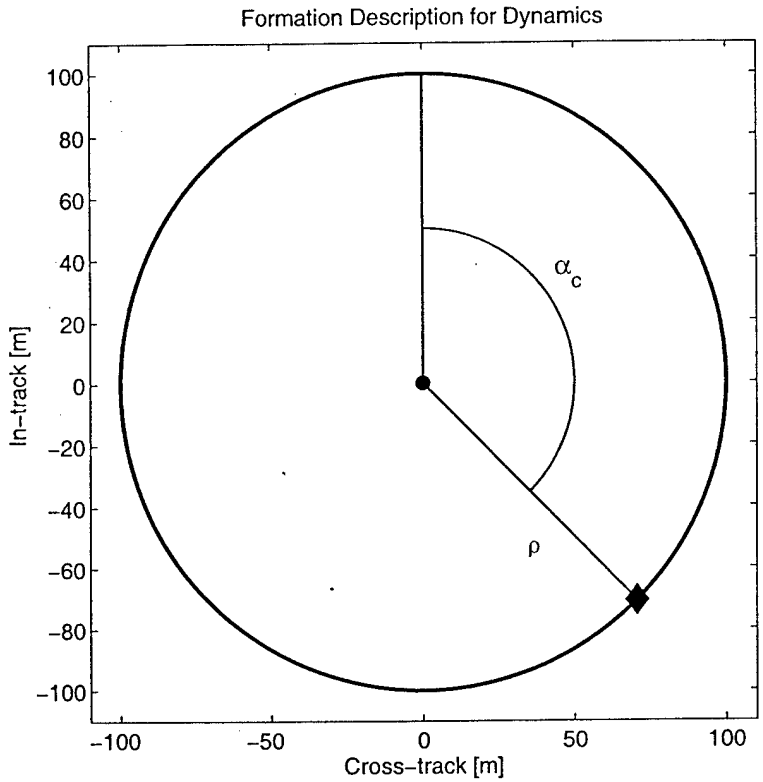

Figure 2-2: Typical formation description for a passive aperture that projects a circle in the in-track–cross-track plane. The cross-track phasing angle is measured by α_c and ρ is the formation radius.

bance specifies whether the cross-track oscillatory motion is due to an inclination difference or ascending node difference. The phasing angle is measured in the in-track–cross-track plane when the spacecraft is in the equatorial plane of the earth. Figure 2-2 shows an example geometry for a formation that projects a circle in the in-track–cross-track plane. If $\alpha_c = 0$ or 180°, the orbit has a maximum inclination difference with respect to the reference orbit and zero node difference, which results in the largest disturbance ($\cos\alpha_c = 1$). If $\alpha_c = \pm\frac{\pi}{2}$, the orbit has maximum node difference and zero inclination difference. As shown, the disturbance disappears because the gravity gradient due to the oblateness of the earth is the same for orbits with the same inclination.

Note that if $J_2 = 0$, then s and c also equal zero and these dynamics simplify to Hill's dynamics in Equation 2.20. This set of dynamics is composed from two sepa-

rate sources because the in-plane dynamics in Reference [24] require an iteration on a parameter to speed up the orbital motion in the dynamics where as Reference [17] provides a direct calculation for the parameter c to achieve the same effect. Conversely, the out-of-plane dynamics in Reference [17] require several calculations involving both relative and absolute measurements to determine the disturbance, whereas the model Reference [24] only requires a relatively straightforward calculation. Furthermore, because the in-plane and out-of-plane dynamics decouple, we can combine these two distinct models.

The homogenous solutions to these equations excluding the out-of-plane disturbance force, d_c, are [17]

$$\begin{aligned} x(t) &= x_0 \cos(\sqrt{1-s}\ nt) + \frac{\sqrt{1-s}}{2\sqrt{1+s}}\, y_0 \sin(\sqrt{1-s}\ nt) \\ y(t) &= -\frac{2\sqrt{1+s}}{\sqrt{1-s}}\, x_0 \sin(\sqrt{1-s}\ nt) + y_0 \cos(\sqrt{1-s}\ nt) \\ z(t) &= z_0 \cos(\sqrt{1+3s}\ nt) + \frac{\dot{z_0}}{n\sqrt{1+3s}} \sin(\sqrt{1+3s}\ nt) \end{aligned} \tag{2.24}$$

Note these equations assume the secular drift terms have been eliminated. The motion described by these equations is periodic in the relative frame. This periodic motion leads to a passive aperture formation that is discussed in the following section.

2.2 Passive Apertures

Passive apertures are formation configurations that result in "drift free" relative motion within the fleet. The baselines of the formations are restricted to be short, less than a kilometer, because the work in this thesis neglects the linearization error. Recent research has lead to correction terms for the linearization error in passive aperture initialization. The drift free configuration can be a simple in-track separation or a more complex passive aperture. Passive apertures take advantage of the natural dynamics of the spacecraft in the absence of disturbance forces to create drift free relative motion. Ideally the formation would remain together over long periods

of time without using any control effort. Passive apertures can be designed using the closed-form solutions provided by the linearized orbital equations presented in Section 2.1. For example, it is well known that the non-periodic in-plane motion terms in the closed form solutions to Hill's equations of motion in Equation 2.21 can be eliminated by requiring $\dot{y}_0 = -2nx_0$. This results in either a constant in-track separation, if $x_0 = 0$, or an elliptical motion when viewed in the reference frame for non-zero radial positions.

Initial conditions for passive apertures in the presence of J_2 have also been investigated. Reference [16] develops two first-order conditions relating the semi-major axis, eccentricity, and inclination such that the average drift among spacecraft is equal. Therefore, on average, the spacecraft will not drift apart over time under the influence of J_2. This requirement is in terms of orbital elements. Another approach uses the solutions to the relative dynamics under the influence of J_2 to determine the following conditions for periodic in-plane motion

$$\frac{\dot{y}(0)}{x(0)} = -2n\sqrt{1+s}\;;\; \frac{\dot{x}(0)}{y(0)} = \frac{n(1-s)}{2\sqrt{1+s}} \tag{2.25}$$

Using these conditions does not eliminate the secular growth experienced in the cross-track direction due to J_2.

Previous work determined initial conditions for periodic motion in eccentric reference orbits for initial true anomaly, $\theta_0 = 0$ [18]. The initial conditions for periodic motion expressed in the θ-domain are

$$\frac{y'(0)}{x(0)} = -\frac{2+e}{1+e} \text{ or } \frac{y'_*(0)}{x_*(0)} = \frac{2+e}{1+e} \tag{2.26}$$

This condition provides a relationship between the initial radial position and in-track velocity for the spacecraft to maintain a periodic motion. Note that this velocity is the true anomaly rate of change of the in-track position. The corresponding condition for the time-domain is

$$\frac{\dot{y}(0)}{x(0)} = -\frac{n(2+e)}{(1+e)^{1/2}(1-e)^{3/2}} \tag{2.27}$$

As $e \rightarrow 0$, Equation 2.27 converges to the differential energy condition for Hill's equations, $\dot{y}(0)/x(0) = -2n$. Another similarity can be observed between the constraints in Equations 2.25 and 2.27. Nonlinear simulations with the gravity perturbations indicate the circular orbit actually will have an eccentricity of 0.001. Using this eccentricity in Equation 2.27, the constraint on in-track velocity and radial position is very similar to Equation 2.25 for a circular orbit with J_2 effects. Both result in a slightly larger ratios than determined from Hill's equations. Therefore, one major effect of J_2 is orbit eccentricity which can be effectively captured in Lawden's dynamics as well as the circular orbit dynamics with linearized J_2 effects. A further examination of the effect of each dynamics model on the desired state and controller is discussed in Section 4.5.

2.2.1 General Initialization in Eccentric Orbits

The initial conditions given above for the time-varying relative dynamics for eccentric orbits only applies for a zero initial true anomaly. This thesis extends the initialization procedure for eccentric orbits to any initial true anomaly. The general initialization procedure involves using the homogeneous solution to the time-varying equations for eccentric orbits presented in Section 2.1.1.

Initialization for periodic motion at other values of θ can also be obtained using Equations 2.16 and 2.18. For example, consider a spacecraft at some $\theta_d \neq 0$ with current values of the scaled position and velocities $x_*(\theta_d)$, $y_*(\theta_d)$, $x'_*(\theta_d)$, and $y'_*(\theta_d)$. Assuming that these values are not consistent with a periodic solution, they can be modified using Equation 2.26. To start, first use Equations 2.16, 2.18 to define

$$\begin{bmatrix} x_*(\theta_d) \\ y_*(\theta_d) \\ x'_*(\theta_d) \\ y'_*(\theta_d) \end{bmatrix} = \begin{bmatrix} r_1 \\ r_2 \\ r_3 \\ r_4 \end{bmatrix} \begin{bmatrix} b_1 \\ b_2 \\ b_3 \\ b_4 \end{bmatrix} \equiv R\,B \tag{2.28}$$

$$\begin{bmatrix} x_*(0) \\ y'_*(0) \end{bmatrix} = \begin{bmatrix} r_{30} \\ r_{40} \end{bmatrix} B \tag{2.29}$$

where the r_i are the appropriate row vectors of coefficients for the b_i's and r_{i0} is the row vector of coefficients evaluated at $\theta = 0$.

Equation 2.26 constrains the relationship between $y'_*(0)$ and $x_*(0)$ which can be rewritten as

$$\left(\frac{2+e}{1+e}\, r_{30} - r_{40}\right) B = 0 \tag{2.30}$$

Note the drift free constraint is equivalent to setting $b_2 = 0$. To complete the initialization, we assume that $x_*(\theta_d)$ and $y_*(\theta_d)$ must be the values provided previously and that only the values of $y'_*(\theta_d)$ and $x'_*(\theta_d)$ can be changed to achieve periodic motion. These assumptions provide three constraints on the four unknowns (the b_i's). The fourth constraint can be developed in a variety of ways, depending on the factors that are most important.

Symmetric Motion

For example, one approach would be to constrain the periodic motion so that it is symmetric in-track about the origin. Evaluating the $y_\star(\theta)$ part of Equation 2.16 at $\theta = 0$ and $\theta = \pi$ and setting the average to zero, yields the constraint

$$\begin{bmatrix} -1 & -(1+e)H(0) + (1-e)H(\pi) & 0 & 1 \end{bmatrix} B = 0 \tag{2.31}$$

Appending this constraint to the three given previously completely defines the periodic motion.

Fuel Optimal

In general, the symmetric initialization requires that both $x'_\star(\theta_d)$ and $y'_\star(\theta_d)$ be modified, which can be fuel intensive. This naturally leads to the question of whether there is an optimal way to select the b_i's that minimizes the fuel cost associated with changing $x'_\star(\theta_d)$ and/or $y'_\star(\theta_d)$ so that the four state values at θ_d are consistent with periodic motion. One solution to this problem is to pose it as an optimization that minimizes the ΔV required to obtain the initial velocities that are consistent

with periodic relative motion at θ_d. Define the desired velocities for periodic motion $x'_*(\theta_d)_{\text{des}}$ and $y'_*(\theta_d)_{\text{des}}$ in terms of the initial velocities, $x'_*(\theta_d)_{\text{init}}$ and $y'_*(\theta_d)_{\text{init}}$, and the required incremental velocity changes, ΔV_x and ΔV_y as

$$\begin{aligned} x'_*(\theta_d)_{\text{des}} &= x'_*(\theta_d)_{\text{init}} + \Delta V_x \\ y'_*(\theta_d)_{\text{des}} &= y'_*(\theta_d)_{\text{init}} + \Delta V_y \end{aligned} \tag{2.32}$$

The $x'_*(\theta_d)$ and $y'_*(\theta_d)$ can be written in terms of the b_i (Equation 2.28) so the total ΔV can be expressed in terms of the knows and the b_i's. Introducing the slack variables ΔV^+ and ΔV^- for each ΔV, the problem can be written as the linear program (LP)

$$\begin{aligned} J &= \min\ c^T U \\ \text{subject to}\quad A_{\text{eq}} U &= b_{\text{eq}} \\ A_{\text{ineq}} U &\leq b_{\text{ineq}} \end{aligned} \tag{2.33}$$

where

$$U^T = \begin{bmatrix} \Delta V_x^+ & \Delta V_x^- & \Delta V_y^+ & \Delta V_y^- & b_1 & b_2 & b_3 & b_4 \end{bmatrix}$$

$$c^T = \begin{bmatrix} 1 & 1 & 1 & 1 & 0 & 0 & 0 & 0 \end{bmatrix}$$

$$A_{\text{eq}} = \begin{bmatrix} 1 & -1 & 0 & 0 & -r_3 \\ 0 & 0 & 1 & -1 & -r_4 \\ 0 & 0 & 0 & 0 & r_1 \\ 0 & 0 & 0 & 0 & r_2 \\ 0 & 0 & 0 & 0 & \frac{2+e}{1+e} r_{30} - r_{40} \end{bmatrix} \quad \text{and} \quad b_{\text{eq}} = \begin{bmatrix} -x'_*(\theta_d)_{\text{init}} \\ -y'_*(\theta_d)_{\text{init}} \\ x_*(\theta_d) \\ y_*(\theta_d) \\ 0 \end{bmatrix}$$

and A_{ineq} is a 4×8 matrix of zeros with $A_{11} = A_{22} = A_{33} = A_{44} = -1$ and b_{ineq} is a 4×1 vector of zeros. These inequality constraints force the slack variables to be positive. The LP problem has four variables and nine constraints. The equality constraints satisfy the position constraints in Equation 2.28, the velocity constraints in Equation 2.32, and the periodicity constraint in Equation 2.30. The solution of the LP problem contains the four b_i's and the ΔV's required to change the initial

velocities to the desired velocities for periodic motion.

The LP problem was tested on many different cases, and the solution always resulted in only a change in the in-track velocity to meet the periodicity constraint. The radial velocity remained unchanged from the (potentially random) initial value that was provided to the problem. This suggests the following simple alternative solution.

Velocity Constraint

The final formulation simply imposes the constraint that the radial velocity not change from the initial value provided. Thus $x_*(\theta_d)$, $y_*(\theta_d)$, $x'_*(\theta_d)$ must be the values provided previously and only $y'_*(\theta_d)$ can be changed by the initialization process. The periodicity constraint in Equation 2.30 then provides the fourth constraint

$$\begin{bmatrix} x_*(\theta_d) \\ y_*(\theta_d) \\ x'_*(\theta_d) \\ 0 \end{bmatrix} = \begin{bmatrix} r_1 \\ r_2 \\ r_3 \\ (\frac{2+e}{1+e} r_{30} - r_{40}) \end{bmatrix} \quad B \equiv \tilde{R}\, B$$

In this case the constants of integration in the problem are given by

$$B = \tilde{R}^{-1} \begin{bmatrix} x_*(\theta_d) \\ y_*(\theta_d) \\ x'_*(\theta_d) \\ 0 \end{bmatrix}$$

which then completely defines the initialization process for any value of θ.

Examples

Sample initializations and resulting trajectories are presented in Figs. 2-3 and 2-4. The initializations were determined for $\theta_d = 5°$ and $\theta_d = 45°$. The $\circ$ represents the given initial position. Using the initial conditions determined by the LP initialization approach, the trajectory was propagated for four orbits using FreeFlyer™ nonlinear orbit propagation software [34]. Note that there was no noticeable drift in either

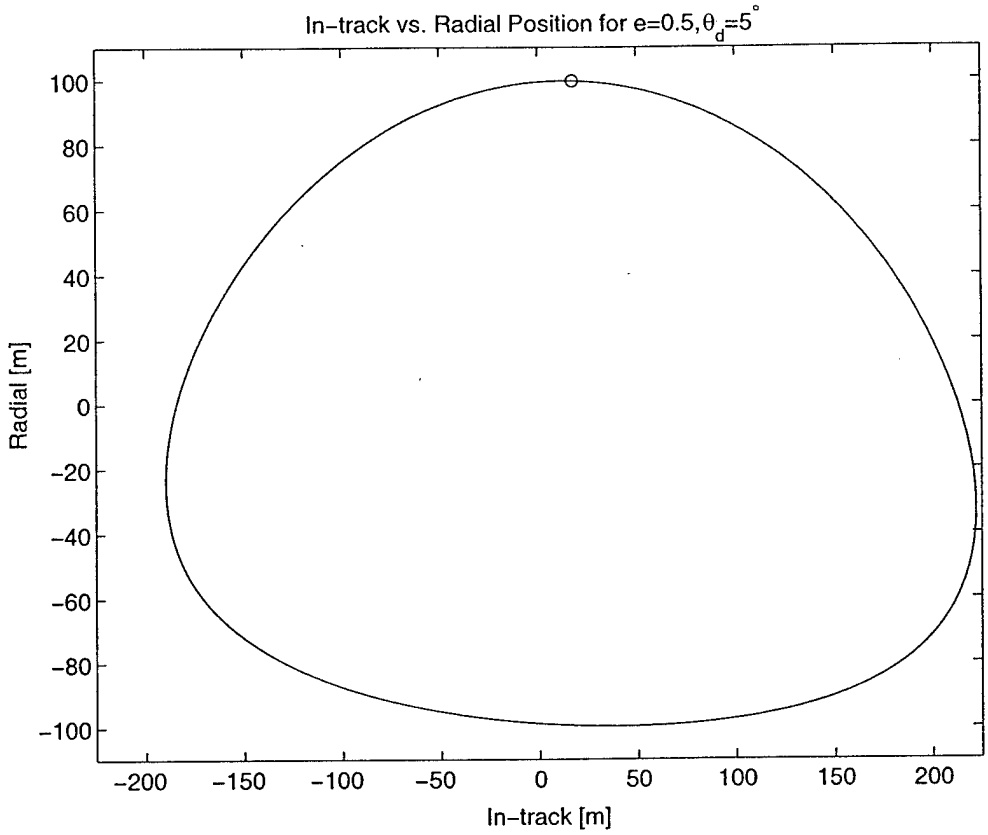

Figure 2-3: Trajectory followed for 4 orbits using initialization at $\theta_d = 5°$. The o represents the initial constrained position. The periodic motion is now shifted off center and is not an ellipse.

example. As is clearly shown for the case initialized at $\theta_d = 45°$, the periodic motion is no longer centered about the reference orbit $(0, 0)$.

The appropriate method for determining the desired relative state for passive apertures involves using the time-varying relative dynamics for eccentric orbits first presented by Lawden [12] and applied to passive formation initialization in References [18, 19]. The small correction for eccentricity is critical in determining the desired state to maintain periodic motion. It is clear from the figure that the desired state changes with time as the spacecraft formation orbits around the earth. Details of passive aperture initialization and desired state propagation for elliptical orbits are in References [19, 21].

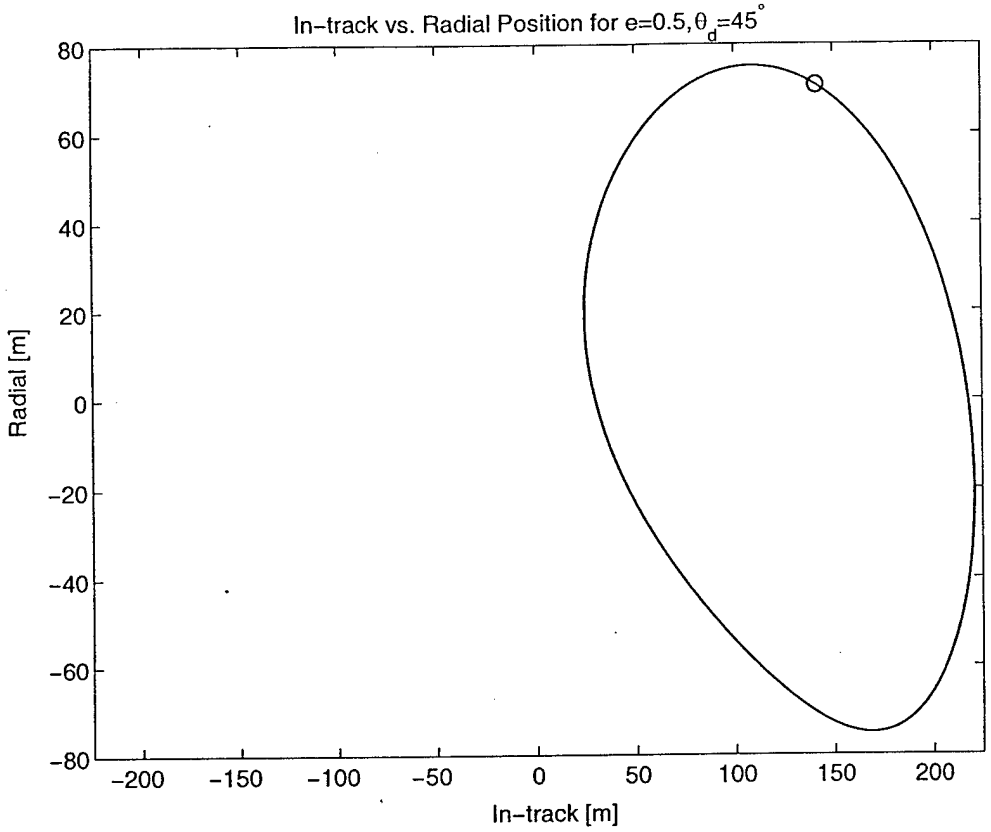

Figure 2-4: Trajectory followed for 4 orbits using initialization at $\theta_d = 45°$. The o represents the initial constrained position. The periodic motion is clearly not centered about the origin.

2.3 Discrete Dynamics

The linear time-varying dynamics in Section 2.1 can be compactly written in the form

$$\dot{x}(t) = A(t)x(t) + B(t)u(t) + B_d(t)w(t) \tag{2.34}$$

where the inputs are now divided into control inputs u and disturbance inputs w. The dynamics can then be discretized using the sampling period, T_s. With the inclusion of the desired output and the direct transition matrices, the discrete relative dynamics

take the following form [35] ($t = kT_s$)

$$\begin{aligned} x(k+1) &= \Phi_k x(k) + \Gamma_k u(k) + M_k w(k) \\ y(k) &= H_k x(k) + J_k u(k) + P_k w(k) \end{aligned} \tag{2.35}$$

where $x(k) \in R^n$ are the states, $u(k) \in R^m$ are control inputs, and $w(k) \in R^p$ are the disturbances acting on the system. The vector $y(k) \in R^l$ are the measured outputs or the variables of interest to the control design. The output $y(k)$ can be calculated using discrete convolution of the form (for $k \geq 1$)

$$\begin{aligned} y(k) &= H_k \Phi^{(k,k)} x(0) + [J_k u(k) + P_k w(k)] \\ &+ \sum_{i=0}^{k-1} H_k \Phi^{(k-i-1,k)} [\Gamma_i u(i) + M_i w(i)] \end{aligned} \tag{2.36}$$

where $\Phi^{(j,k)}$ corresponds to

$$\Phi^{(j,k)} = \begin{cases} \Phi_{(k-1)} \cdots \Phi_{(k-j+1)} \Phi_{(k-j)} & 2 \leq j \leq k \\ \Phi_{(k-1)} & j = 1 \\ I & j = 0 \end{cases}$$

If the formation follows a circular reference orbit, then the dynamics are time-invariant and the system matrices $(\Phi_k, \Gamma_k, H_k, J_k, M_k, P_k)$ will be independent of time and $\Phi^{(k-i-1,k)}$ simply corresponds to Φ^{k-i-1}.

Equation 2.36 can be manipulated into the following simple matrix notation, resulting in a linear matrix equation in U

$$y(k) = A(k) U_k + b(k) \tag{2.37}$$

where the matrix $A(k)$ and vector $b(k)$ correspond to

$$A(k) = \begin{bmatrix} H_k \Phi^{(k-1,k)} \Gamma_0, \cdots, H_k \Phi^{(0,k)} \Gamma_{k-1} & J_k \end{bmatrix} \tag{2.38}$$

$$b(k) = \left[H_k\Phi^{(k-1,k)}M_0, \cdots, H_k\Phi^{(0,k)}M_{k-1}, \; P_k \right] \begin{bmatrix} w(0) \\ w(1) \\ \vdots \\ w(k) \end{bmatrix} + H_k\Phi^{(k,k)}x(0) \quad (2.39)$$

and $H_k\Phi^{(k-1,k)}\Gamma_0$ is the pulse response of the system which maps the inputs

$$U_k = [\; u(0)^T \; u(1)^T \; \ldots \; \ldots \; u(k-1)^T \; u(k)^T \;]^T \quad (2.40)$$

to the output observed at the k^{th} step.

This plant description, Equation 2.37, is the basis of the trajectory and control algorithm design using linear programming. Note that for use with the eccentric orbit dynamics, the index k actually corresponds to steps in the true anomaly. The solution, using the theta-varying dynamics for eccentric orbits, is a function of k steps in the true anomaly which is converted back to the time domain for implementation in the real-time controller. The conversion from true anomaly to time is straight forward using the relation between true anomaly and eccentric anomaly

$$\tan\frac{E}{2} = \left[\frac{1-e}{1+e}\right]^{1/2} \tan\frac{\theta}{2} \quad (2.41)$$

and then using Kepler's Equation to solve for the time

$$n(t-\tau) = E - e\sin\; E \quad (2.42)$$

The only additional required information is the time of perigee passage τ.

2.4 Chapter Summary

This chapter derives the relative dynamics for the motion of one spacecraft relative to a reference orbit. Three forms of linearized dynamics are presented, each capable of modeling different properties of the relative motion. The closed-form solutions are

also presented for each of the form of dynamics. The closed-form solutions are used to calculate the required state for a passive aperture. The relative dynamics provided are necessary for determining the desired state and describing the relative motion of the spacecraft in the formation flying control problem. The discretization process is presented which transforms the continuous dynamics to the discrete form used in the linear programming formulation in the following chapter.

Chapter 3

Formation Flying Coordination and Control Algorithms

The passive aperture designs discussed in Section 2.2 provide a fleet formation that takes advantage of the natural dynamics to keep the spacecraft together in the absence of disturbances. The spacecraft will require a control scheme to achieve these passive apertures and once the aperture has been formed, disturbances such as differential drag will cause the aperture to disperse without including some method of control. This thesis develops a control algorithm using linear programming (LP) to solve for the fuel optimal control inputs and trajectories over a fixed time interval. An LP formulation is presented for 1) the terminal constraint problem required for formation initialization and reconfiguration maneuvers and 2) the formation-keeping problem to maintain the passive aperture over extended time periods. The control algorithm is capable of using any of the three forms of relative dynamics presented in Section 2.1. The chapter also discusses the coordination aspects of each of these problems and presents a method of distributing the algorithm to reduce computational load.

3.1 Trajectory and Control Generation

This section presents the formulation of the basic trajectory planning problem as an LP optimization [36, 37]. There are two primary trajectory design problems of

interest for formation flying spacecraft:

1. Formation initialization or reconfiguration control problem; and
2. Formation-keeping control problem.

The formation initialization or reconfiguration control problem is a terminal constraint problem. The general problem is to determine the control inputs and trajectories to maneuver the N vehicles in the fleet to the desired relative positions with the desired relative velocities after n time-steps, while minimizing a weighted sum ($c_j \geq 0$) of the $\|\cdot\|_1$ norm of the control inputs by each spacecraft. The objective statement for a single spacecraft is

$$\min_{U_n} \sum_{j=1}^{m} c_j \|u_j\|_1 \quad \text{subject to} \quad y(n) = y_{\text{des}}(n) \tag{3.1}$$

where $u_j = [\ u_j(0)\ u_j(1)\ \ldots\ u_j(n)\ ]^T$ is the fuel used by the j^{th} thruster on the spacecraft. Equation 3.1 is the cost function used to design trajectories for a single spacecraft. The control and trajectory design could be performed simultaneously for the entire fleet by extending the cost in Equation 3.1 to include all control inputs for all spacecraft and including terminal constraints for each vehicle. In order to perform a fleet level maneuver, the final state must be specified for each spacecraft. Section 3.2 discusses a method of coordinating and optimizing the selection of these final states.

The terminal constraint problem determines control inputs to reach the final desired state; however, differential disturbances such as J_2 or drag will cause the spacecraft to drift from the desired state. Formation-keeping is required to maintain the desired state in the presence of disturbances. The objective of the formation-keeping control problem is to use the minimum control effort necessary to maintain the vehicle to within some tolerance of a specified desired set of coordinates at each time-step k. The performance specification is represented by a "slab"

$$|y_j(k) - y_{j_{\text{des}}}(k)| \leq \epsilon_j, \quad \epsilon_j \geq 0 \ \Rightarrow\ -\epsilon_j \leq y_j(k) - y_{j_{\text{des}}}(k) \leq \epsilon_j \qquad \forall\ j = 1, \ldots, l \tag{3.2}$$

where ϵ_j is the error bound associated with each coordinate y_j. For example, these bounds are specified by an error box, *e.g.*, separation of ± 10 m in-track, ± 5 m radial, and ± 10 m cross-track. Formation-keeping under differential disturbances is achieved by placing constraints on the position of the spacecraft relative to the desired coordinates, which corresponds to the center of the error box. Note that the center of each error box is referenced to the formation center, which could be a reference orbit or another spacecraft.

In Equation 3.1, $y_{\text{des}}(n)$ can represent the states $x(n)$ directly or any affine relationship between the states, such as the constraint $S(n)y_{\text{des}}(n) \leq T(n)$. This more general form can be used to place constraints on only part of the system state. For example, one important problem [19] is to control a group of spacecraft so that they have the same energy level, which tends to reduce the rate that they will drift apart. This type of energy constraint can be written as

$$\dot{y}_j + 2n_0 x_j = c, \quad \forall\ j \ \text{ spacecraft}$$

where c is an arbitrary, but common, constant. Note that this process does not specify any fixed values for the relative states such as radial position, x_j or in-track velocity, $\dot{y}_j$.

3.1.1 Additional Constraints

Equation 3.1 is the basic form of the general formation control problem, but other constraints must be included to address the following issues:

1. The formation-keeping requires that the state variables (coordinates) be constrained at each time-step to ensure that the vehicles stay with a specified tolerance of the desired location.
2. The thrust levels of each actuator on each spacecraft typically have unique bounds that must be correctly addressed in the optimization to obtain precise formation flying.
3. For spacecraft utilizing micro-propulsion, large maneuvers require long periods

of thruster firings and an impulsive ΔV assumption does not hold for these transfers.

4. Some actuation methods have a very slow slew rate (such as drag panels), and this must be accounted for in the control design.

This section demonstrates how to include these constraints and presents solutions to several other problems typically encountered in formation coordination and control.

The different aspects observed in these examples can be structured into a standard format that can easily be included in the basic optimization problem given previously:

- **State-Space Constraints**

  State-space constraints are used in the formation-keeping control problem to constrain the position of the spacecraft to remain within a desired tolerance of a specified state. State-space constraints could also be used to place limits on the maximum relative velocity obtained by the spacecraft. State-space constraints are described via

$$S(k)y(k) \leq T(k) \quad \forall\, k \in \{0, 1, \ldots, n\} \tag{3.3}$$

  which can be written as a function of the control input sequence using Equation 2.37

$$[S(k)A(k)]U(k) \leq [T(k) - S(k)b(k)] \quad \forall\, k \in \{0, 1, \ldots, n\} \tag{3.4}$$

$$\text{or in general} \quad \bar{S}\, U_n \leq \bar{T} \tag{3.5}$$

- **Control Input Saturation**

  Control input saturation constraints are imposed to restrict designed control inputs to be within the limits of the actuators on the spacecraft. Control input saturation constraints are described through the following

$$u_j^{\min}(i) \leq u_j(i) \leq u_j^{\max}(i) \tag{3.6}$$

which can be written in a compact form for n steps using the previous definition of U_n

$$\begin{bmatrix} I \\ -I \end{bmatrix} U_n \leq \begin{bmatrix} U_n^{\max} \\ -U_n^{\min} \end{bmatrix} \tag{3.7}$$

Note that typically $u^{\min} = -u^{\max}$. A minimum impulse bit constraint may also be required. This constraint cannot be included in an LP formulation because the constraint would make the problem non-convex. Section 4.6 discusses a method to include this type of constraint using a binary switch variable and mixed integer linear programming.

- **Actuator Rate Limits**

  Actuator rate limits are described as

$$r_j^{\min}(i) \leq u_j(i+1) - u_j(i) \leq r_j^{\max}(i) \tag{3.8}$$

and can be expressed in the compact form

$$\begin{bmatrix} \nu_n \\ -\nu_n \end{bmatrix} U_n \leq \begin{bmatrix} R_n^{\max} \\ -R_n^{\min} \end{bmatrix} \tag{3.9}$$

where

$$\nu_n = \begin{bmatrix} -1 & \dots & 1 & \dots & \dots & \dots \\ & -1 & \dots & 1 & & \\ & & \ddots & & \ddots & \\ \dots & \dots & \dots & -1 & \dots & 1 \end{bmatrix} \tag{3.10}$$

The inequality constraints involving the control input set U_n can be combined with state-space constraints to form the inequality

$$\begin{bmatrix} I \\ -I \\ \nu_n \\ -\nu_n \\ \bar{S} \end{bmatrix} U_n \leq \begin{bmatrix} U_n^{\max} \\ -U_n^{\min} \\ R_n^{\max} \\ -R_n^{\min} \\ \bar{T} \end{bmatrix} \quad \text{or} \quad \Gamma_n U_n \leq \beta_n \tag{3.11}$$

With the addition of these constraints, the formation initialization control problem in Equation 3.1 can be written as

$$J_{\text{sp}}^{\star} = \min_{U_n} \sum_{j=1}^{m} c_j \|u_j\|_1 \tag{3.12}$$

$$\text{subject to} \quad \begin{cases} A(n)U_n = y_{\text{des}}(n) - b(n) \\ \Gamma_n U_n \leq \beta_n \end{cases} \tag{3.13}$$

3.1.2 Linear Program Formulation

To rewrite the formation control problem as a linear program, two slack variables are introduced that define the positive and negative parts of the control [36, 37] input

$$U_n = U_n^+ - U_n^-, \quad U_n^+ \geq 0, \; U_n^- \geq 0 \tag{3.14}$$

Using c_{ij} as the weight for the input from the j^{th} actuator at the i^{th} time-step, define $C^T = [c_{00}\ c_{01}\ \ldots\ c_{nm}\ c_{00}\ c_{01}\ \ldots\ c_{nm}]$ as the weights (typically all set to 1) on each of the positive and negative parts of the control inputs. Also define the control input vector as

$$\hat{U}_n = \begin{bmatrix} U_n^+ \\ U_n^- \end{bmatrix} \tag{3.15}$$

The formation initialization and reconfiguration problem can then be rewritten as

the standard linear program

$$
\begin{aligned}
& J^* = \min_{\hat{U}_n} C^T \hat{U}_n \\
\text{subject to} \quad & \begin{cases} \begin{bmatrix} A(n) & -A(n) \end{bmatrix} \hat{U}_n = y_{\text{des}}(n) - b(n) \\ \begin{bmatrix} \Gamma_n & -\Gamma_n \\ -I & 0 \\ 0 & -I \end{bmatrix} \hat{U}_n \leq \begin{bmatrix} \beta_n \\ 0 \\ 0 \end{bmatrix} \end{cases}
\end{aligned} \tag{3.16}
$$

As given in the structure of the problem, the information necessary to complete the coordination problem are the initial states x_0, the desired goal $y(n)$, and the system limitations embedded in the inequality constraints.

The formation-keeping control problem is formulated by replacing the terminal equality constraint with inequality constraints at each time-step k to constrain the state to be within some tolerance, y_{tol}

$$
\begin{aligned}
& J^* = \min_{\hat{U}_n} C^T \hat{U}_n \\
\text{subject to} \quad & \begin{cases} \begin{bmatrix} A(k) & -A(k) \\ -A(k) & A(k) \end{bmatrix} \hat{U}_k \leq \begin{bmatrix} y_{\text{des}}(k) - b(k) + y_{\text{tol}} \\ -y_{\text{des}}(k) + b(k) + y_{\text{tol}} \end{bmatrix} \\ \begin{bmatrix} \Gamma_n & -\Gamma_n \\ -I & 0 \\ 0 & -I \end{bmatrix} \hat{U}_n \leq \begin{bmatrix} \beta_n \\ 0 \\ 0 \end{bmatrix} \end{cases}
\end{aligned} \tag{3.17}
$$

The equality terminal constraint given in Equation 3.16 can also readily be replaced with an inequality constraint of this form with $k = n$.

Remark 1 It can easily be shown that the LP cost in Equation 3.16 is equivalent to the $\|\cdot\|_1$ in Equation 3.12. For example, given an optimal command $u_k^\star$ at the k^{th} time-step, the LP problem essentially solves the following optimization

$$
\min_{u_k^+, u_k^-} u_k^+ + u_k^-, \quad \text{subject to} \quad u_k^+ - u_k^- = u_k^\star \,, \quad u_k^+ \geq 0 \,; \quad u_k^- \geq 0 \tag{3.18}
$$

The optimal answer to this problem is (i) $u_k^+ = u_k^\star$, $u_k^- = 0$ if $u_k^\star \geq 0$ or (ii) $u_k^+ = 0$, $u_k^- = -u_k^\star$ if $u_k^\star < 0$. Thus the cost function $u_k^+ + u_k^-$ is equivalent to $|u_k^\star|$, as specified in the standard optimization in Equation 3.12. Of course, the LP optimization actually solves for u_k^+, u_k^- not $u_k^\star$. □

The LP in Equations 3.16 and 3.17 can be solved very efficiently using many free and commercially available optimization programs [38, 39, 40]. The convexity of the LP problem essentially means that, if a solution exists, the solution result will be the global optimum. Thus, under these given dynamics, constraints, and cost assumptions, no other coordination or control method will outperform the LP solution. Another benefit of the LP approach is that the solution time increases slowly as the number of variables grows, which is true for all convex optimization problems.

In a typical implementation of the formation-keeping algorithm, each spacecraft is constrained to remain close (specified by the error box) to a desired location in the formation. When the vehicle reaches the edge of the error box, the LP approach is used to design a trajectory that moves the spacecraft to a final position (*e.g.*, near the center or the far end of the box) while remaining within the error box and using a minimum amount of fuel. The terminal constraint is specified as in Equation 3.16, while the constraints for remaining inside the box are specified as in Equation 3.17.

Figure 3-1 shows a trajectory that moves the spacecraft to within 1 m of the center of the error box at the end of four orbits. Note that the vehicle begins near the center and drifts to the right under the differential drag. Figure 3-2 shows the control inputs used to generate the trajectory. Only inputs in the in-track direction were required to complete the maneuver, and all inputs occur at the beginning of the maneuver. Disturbances such as differential drag and differential J_2 can be included as additional inputs to the system dynamics as in Equation 2.37. With these inputs, the LP approach can be used to generate fuel optimal trajectories for long-term formation-keeping that account for these disturbances. Differential drag can be modeled as a constant or sinusoidal input for each spacecraft, and its effect will depend on whether the vehicle's drag is more or less than the average drag of the entire fleet (*i.e.*, the vehicle will tend to drift ahead or lag behind). The differential drag in this LP is

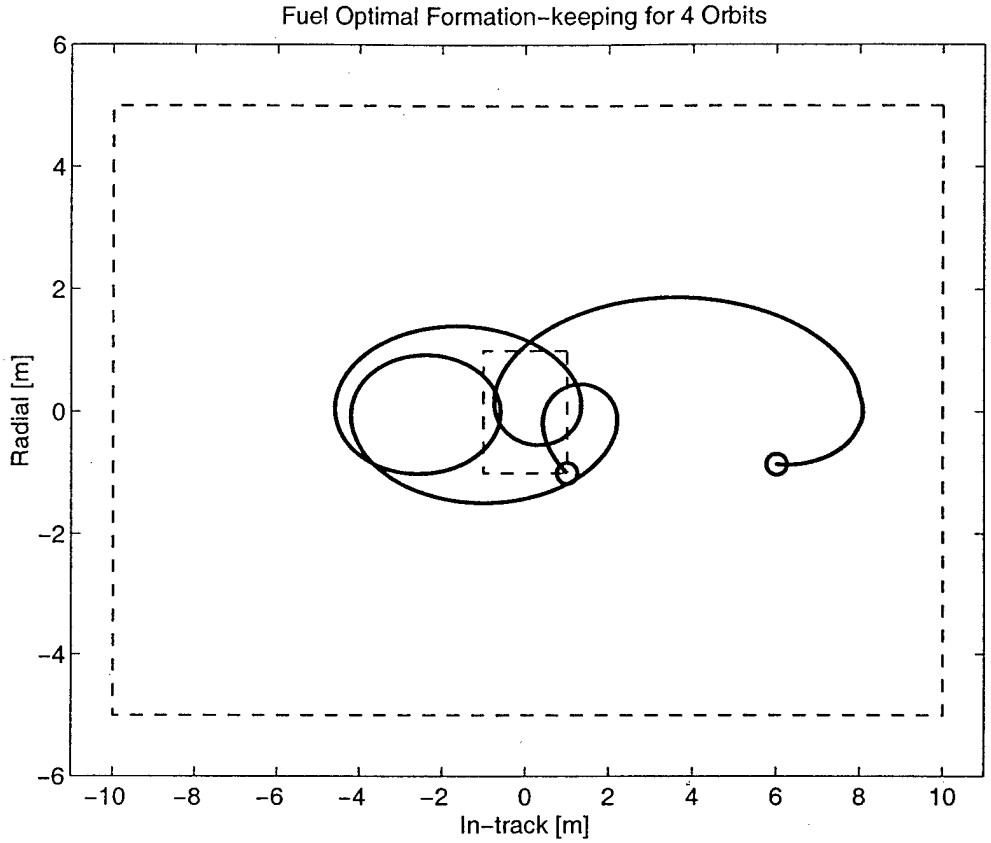

Fig. 3-1: Resulting trajectory for the minimum fuel solution to a four orbit horizon formation-keeping LP.

modeled as a constant $\pm 0.5 \times 10^{-7}$ m/s^2 acceleration. This acceleration depends on the difference between the drag coefficient for each spacecraft and the average drag coefficient for the fleet.

3.2 Coordination

This section addresses coordination between spacecraft in the fleet. Coordination provides benefits in terms of reducing computational load and control effort. A method for solving the formation initialization or reconfiguration is presented that allows the computational effort to be distributed across the fleet. This is an example of using coordination to ease computational load. A coordinated method of specifying the passive aperture is also presented for the formation-keeping control. This coordination

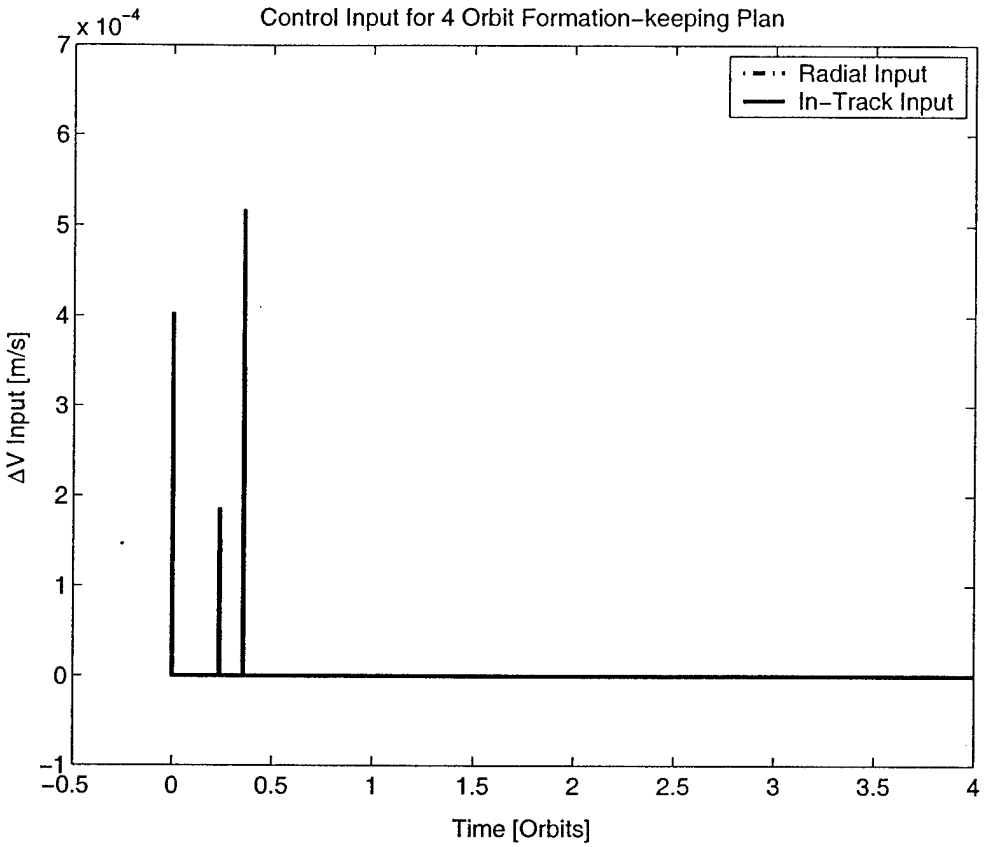

Fig. 3-2: Control inputs for trajectory in Figure 3-1. No radial inputs were required.

reduces sensitivity of the control to errors of any particular spacecraft.

3.2.1 Formation Initialization and Reconfiguration

With a large number of vehicles, the computational aspects of the fleet trajectory planning are complicated by the large information flow and the amount of processing required. This computational load can be balanced by distributing the effort over the fleet using a bidding process [41, 42]. For example, in a typical formation flying scenario [2, 8], the vehicles will be arranged as part of a *passive aperture*. These apertures provide relatively stable configurations that do not require as much fuel to perform the science observations. But changing the viewing mode of the fleet could require that the formation change configuration, moving from one aperture to another. In this case it is essential to find fuel- and time-efficient ways to move each

spacecraft to their locations in the new aperture, which is a challenging optimization problem with many possible final configurations.

The following describes a distributed solution to this problem, which builds on the results of References [41, 42]. The approach partially alleviates the computational difficulties associated with solving the aperture optimization problem by distributing the effort over the entire fleet, and then using a coordinator to recombine the results. In this approach, the vehicles analyze the possible final locations in a discrete set of global configurations and associate a cost with each. The linear programming tools in Section 3.1.2 are used to compute the fuel costs (and trajectories) to move each spacecraft from their current location to each possible final location. These simple calculations can be done in parallel by each spacecraft. The result is a list of predicted fuel costs for every possible final location (called a ΔV map), which are used to generate the fuel cost to move the fleet to each global configuration. These costs are based on fuel usage, but they could include other factors, such as the vehicle health.

Note that, in the placement of the formation around the passive aperture, the only requirement is that the vehicles be evenly spaced. Because the spacecraft are assumed to be identical, their ordering around the aperture is not important, so this corresponds to an assignment problem. In addition, the rotation of the entire formation around the aperture is not important. Each rotation angle of the formation around the ellipse corresponds to what is called a "global configuration." To consider only a discrete set of configurations, the aperture is typically discretized at 5° intervals. The ΔV maps are given to a centralized coordinator to perform the assignment process, which can be done in a number of ways.

To consider this assignment process in more detail, start by selecting one of the possible locations on the closed-form aperture, and then the $N-1$ equally spaced locations from that point. The N columns corresponding to these locations are then

extracted from the overall ΔV map to form the $N \times N$ matrix

$$F = \begin{bmatrix} f_{11} & f_{12} & \cdots & f_{1N} \\ f_{21} & f_{22} & \cdots & f_{2N} \\ \vdots & & \ddots & \\ f_{N1} & \cdots & \cdots & f_{NN} \end{bmatrix} = \begin{bmatrix} f_1 & f_2 & \cdots & f_N \end{bmatrix} \tag{3.19}$$

the elements (f_{ij}) of which are the fuel cost for the i^{th} spacecraft to relocate to the j^{th} position.

The following heuristic, which is based on the results of numerous examples, provides one way to solve the coordinator's assignment problem. The approach is to determine which position, on average, would require the most fuel to fill. This fuel cost is calculated by simply summing the ΔV's for each position. The location with the highest fuel total is then filled first by selecting the vehicle that requires the minimum amount of fuel to reach that position. The procedure is repeated until all positions are filled.

Algorithm: Initialize $I = \begin{bmatrix} 1 & \ldots & N \end{bmatrix}$ and $J = \begin{bmatrix} 1 & \ldots & N \end{bmatrix}$

Step 1: Find $j^\star = \arg\max_{j \in J} \sum_{i \in I} f_{ij}$

Step 2: Find $i^\star = \arg\min_{i \in I} f_{ij^\star}$

Step 3: Remove $i^\star$ from I and $j^\star$ from J: $I \rightarrow I \setminus \{i^\star\}$, $J \rightarrow J \setminus \{j^\star\}$

Step 4: Remove the $i^\star$ row and $j^\star$ column from F and return to step 1.

This heuristic algorithm is typically used to reduce the problem until only three vehicles (and three positions) remain. The six remaining scenarios can easily be examined to determine the best possible configuration. This heuristic algorithm can be computed very quickly, but it typically does not provide the optimal solution. However, experience has shown that it is very good at avoiding poor configurations, and thus provides a viable solution approach.

The coordinator's assignment problem can also be solved using integer programming (IP) techniques [43, 44, 45, 46]. Define the $N \times N$ matrix Y, the elements y_{ij} of which are binary and can be used to include logical conditions in the optimization.

For example, $y_{ij} = 1$ would correspond to the i^{th} spacecraft being located at the j^{th} position on the aperture (and $y_{ij} = 0$ would mean that it is not).

$$Y = \begin{bmatrix} y_{11} & y_{12} & \cdots & y_{1N} \\ y_{21} & y_{22} & \cdots & y_{2N} \\ \vdots & & \ddots & \\ y_{N1} & \cdots & \cdots & y_{NN} \end{bmatrix} = \begin{bmatrix} y_1 & y_2 & \cdots & y_N \end{bmatrix} \tag{3.20}$$

With the vectors

$$\tilde{F} = \begin{bmatrix} f_1^T & f_2^T & \cdots & f_N^T \end{bmatrix} \ , \ \tilde{Y} = \begin{bmatrix} y_1 \\ \vdots \\ y_N \end{bmatrix} \tag{3.21}$$

then the assignment problem for the coordinator can be written as

$$J^{\star}_{\text{coord}} = \min_{\tilde{Y}} \tilde{F}\tilde{Y} \tag{3.22}$$

$$\text{subject to} \quad \begin{cases} \sum_{i=1}^{N} y_{ij} = 1 \ , \quad \forall \ j = 1, \ldots, N \\ \sum_{j=1}^{N} y_{ij} = 1 \ , \quad \forall \ i = 1, \ldots, N \\ y_{ij} \in \{0, 1\} \quad \forall \ i, \ j \end{cases} \tag{3.23}$$

Note that $\tilde{F}\tilde{Y}$ calculates the fuel cost associated with each configuration, and the coordinator selects the configuration that minimizes the total fuel cost for the fleet. The two summation constraints ensure that each vehicle is given a location and that only one vehicle is placed at each location (an *exclusive or* condition) [43, 44, 45, 46]. The selection algorithm can be modified to include the initial fuel conditions of each vehicle by simply adding the initial fuel state to the corresponding row of the ΔV map. Fuel balancing across the fleet can be addressed by weighting each row of the ΔV map by a factor $\alpha_i = \Delta V_{i0}/\Delta V_{avg0}$, where ΔV_{i0} is the initial fuel used by the i^{th} spacecraft and ΔV_{avg0} is the average initial fuel used by the entire fleet. By design

$\alpha_i > 1$ for vehicles that have used more fuel than the average, which tends to penalize their additional fuel expenditures more heavily.

The formation coordinator approach was applied to a reconfiguration example with 8 vehicles. The vehicles start on one aperture (100 m semi-major axis) and recombine on a second one (200 m semi-major axis), see Figure 3-3. The maneuver also changes the orientation of the cross-track motion. The only hard constraint on the planning process is that the vehicles be placed with equal phasing on the new aperture. The cost maps for the spacecraft are based on their predicted fuel usage vs. aperture location, and are shown in Figure 3-4. The circles in the figure show which location each vehicle was given in the fleet-optimal configuration. As is evident from the figure, all of the spacecraft received solutions that are close to the locations that would minimize their predicted fuel cost (all spacecraft are within 4% of their minima, and four are within 2%). However, it is also clear that two of the vehicles (#1 and #5) are forced to expend more fuel than the others, and two others (#2 and #6) are forced to select locations that are much higher compared to their fuel-optimal choices (4% above). This is an example of a case where the team objectives and individual control objectives are in conflict, and sacrifices by some team members are required to obtain better overall performance.

For this example, the integer optimization takes approximately 1 second to solve using MATLAB™ code [47] on a Pentium III (500 MHz). The heuristic algorithm takes significantly less time ($\leq$ 0.1 seconds), and in this case, gave the same answer. Note that Reference [48] shows that the linear assignment problem can also be solved using linear programming with equality constraints, which in this example takes approximately 0.17 seconds. Figure 3-5 compares the fuel cost associated with the $(360/5)/8 = 9$ best configurations (there is an N-fold symmetry in the selection process). The ($\diamond$)'s show the costs associated with 800 other cases that were investigated for each configuration. These results show that some aperture configurations have a fuel cost that is 33% higher than the optimal one given above.

With the discretization of the target aperture, this process is not guaranteed to be globally optimal, but this hierarchical approach offers some key benefits in that it:

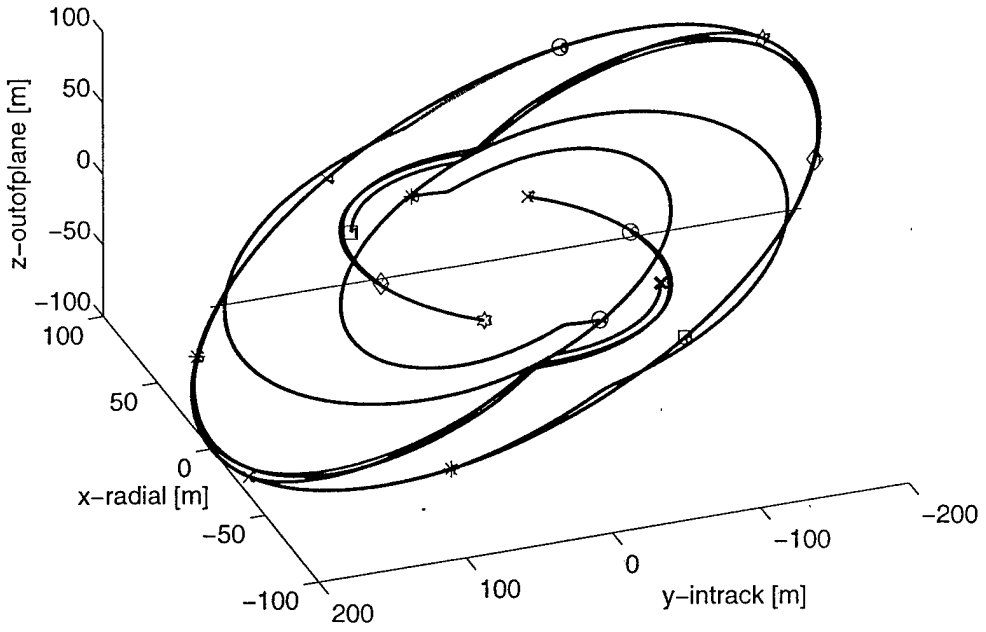

Figure 3-3: Hill's frame showing the optimized trajectories followed by the spacecraft to reconfigure the aperture.

1. Distributes the computational effort of the reconfiguration optimization since most calculations are done in parallel on much smaller-sized (LP and IP) problems;
2. Provides a simple method of finding optimized solutions that are consistent with the global constraints since the centralized coordinator determines the final solution; and
3. Allows the vehicles to include individual decision models (e.g., bidding highly for a maneuver that requires less reorientation if there is a reaction wheel failure).

While the heuristic approach is faster to compute on this simple example, the advantage of integer optimization approach to the coordination is that it enables the trajectory design and target aperture assignment to be combined into one centralized algorithm [45, 46]. This allows the coordinator to explicitly include additional constraints, such as collision avoidance and plume impingement, in the optimization. The technique has been demonstrated on small fleets (*e.g.* $N = 4$) [46].

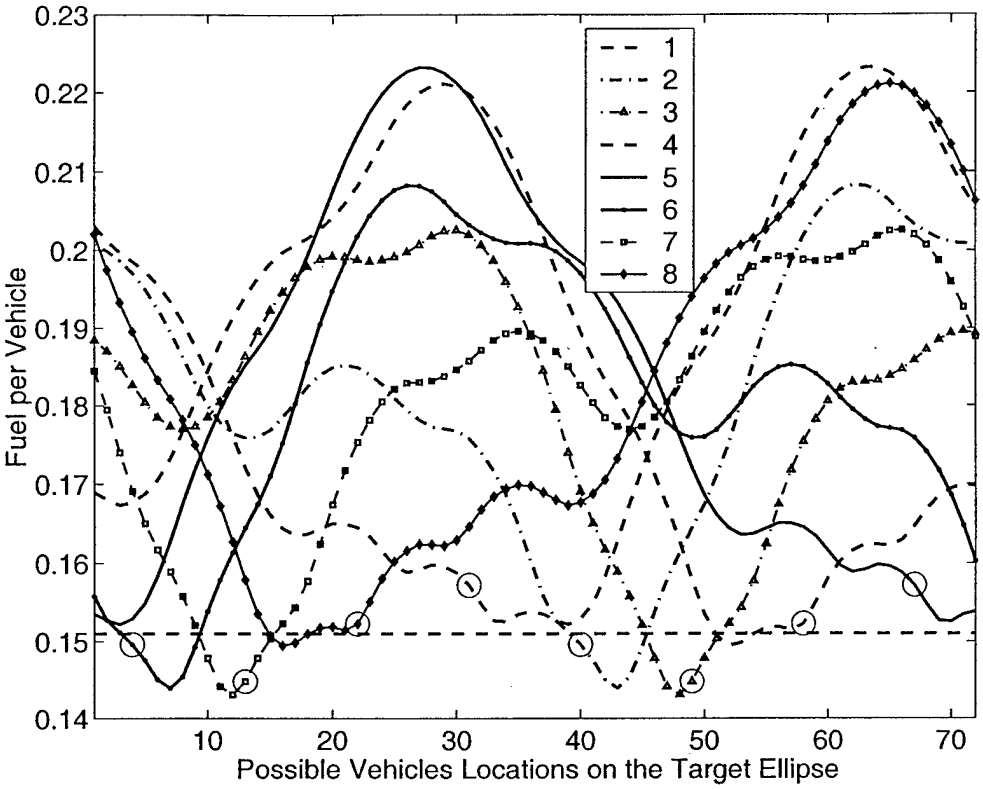

Figure 3-4: Associated predictions of the ΔV fuel cost to move to each location on the target aperture. Uses a 5° discretization of the target ellipse.

3.2.2 Formation-keeping

The formation-keeping LP algorithm in Section 3.1.2 is formulated to control a single spacecraft to maintain a desired state to within some tolerance specified by an error box centered on the desired state. Figure 3-6 shows the typical motion of a spacecraft relative to a reference point. The reference point is the • in the center. The error box is centered on the desired state represented by a ♦. The desired state moves around the aperture over time. The formation-keeping algorithm is applied independently to each spacecraft and thus can be completely distributed across the fleet. Each spacecraft determines the control sequence to maintain the desired state for that vehicle. As described, there is not much cooperation between the vehicles in the fleet. However, the cooperation and coordination for formation-keeping occurs in the specification of the desired state for each individual spacecraft. In particular, the

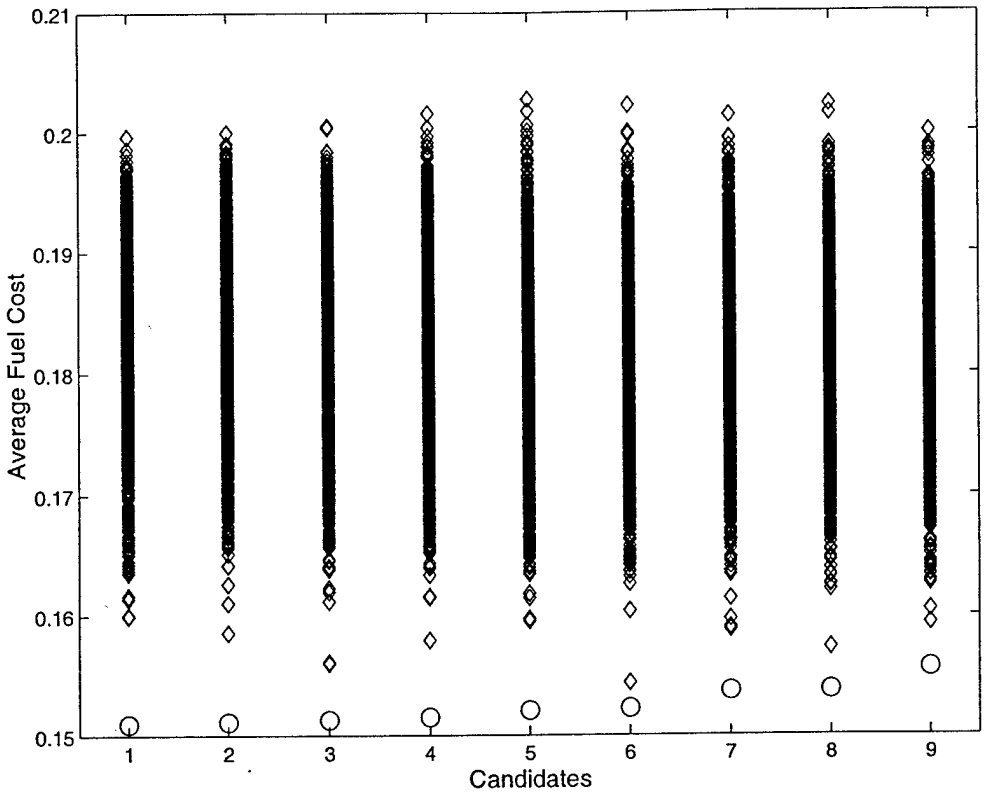

Figure 3-5: Comparison of the nine best alternative fleet configurations. The final design is #1. The ($\diamond$) symbols show 800 alternatives for each possible configuration.

desired state is specified relative to the reference point which can be chosen to enable cooperation within the fleet.

Figure 3-7 shows a basic description of a formation of three spacecraft. Clearly the desired state for a spacecraft changes as the vehicle moves around the aperture. The desired state can be described in terms of a "formation radius" for the aperture and a "formation angle" for the vehicle. The formation radius is a parameter to define the size of the aperture. The formation angle describes where the vehicle is located on the aperture. Based on the closed form solution in Equation 2.21 at $t = 0$, the formation angle is measured from maximum positive radial displacement. The initial conditions and the closed-form solutions to the relative dynamics are used with the drift free constraints to determine the desired state at some future time. This desired state is specified relative to the formation center which is determined relative to the

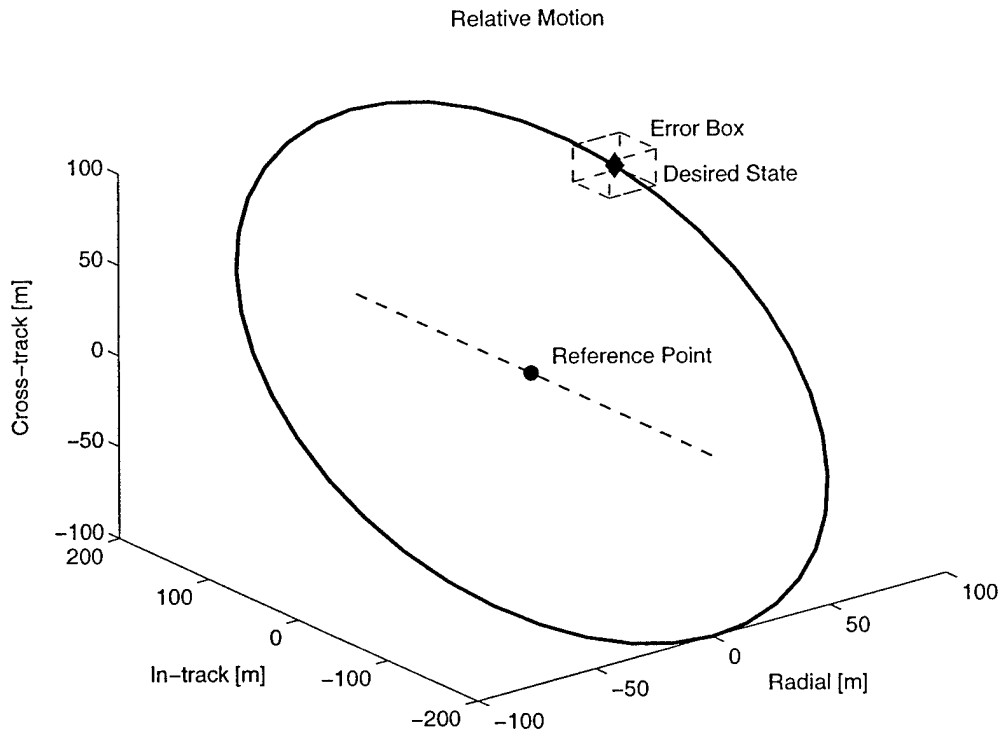

Figure 3-6: Motion of spacecraft relative to the reference point. The reference point is denoted with a •, and the current desired relative position with a ♦. An error box is centered on the desired state.

reference point for the formation. The reference point can be the formation center but this is not a requirement.

The reference point orbits the earth in a similar orbit to the spacecraft in the fleet. Three methods for determining the reference point are presented in this thesis. Each method is discussed in terms of the complexity of the method as well as the amount of information flow required to perform the calculation. The complexity of the calculation involves the mathematical calculation of the reference point state as well as any propagation of the state forward in time. The propagation will also require a detailed dynamics model that may need to be updated to match the fleet motion. The information flow is important in terms of communication bandwidth and any time delay issues in gathering and distributing information across the fleet. The information flow can include individual spacecraft states, dynamics model parameters, and the reference point state.

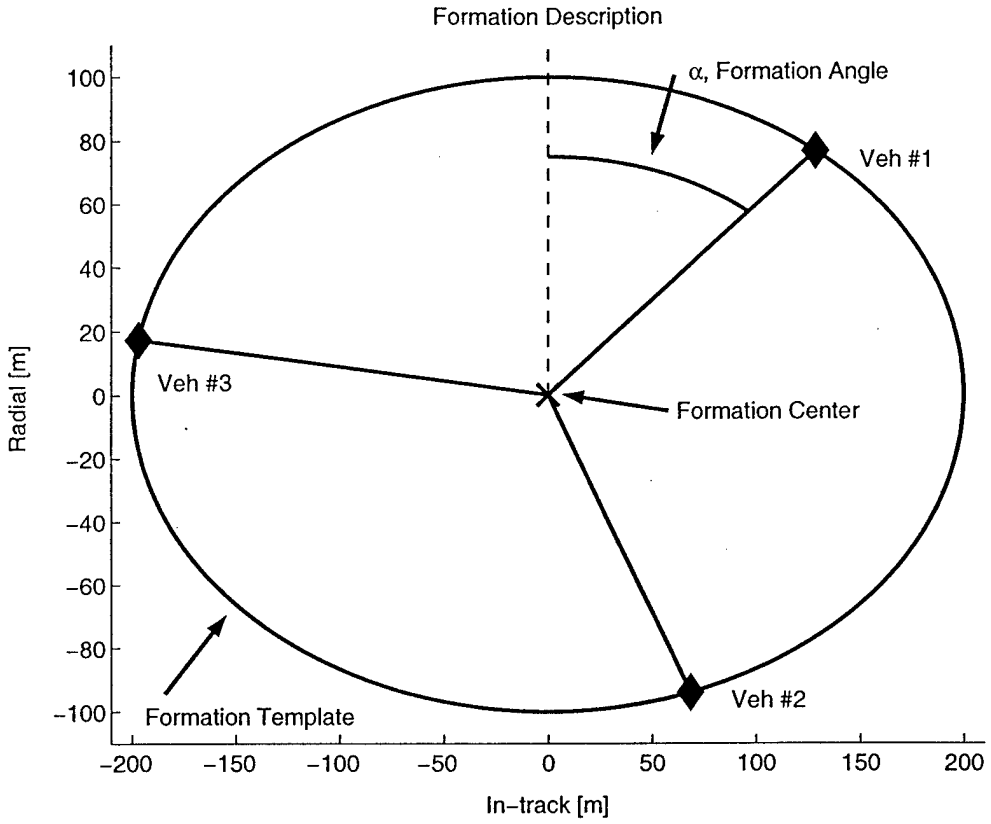

Figure 3-7: The formation geometry is described relative to the formation center, marked with a $\times$. Each vehicle state can be specified in terms of a formation radius and angle.

Reference Orbit

The most basic method of specifying the reference point is by a predetermined reference orbit. The reference orbit is a point in space that is propagated forward in time using a model that best describes the average fleet orbit. The formation center is attached to this reference orbit and used to specify the desired states for the vehicles in the fleet. Because the reference point is described by mathematical equations, little information flow from the vehicles in the fleet is required. For example, the reference state is calculated independent from the fleet state, therefore the individual state of the vehicles are not communicated across the fleet. Also, because the reference point is specified by equations and not through sensor measurements, there is no uncertainty in the state due to sensor noise. The major disadvantage to this approach is that the point does not experience the disturbances of the fleet. Instead a model

of the disturbances must be included in the propagation. If the disturbance model is inaccurate, the fleet will be tracking a reference orbit that does not naturally describe the motion of the fleet. Instead of using control effort to maintain the fleet, much of the control effort is wasted "chasing" a mathematical point in space that does not move with the fleet. The model used to propagate the reference orbit could be improved by using measurements of the fleet motion to alter parameters in the dynamics of the reference orbit; however, this will require a large increase in complexity and information flow and negates the major benefits of this method.

Leader-Follower

Another method of specifying the reference point is to declare one vehicle in the fleet to be the leader and fix the reference point to the leader spacecraft. The reference state is now the state of the leader spacecraft. The reference point acts as the origin for the reference frame in which the relative dynamics are described as well as the origin from which all measurements of the follower spacecraft relative states are made. The advantage of this method is that the reference point is represented by a spacecraft in the fleet. This eliminates the need for propagating the reference state. The absolute disturbance effects will also be captured by the leader spacecraft which means all fleet disturbances are relative to the disturbances experienced by the leader. The differential disturbances will require less control effort to maintain the fleet. The orbital elements for the relative dynamics equations can also be directly obtained from the orbital elements of the leader spacecraft. The leader-follower method also requires little information flow because the reference state is just the state of the leader spacecraft. The dynamics of the reference point are also determined from the leader spacecraft. The calculation of the desired state can be distributed to each vehicle in the fleet, the only information required is the desired state of the leader satellite and the orbital parameters required for the relative dynamics. The desired state of the leader spacecraft is used to determine the formation center which is then used to calculate the desired state for the individual vehicle.

The disadvantage of this method is that all follower spacecraft are forced to overcome any disturbances experienced by the leader vehicle but not by the followers.

The leader spacecraft will also never use any fuel because the state of the leader is always fixed to the origin and therefore never experiences any error. One possible solution to spread the control effort across the fleet is to alternate which spacecraft is the leader. There are two possible configurations for the leader spacecraft in the fleet. If the leader spacecraft is at the center of the aperture, the reference point is the formation center. Alternating leaders requires a formation maneuver between the previous leader and new leader, which is often more fuel intensive than formation-keeping. The transition period during this maneuver also presents problems in terms of describing the formation center during the transition between leaders because the leader spacecraft no longer occupies the formation center. The current control plans were also formulated using the previous leader and therefore are no longer applicable.

The second leader configuration is to make the leader spacecraft one of the vehicles on the same aperture as the followers rather than at the center of the aperture. The desired state for each follower spacecraft is just the desired state for the follower relative to the center of the aperture minus the desired state of the leader from the center of the aperture. In this configuration the transition between leaders is relatively simple. With the leader on the aperture, no formation maneuvers are required to transition leaders, but the instantaneous switch of leaders will cause a jump in the location of the desired state for each spacecraft. The discontinuity can lead to violations of the position tolerance and will require the LP controllers to be reset to correct for the change in desired state.

Virtual Center

A third approach is to use a "virtual center" as the reference point. In this method, there is not a physical spacecraft at the reference point, but the reference state is estimated based on measurements between the spacecraft in the fleet. Figure 3-8 shows an example formation of three spacecraft. The thick solid lines are known or measurable distances, the thin solid lines represent the true distances to the virtual center that are compared to the specified desired state relative to the virtual center (dashed lines).

In order to calculate the relative position and velocity of the center, a reference for

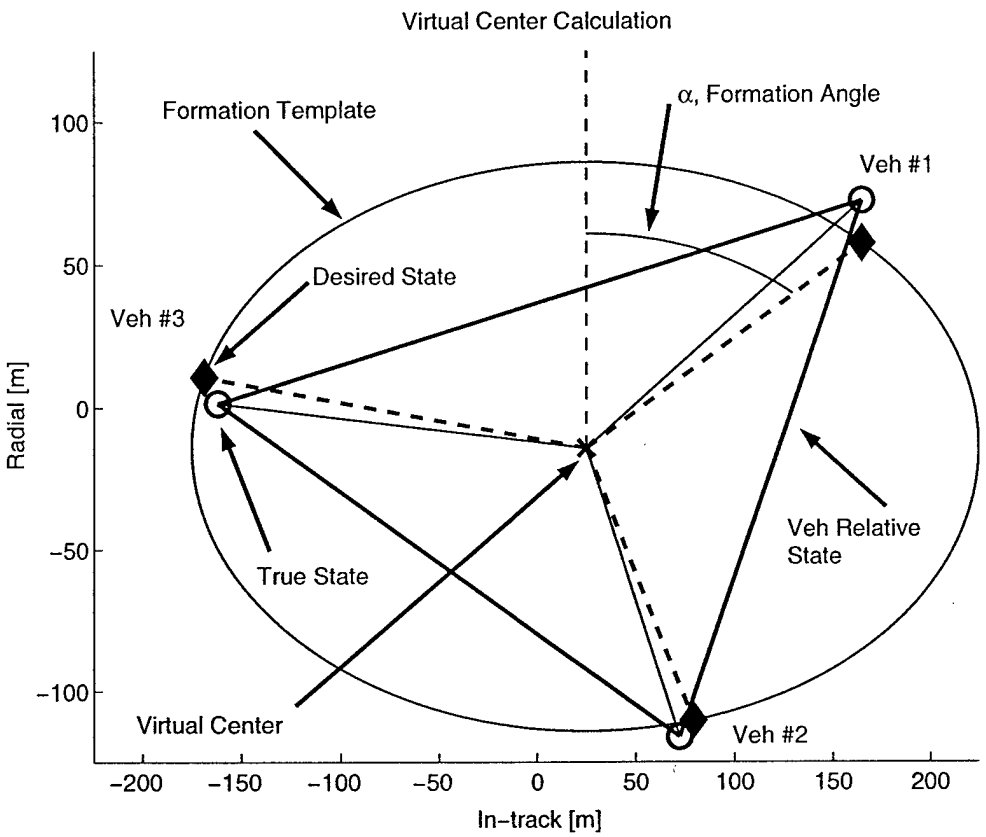

Figure 3-8: The virtual center can be calculated from the measured relative states (thick solid lines) and then used to determine the desired states (dashed lines) and actual state (thin solid lines) of each spacecraft relative to the center.

measurements must first be specified, typically taken to be one of the spacecraft in the fleet. In the figure, the reference frame is attached to spacecraft # 1, which will be referred to as the reference spacecraft. All inter-spacecraft states, $\vec{x}_{1i}$, are measured relative to the reference spacecraft, represented by the solid lines in Figure 3-8. The virtual center state, $\vec{x}_c$, is also specified relative to the reference spacecraft. The state of each spacecraft relative to the virtual center can then be written as

$$\vec{x}_{ci} = \vec{x}_{1i} - \vec{x}_c \tag{3.24}$$

The error states are then calculated as the difference between the state of each spacecraft relative to the center, x_{ci}, and the desired state for that spacecraft, which is

also specified relative to the center. The error states in the figure are the differences between the ♦ and ○ for each spacecraft.

$$\vec{x}_{ci} - \vec{x}_{i,des} = \vec{e}_i \tag{3.25}$$

Substituting Equation 3.24 for x_{ci} results in the following expression for the error of each vehicle in terms of known quantities and the unknown virtual center, $\vec{x}_c$,

$$\vec{x}_{1i} - \vec{x}_c - \vec{x}_{i,des} = \vec{e}_i \tag{3.26}$$

The error equation for each spacecraft can be grouped together as in the following

$$\begin{bmatrix} \vec{x}_{11} - \vec{x}_{1,des} \\ \vec{x}_{12} - \vec{x}_{2,des} \\ \vdots \\ \vec{x}_{1N} - \vec{x}_{N,des} \end{bmatrix} - \begin{bmatrix} I \\ I \\ \vdots \\ I \end{bmatrix} [\vec{x}_c] = \begin{bmatrix} \vec{e}_1 \\ \vec{e}_2 \\ \vdots \\ \vec{e}_N \end{bmatrix} = \vec{e} \tag{3.27}$$

$$\text{or } b - Ax = \vec{e}$$

The best virtual center will minimize the sum of the errors, specifically $\vec{x}_c$ is chosen to minimize $\|\vec{e}\|_2 = (b - Ax)^T(b - Ax)$. A weighting matrix, W, can also be included to increase the importance of a particular vehicle or state. The goal is now to minimize the weighted sum of the squares of the state errors. The center that minimizes $\|W\vec{e}\|_2$ is found by differentiating $(Wb - WAx)^T(Wb - WAx)$ which results in the following expression for $\vec{x}_c$

$$\hat{x}_c = \left(A^T W^T W A\right)^{-1} A^T W^T W b \tag{3.28}$$

The weighting matrix can be used several ways to adjust the cooperation amongst the vehicles in the fleet. One possible weighting matrix would be based on current fuel use. If one spacecraft has used more fuel than the rest of the fleet, the weight on the error for this vehicle can be increased. This results in the virtual center being chosen to reduce this particular error more than the others. The error of the spacecraft will be reduced through the calculation of the center rather than individual control effort.

Over time the weighting would equalize the fuel use across the fleet.

With the state of the virtual center determined, the reference point state is assigned the state of the virtual center. The state of the virtual center can either be updated at every time step using this method, or only periodically updated (once an orbit) with a propagation of the virtual state between updates. The propagation of the virtual state requires the determination of a weighted average of absolute disturbances experienced by the individual members of the fleet. A dynamics model estimator could be used to adjust the disturbance forces and orbital elements of the virtual center to match that of the weighted average motion of the fleet. Again the advantage of this method is that the disturbances effecting each spacecraft are now differential disturbances with respect to the fleet average instead of the absolute disturbance force, which will lower fuel costs. The disadvantage of this method is that the virtual center calculation must be centralized. Particularly, the current and desired states of all spacecraft in the fleet must be collected in one place to determine the virtual center. This requires an increase in information flow throughout the fleet. Also, the virtual center state is determined from several measurements that contain sensor noise as well as noise introduced through data transmission. This could lead to uncertainty in the virtual center state.

Because the virtual center is a function of the states of all the vehicles in the fleet, any control effort by one vehicle will have an effect on the other vehicles. Particularly, when one vehicle uses a control input to correct for an error, the control input is based on the virtual center being fixed over the plan horizon. However, as the vehicle moves back towards the desired state, the virtual center is changed to minimize other errors. The result is that the virtual center is effected by the individual control input which then effects the desired states of the other spacecraft. The movement of the virtual center due to control inputs of other vehicles is not directly accounted for in the LP.

One method of including these external control inputs while maintaining the distributed formation-keeping architecture is to include the control inputs as disturbance inputs, $w(k)$, in Equation 2.39. The control inputs would be scaled according to the same weighting that is used to calculate the virtual center. For example, with n

spacecraft, equally weighted, the control inputs contribution from one satellite on another is $u(k)/n$. Including the external control inputs requires that all vehicles "publish" a current list of planned control action. However, there is no guarantee that the published control action is entirely implemented, which could still lead to errors in the LP from modeling control inputs that were not actually implemented.

Another method of including the effect of external control inputs on the virtual center is to formulate one large LP to solve for the control inputs of all the vehicles at once. The state of the virtual center at each time step in the LP can be described in terms of the states of the vehicles in the fleet as in Equation 3.28, capturing the motion of the center due to all control inputs. This LP is obviously a centralized problem with a large number of variables and constraints that could lead to slow solution times and large memory requirements. The control input solutions and trajectories will also have to be sent back to the individual vehicles, increasing communication load.

Comparison

Figures 3-9 through 3-11 demonstrate the differences between the methods for specifying a formation center. A simulation was performed with three spacecraft initialized on a passive aperture. All three spacecraft experience the exact same drag disturbance. The vehicle states are propagated forward for eight orbits without any control action to correct the errors. The first example specifies the reference point with a reference orbit which experiences a drag that does not correctly match the fleet drag. Figure 3-9 shows the motion of the three spacecraft relative to the reference point which represents the formation center. The three spacecraft have similar errors and drift off the passive aperture. If control were applied, the control would have to overcome this drag effect.

The second case, shown in Figure 3-10 uses a coordinated reference point. This reference point would be either a leader spacecraft acting as the formation center with the same dynamic properties as the rest of the fleet or a virtual center with dynamic properties specified to match the weighted fleet average response. The motion relative to the reference point remains periodic as desired for the aperture.

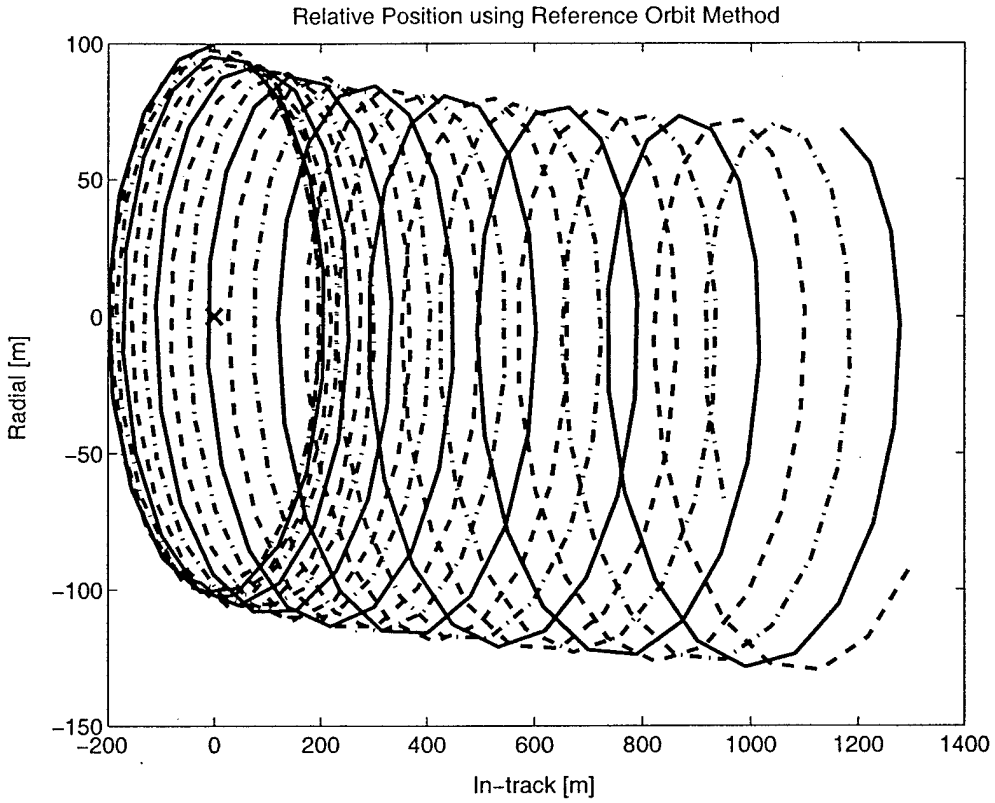

Figure 3-9: Relative motion with a reference point described by a reference orbit where the drag is modeled incorrectly. All the spacecraft drift from the aperture in the same direction due to a drag disturbance. The × marks the reference point which is also the formation center.

Figure 3-11 shows the motion using this second method as viewed from the reference orbit used in the first simulation. The virtual center, × , moves with the fleet, experiencing the same disturbance as the fleet. Normally the fleet would not experience equal disturbances. Differential disturbances such as differential J_2 would exist, resulting in some error in the passive aperture even though the reference point is coordinated with the fleet. However, these disturbances would only be relative to the fleet average and not a predetermined orbit that does not follow the natural fleet dynamics.

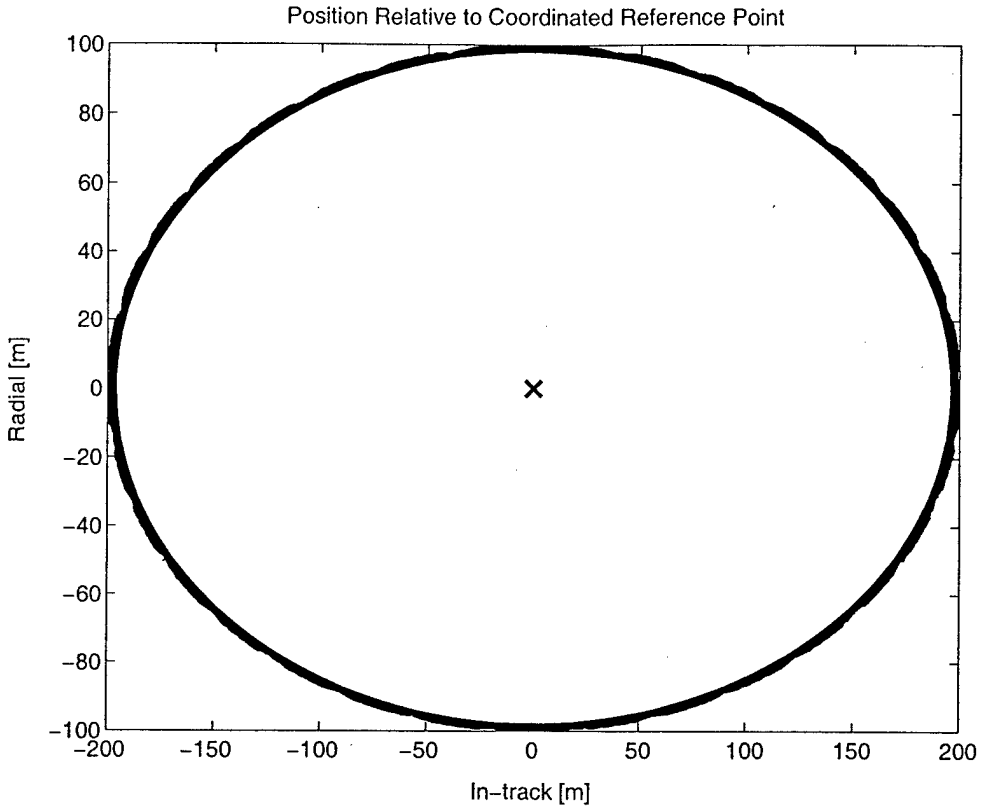

Figure 3-10: Relative motion with a reference point calculated using the virtual center method. The virtual center moves with the fleet resulting in no net disturbance force and the aperture is maintained. The $\times$ marks the center.

3.3 Chapter Summary

Chapter 3 presents the linear programming formulation for the spacecraft formation flying controller. A control algorithm for terminal constraint formation maneuvers and an algorithm for formation-keeping maneuvers are developed. The chapter also discusses the coordination algorithms for each type of maneuver. A distributed method of determining costs for each vehicle to perform the maneuver is combined with a centralized coordinator to solve the fleet initialization or reconfiguration maneuver control problem. The coordination for formation-keeping maneuvers is achieved through the specification of the reference point for the fleet and desired state for each vehicle. Three methods for determining the reference point are presented.

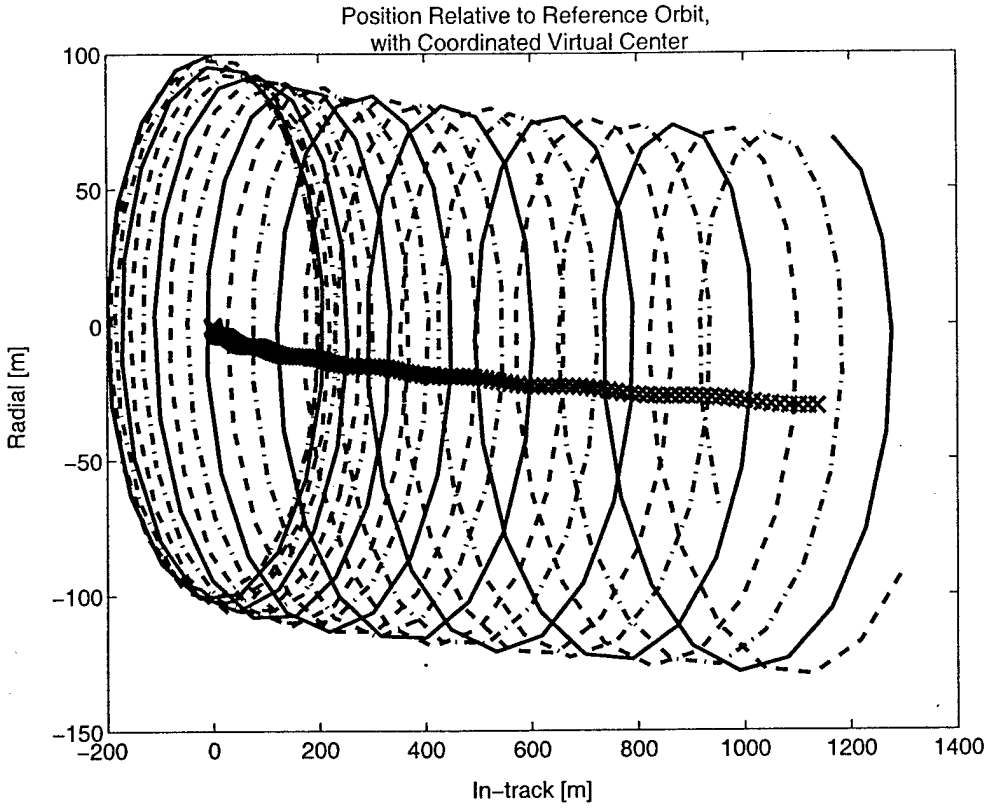

Figure 3-11: Relative motion with a coordinated reference point as viewed from the original reference orbit. All of the spacecraft experience equal drag and the center experiences the drag as well. The $\times$ marks the virtual center.

Chapter 4

Implementation Issues

The control algorithms presented in Chapter 3 provide the framework to calculate fuel optimal control inputs and trajectories for various maneuvers in spacecraft formation flying. However, there are several implementation issues that must be addressed in order to use the control algorithms in a spacecraft formation control architecture. These implementation issues include a method of initiating the LP control algorithm, robustness to initial condition uncertainty from sensor noise, LP solution feasibility, algorithm convergence times, and the selection of appropriate dynamics to use in the controller. This chapter discusses each of these issues and presents possible solutions.

Several nonlinear simulations are performed using FreeFlyer™ orbit simulation software [34] in order to demonstrate the effectiveness of the LP control method. FreeFlyer™ is used to propagate the absolute states of the vehicles in the formation in the Earth centered inertial (ECI) frame. The simulator allows the option of including or excluding disturbances such as drag, lift, solar radiation pressure, and J_2. The simulator software interfaces with MATLAB™, where the control calculations are performed. In MATLAB™, the spacecraft states are converted to the appropriate local reference frame for the relative dynamics being used in the LP controller. The LP controller then calculates the fuel optimal control inputs and trajectory for the desired maneuver. The control inputs, if required, are converted to small displacements and velocity changes using the time-varying dynamics. These relative state variables are transformed back to the ECI frame and are added to the absolute state vector of the

vehicle after the force-free propagation is performed by the FreeFlyer™ software. The result is a simulation with a linear controller in MATLAB™ with nonlinear dynamics for the spacecraft motion in FreeFlyer™.

4.1 Algorithm Initiation

The control algorithms presented in this thesis provide a method for determining the control inputs and resulting trajectories that minimize fuel cost subject to constraints over some time interval. Because the control inputs are not determined for every discrete step in time, a method for initiating the control algorithm is required. In formation reconfiguration maneuvers, the initiation is triggered by a desire to initialize a fleet on a passive aperture or reconfigure an aperture size or pointing direction. The initiation is coordinated between the fleet to ensure that each vehicle arrives at the final state at the prescribed time.

In formation-keeping maneuvers, the individual spacecraft determine control inputs to maintain a desired state over a period of time based on the error state for that particular spacecraft. Figure 3-6 shows the typical relative motion of a spacecraft around a passive aperture centered on a reference orbit. Because the control algorithms are distributed and independent of each other, there is no clear initiation procedure for each spacecraft. The formation-keeping control algorithm is designed to maintain a desired state, so a natural initiation method is to start the controller based on the spacecraft deviation from the desired state. An error box is introduced to provide a position tolerance and initiate the formation-keeping algorithm for each vehicle. The error box is centered on the current desired state for the vehicle and is also shown in Figure 3-6. Figure 4-1 shows an in-plane view of the error box. The deviation of the current position from the desired position (called the *error state*) is used to initiate the LP algorithm and determine the control inputs and trajectories to maintain the position tolerance throughout the plan horizon. At each time-step in the controller, the error position state is calculated and used to determine: 1) if control action is needed when a plan does not exist; 2) if the controller should continue to

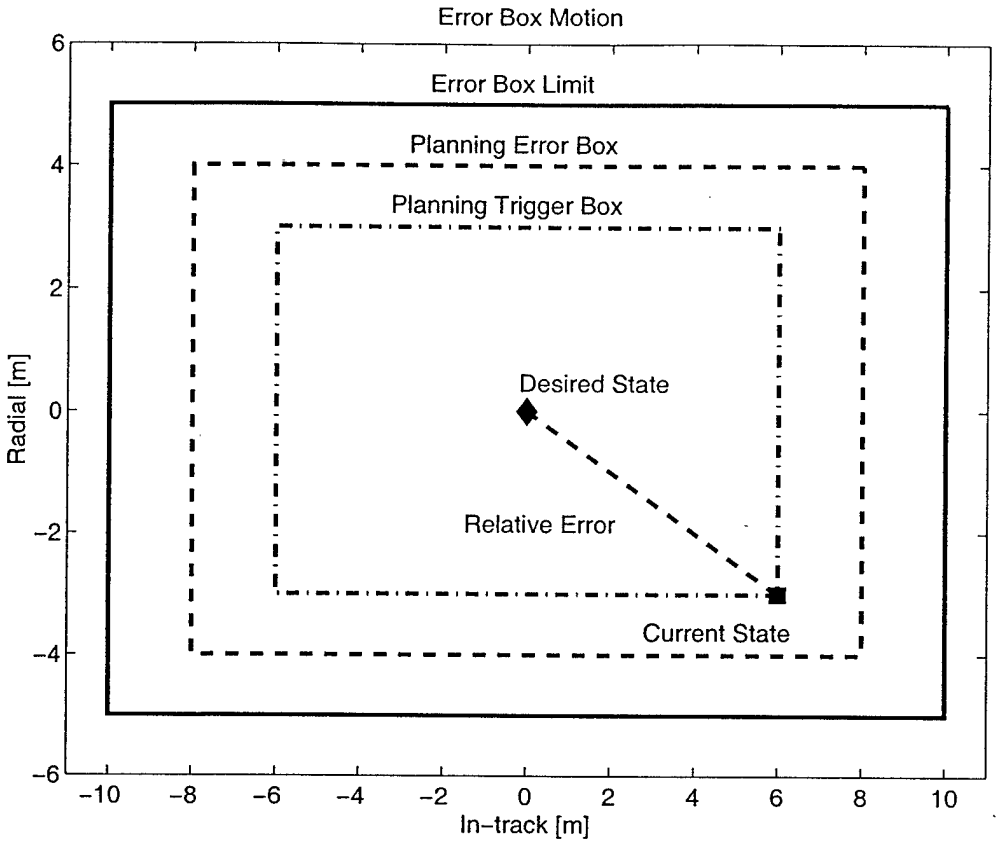

Figure 4-1: In-plane view of error box. Three limits: plan trigger limit, planning error box constraint limit, hard performance (error box limit) constraint. The desired state is represented by the diamond while the current state is the square.

use the existing plan; or 3) make a new plan. The method for determining each of these actions is discussed in the following.

There are three parts to the error box. The error box *limit* is the largest box and represents the position tolerance not to be exceeded. The *planning* error box is slightly smaller and is the limit used in the constraints of the LP. The planning tolerance is slightly smaller because the dynamics used in the LP do not exactly match the nonlinear orbital dynamics, so the path followed by the spacecraft will not exactly match the designed trajectory. The smaller box allows some deviation in the path without exceeding the ultimate limit. The *planning trigger* box is the smallest box. When the state exceeds the trigger box and no plan exists, then a new plan is developed. When a plan does exists, the first half of the plan is implemented regardless

of the current error position and then, if the position exceeds the planning error box, a new plan is formed. This limits the deviation from the designed trajectories.

The relative sizes of the three boxes is a variable in the control scheme that can be used to increase or decrease performance at the expense or relief of fuel cost. The geometry of the error "box" is also a variable in the control implementation. The form of the dynamics suggests that using an oblate sphere rather than a cube could yield some performance benefits [49]. The sphere can be approximated in the LP using a polygon with a constraint for each side. Using a "sphere" would also avoid initial conditions to LP problems that result in higher fuel costs, such as when a vehicle is near the corner of the error box with little room to maneuver.

The LP controller is a feed-forward controller. The control inputs and expected trajectories are designed based on linearized dynamics and disturbance models that will contain errors. As a result, the actual motion followed by the vehicle will not match the expected motion. To ensure the spacecraft follows the desired trajectory, the error box is used in a state feedback scheme. At each time-step the state of the vehicle is determined and checked with the error box. In reconfiguration maneuvers the error box is centered at the expected position of spacecraft for that particular time-step. In formation-keeping the error box is centered on the desired state. The error box is used to determine whether to continue using the existing plan or make a new plan. The state feedback method with the error box prevents errors from increasing over the plan interval for the controller. If the error exceeds the box, a new plan is formed based on the current state. The dynamics and disturbance models used in the LP can also be adjusted based on the actual motion compared to the expected motion to provide a more accurate plant description for the next control sequence generation.

4.2 Sensor Noise

Designing a fuel-optimized control input sequence will typically require a trajectory planning technique, but these planning techniques will heavily rely on the knowledge

of the spacecraft's initial conditions. Since these initial relative positions and velocities must be determined from measurements, they will be corrupted by noise. For example, with filtered Carrier-Phase Differential GPS (CDGPS) signals as the relative navigation sensor, the position noise at the time of this study in late 2000 was predicted to be on the order of σ_p =2–5 cm and velocity noise on the order of σ_v =2–3 mm/s [50]. The current sensor noise is now predicted to be about σ_p =2–5 cm position noise and σ_v =0.1–1 mm/s velocity noise [51]. The following section will examine the effects of these measurement errors from three perspectives: spacecraft dynamics, ability to plan fuel-optimal trajectories, and expected fuel consumption.

4.2.1 Effects on Relative Motions

To analyze the effects of measurement errors, consider the dynamics of the relative motion of two spacecraft in a circular reference orbit using Hill's equations as shown in Equation 2.21 in Section 2.1. Taking x_0, y_0, $\dot{x}_0$, and $\dot{y}_0$ to be nominally zero, each initial condition can then be perturbed to values of ± 0.02 m for the position and ± 0.002 m/sec for the velocity to calculate the resulting relative error. Initial errors in position as well as radial velocity only result in small errors in predicted motion, on the order of less than a meter. However, a ± 0.002 m/s in-track velocity error results in approximately a 30 m in-track position offset after only one orbit. For comparison, the relative error (as predicted by the FreeFlyer™ orbital simulation software [34]) due to differential J_2 for a pair of satellites in an orbit with a 35° inclination angle results in a drift rate of ≈5 m per orbit. For this simulation one satellite is on a closed-form ellipse centered on the other satellite. The relative error is determined as the difference between where the satellite should be, based on the best dynamic models currently available [19], and the path actually followed by the spacecraft under the influence of J_2. The errors caused by both the velocity and differential J_2 effects are shown in Figure 4-2.

Another way to analyze these errors is to note that the last term of the in-track velocity expression in Equation 2.21 shows that the relative velocity errors ($\dot{y}_0$) have an effect that is $1/(2n) \approx 450$ times larger (in terms of the secular in-track drift) than

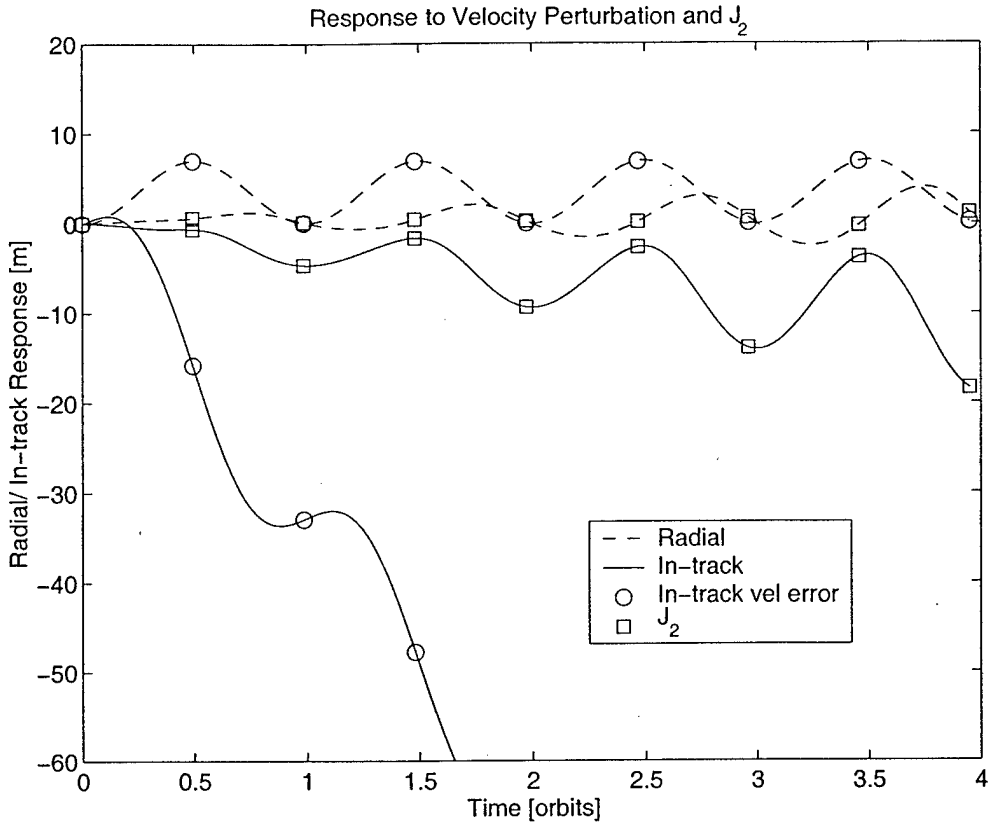

Figure 4-2: Comparison of the resulting error due to initial error in the in-track velocity (+0.002m/sec in-track) (o) and due to differential J_2 effects (□). The results show that there is an in-track drift of $\approx$30 m per orbit for in-track velocity error and $\approx$5 m per orbit due to J_2.

the relative position errors (x_0). However, the filtered CDGPS is only predicted to provide velocity knowledge that is a factor of ten better (comparing 0.002 to 0.02). These results indicate that obtaining better velocity estimates is an important issue for future work in formation flying. From the control perspective, these results also indicate that it is important for any control technique that designs fuel-optimal trajectories to account for uncertainty in the spacecraft's initial conditions. Modifications to account for these sensing errors in the formation-keeping algorithm developed in Section 3.1 are outlined in the following section.

4.2.2 Robust LP for Formation-keeping

As a result of the estimation process associated with the relative navigation [50, 51], it is expected that there will be an uncertainty associated with the current positions and velocities (initial states in the trajectory optimization). A key question that arises for any trajectory generation process is the effect of uncertainty in the initial state knowledge on the optimal plan. This subsection analyzes the effects of initial condition uncertainty on the LP control algorithm presented in this thesis and presents a simple technique to add robustness in the planning process to these uncertainties.

To examine the effect of sensor noise on the LP controller, consider a velocity uncertainty of ± 2 mm/s for a formation-keeping problem with a plan horizon of four orbits. Figure 4-3 shows the response to the nominal plan for the nominal case (solid line terminating at the circle marked 0) as well as responses when the velocity initial conditions are perturbed (± 2 mm/s in-track, ± 2 mm/s radial). As expected, for the nominal case, the inputs keep the vehicle within the error box for four orbits and the path terminates near the center. However, when the velocity is perturbed, three of the trajectories violate the constraint box and two of the paths leave the box and never return. The alternatives at this point are to increase the size of the error box, which will impact the payload performance, or to modify the algorithm so that it is less susceptible to measurement noise.

Uncertainty in the initial conditions can be addressed by developing a trajectory design that is robust to errors in $x(0)$. Based on the "multiple-model" techniques successfully used for robust feedback control design [52, 53, 54], one approach to increasing robustness in the trajectory planner is to design the input sequence to simultaneously satisfy the constraints for several (m_{ic}) initial conditions. Note that, as shown in Equation 2.39, the initial condition only enters the problem though the righthand side $b(k)$. Thus in the general formulation given in Equation 3.1, the first constraint would be written in the form

$$\begin{bmatrix} -A(k) & A(k) \end{bmatrix} \begin{bmatrix} \hat{U}_n \end{bmatrix} \leq y_{\text{des}}(k) - b_i(k) \quad \forall\, i = 1, \ldots, m_{ic} \tag{4.1}$$

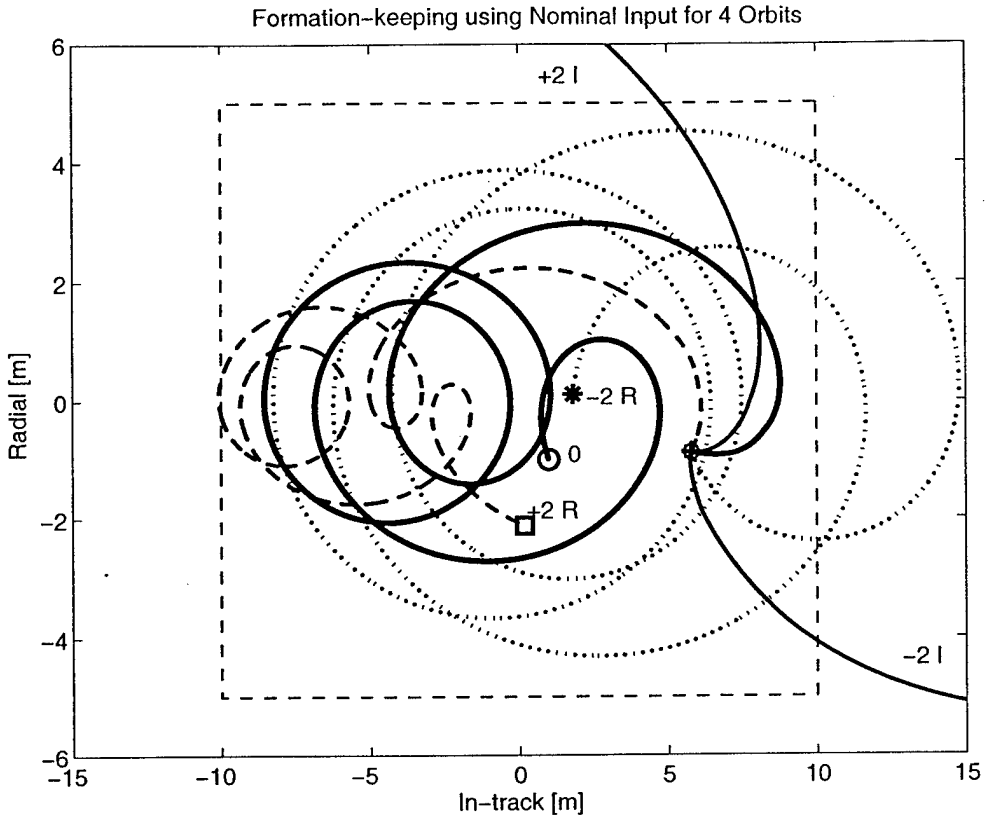

Figure 4-3: Trajectory followed using the nominal plan designed for four orbits without considering initial condition uncertainties. Trajectories for ± 2 mm/s in-track error had final position errors of approximately ± 130 m.

where $b_i(k)$ from Equation 2.39 captures the response associated with each of the initial conditions $x_i(0)$.

To avoid adding a large number of constraints to the LP problem, these m_{ic} constraints can be replaced with a single constraint

$$\begin{bmatrix} -A(k) & A(k) \end{bmatrix} \begin{bmatrix} \hat{U}_n \end{bmatrix} \leq y_{\text{des}}(k) - b_{\max}(k) \tag{4.2}$$

where $b_{\max}$ is formed using the following. Form the matrix B

$$B = \begin{bmatrix} b_1 & \dots & b_{m_{ic}} \end{bmatrix} \tag{4.3}$$

whose columns are the b_i vectors associated with each initial condition. Then deter-

mine the vector $b_{\max}$, the i^{th} element of which is given by

$$b_{\max}(i) = \max_j B_{ij}; \quad \forall\, i = 1, \ldots, N \tag{4.4}$$

Because the approach typically only considers several ($m_{ic} = 1 - 10$) perturbed initial conditions, it is not guaranteed to provide an input sequence that will not violate the specified constraints. However, as with the robust feedback control design, experience indicates that the results from this approach are much less sensitive to errors in the initial conditions. Guaranteed techniques for robustness in LPs are addressed in Reference [55].

By considering several different initial conditions, the result of this LP design should be more robust to measurement errors, but due to the large effect of the initial velocity errors, the length of the planning horizon has to be reduced in order to achieve a feasible solution. For the examples considered in the remainder of this section, the horizon was reduced to approximately one quarter of an orbit and the terminal constraint on the optimization (*e.g.*, finish within 1 m of the origin) was removed. Figure 4-4 shows the response to the perturbed velocity initial conditions as well as two additional initial conditions for a quarter orbit plan designed using only the nominal case. The additional two cases have initial velocity errors of $+\sqrt{2}$ mm/s in-track, $+\sqrt{2}$ mm/s radial and $+\sqrt{2}$ mm/s in-track, $-\sqrt{2}$ mm/s radial. Note that four of the paths exit the error box. This is not unexpected, as the LP was only designed for the nominal case. The control inputs from the robust LP were applied to the same set of initial conditions to generate the trajectories in Figure 4-5. Only four of these initial conditions were included in the LP design (the labeled ones). However, as shown, all six trajectories remain within the box during this first quarter orbit.

With increasing noise levels and subsequent increasing uncertainty in the initial conditions, the variation in trajectories for a set of inputs can become quite large. As a result, the control can only be successfully applied over a reduced time horizon. The size of the error box also determines the maximum allowable plan horizon. For

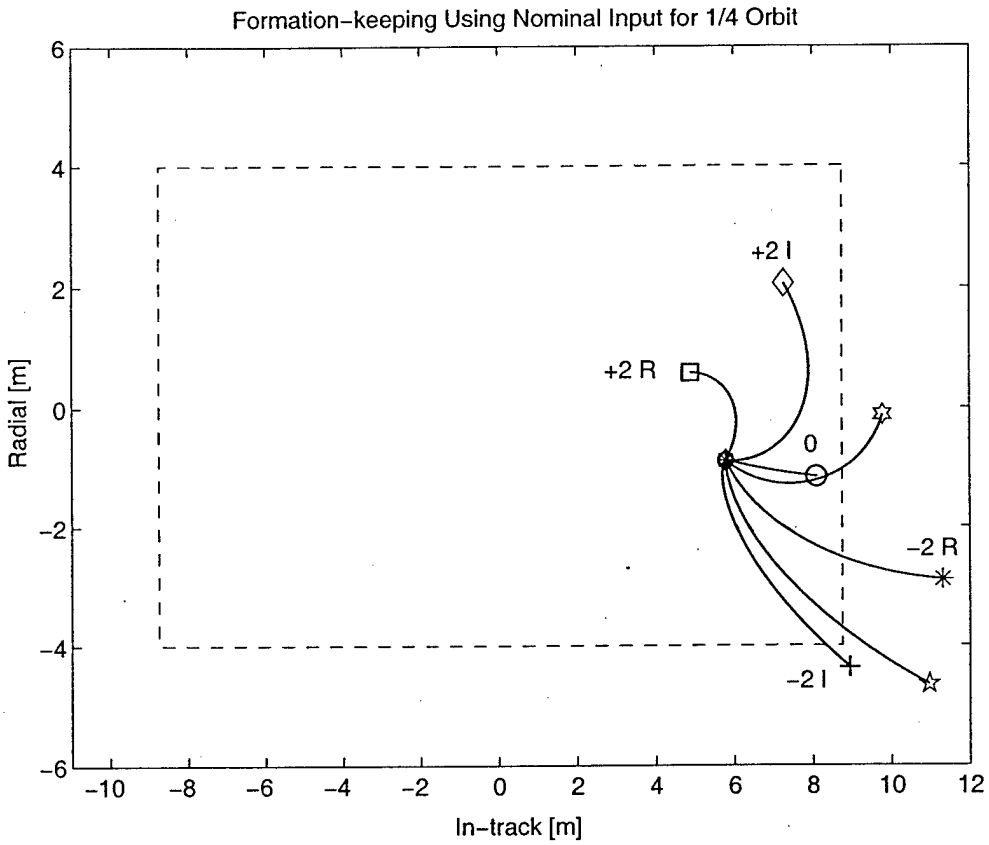

Figure 4-4: Trajectories for each of the five possible initial conditions using the plan for nominal case. The pentagram and hexagram represent two additional cases within the uncertainty ellipsoid but not considered in the plan.

example, a 2 mm/s deviation in in-track velocity results in a 30 m drift over one orbit. If the error box is smaller than 30 m in the in-track direction, then the plan horizon clearly must be less than one orbit. However, a larger error box may be able to sustain this drift from the planned destination. Figure 4-6 shows a plot of feasible plan times versus the noise level for increasing error box size. The LP optimization for the plot only constrained the spacecraft to remain within the specified error box for the duration of the plan time. Note that as the noise level increases the plan time drops very rapidly, but increasing the error box size relieves the position constraint and allows for a longer plan horizon. Of course, shorter plan horizons correspond to more frequent thruster firings, which will result in a much higher fuel cost.

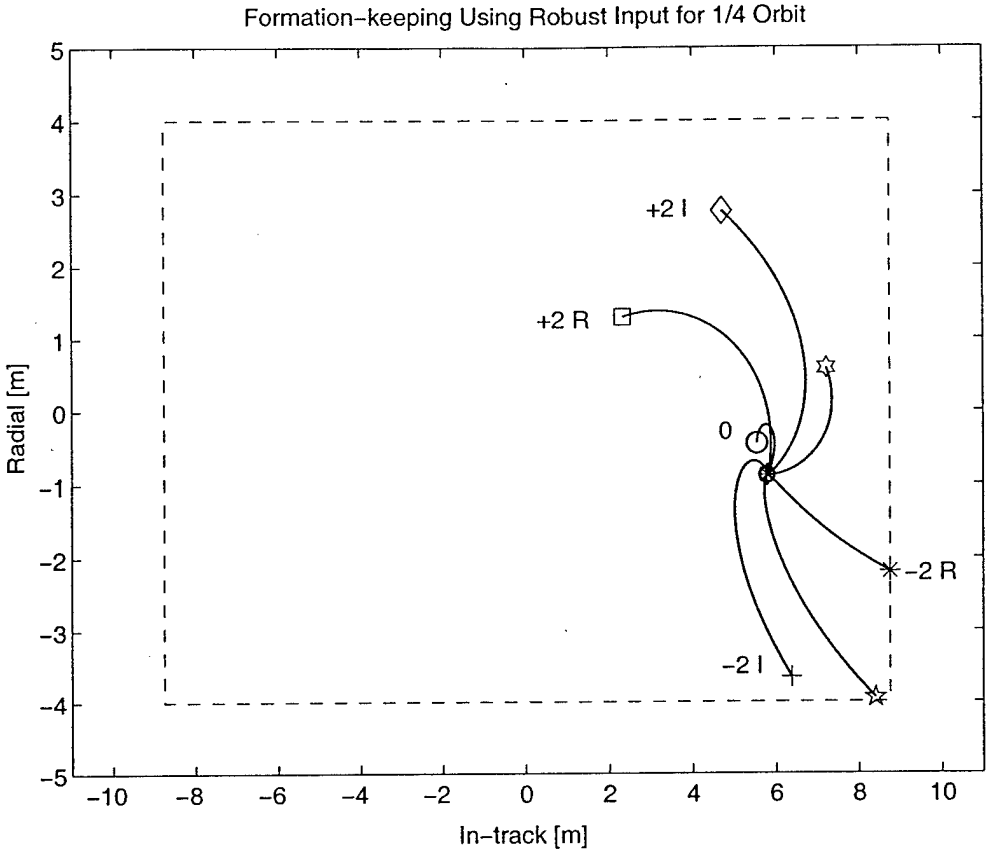

Figure 4-5: Trajectory followed using the robust plan for each initial condition. The pentagram and hexagram represent two additional cases within the uncertainty ellipsoid but not considered in the plan.

Effects on Fuel Use

Several nonlinear simulations were performed using the FreeFlyer™ orbit simulator in order to determine the effect of sensor noise on fuel use for formation-keeping maneuvers. The simulations consist of two vehicles, in approximately 90 minute circular orbits, on a closed form ellipse with 200 m semi-major axis. The differential drag is modeled as a constant $\pm 0.5 \times 10^{-7}$ m/s^2 acceleration. In order to clearly examine the effect of sensor noise on fuel use for formation-keeping, only the differential drag disturbances are implemented in the FreeFlyer™ [34] simulation, although other disturbances such as J_2 effects and solar radiation pressure could be implemented. The J_2 and other disturbances are disabled in the FreeFlyer™ simulations because the

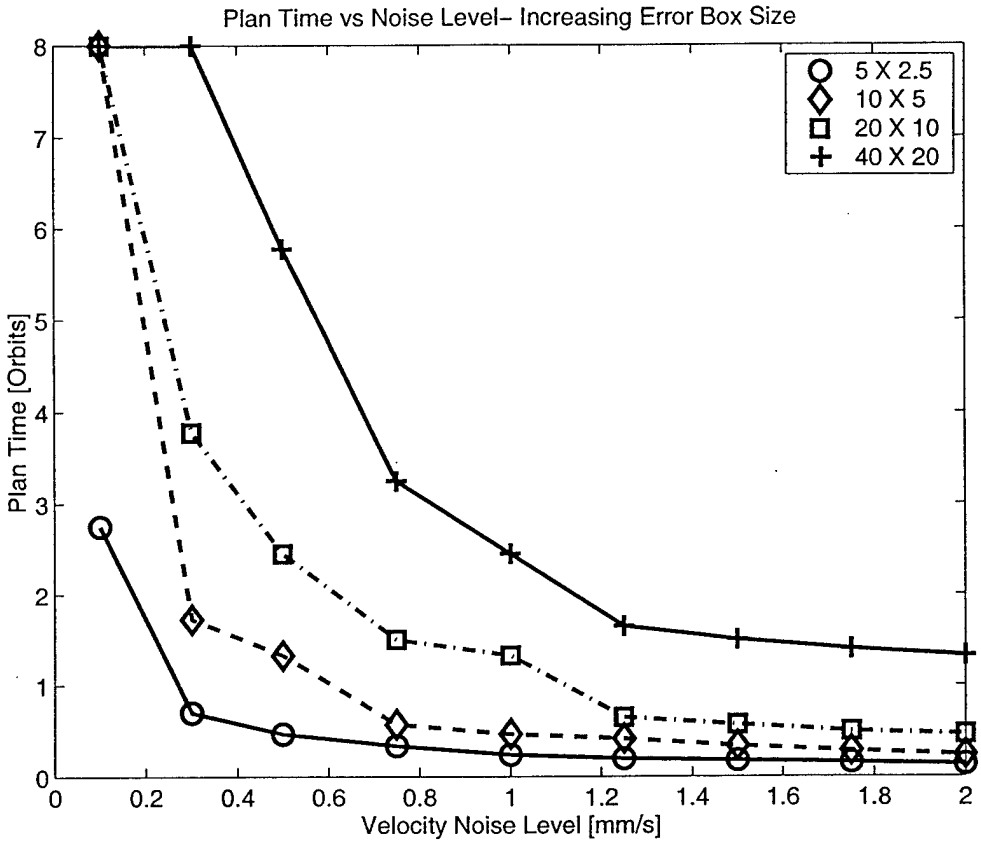

Figure 4-6: Maximum plan time achievable versus noise level for increasing error box size. Error box sizes are in meters (± in-track×± radial).

dynamics in the LP do not account for these disturbances. With these disturbances eliminated, the increase in fuel use is caused by the sensor noise rather than a combination of noise and plant uncertainty. During maneuvers, the spacecraft thrusters are restricted to provide a maximum acceleration of 0.003 m/s^2 and a minimum of 5×10^{-6} mm/s^2. The maximum thrust is produced by turning the thruster on for the full time-step. The minimum thrust is determined from a minimum impulse bit of 10 msec during the 5.4 second time-step. The ±10 m in-track × ±5 m radial error box is selected to meet the requirements of the TechSat 21 mission. Simulations were performed for position noise levels of 2 cm and velocity noise levels ranging from 0.1 mm/s to 2 mm/s. Only the velocity noise is varied because the LP is much more sensitive to velocity errors than position errors, as demonstrated by the simulations

in Section 4.2.1. The noise is modeled in the simulations as the true state vector plus a white noise component. Multiple simulations are required for each noise level because of the stochastic nature of the system response. Three, one day simulations are performed for each noise level. The fuel use, ΔV, is determined as an average fuel use per orbit for each noise level.

For each simulation, the spacecraft begins in the center of the error box and drifts to the edge due to a differential drag. When the vehicle nears the edge, a control input sequence is determined to keep the spacecraft within the box using the robust LP. The constraints for the LP are the same for each noise level, only the planning horizon is altered in order to arrive at a feasible solution. The vehicle is constrained to remain inside the error box for the duration of the plan.

Figures 4-7 and 4-8 display the typical relative error box motion of a spacecraft for a low noise level of 0.1 mm/s and a high noise level of 2 mm/s, respectively. Notice that the low noise case results in a smooth continuous motion, but the high level case is disjointed. The abrupt changes in motion for the high noise case result from the uncertainty in initial conditions. The robust LP plans for the worst case possible and, as a result, often uses a large control input that completely reverses the motion of the vehicle.

To summarize these simulations, Figure 4-9 shows a plot of fuel use versus noise level. The average fuel used increases proportionally to the sensor noise, from $\Delta V =$ 1.15 mm/s per orbit for a noise level of 0.1 mm/s to $\Delta V = 33.3$ mm/s per orbit for 2 mm/s noise. Also note that the variation in fuel use increases as the noise level increases from 0.1 to 1.0 mm/s, and then decreases again. The variation in the fuel used arises from the uncertainty in the effectiveness of the LP generated inputs. The LP is designed to compensate for the worst case effects of the initial condition errors, which turns out to be more fuel efficient in some cases than in others. The decrease in the variability of fuel used for higher noise levels is most likely due to the reduced plan time. The shorter the plan time, the less the vehicle will diverge from a designed plan. The plot suggests that a reduction in sensor noise by 50% (from 2 mm/s) will reduce fuel use by $\approx$50%. The results of this simulation show that a $\Delta V \approx 33.3$ mm/s

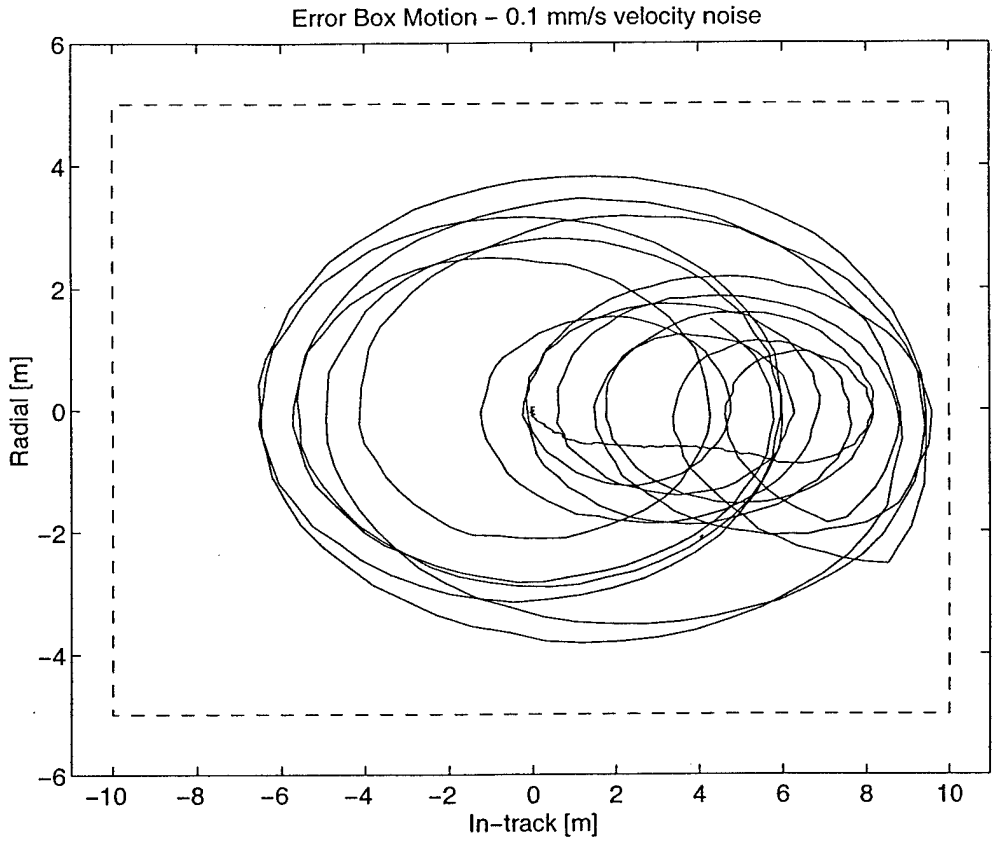

Figure 4-7: Typical error box motion for 0.1 mm/s velocity noise level.

per orbit is needed to account for a velocity noise level of 2 mm/s. These ΔV values are roughly of the same order of magnitude as the ΔV predictions to account for differential J_2 disturbances.

Figure 4-10 compares the fuel cost for formation-keeping using LP with no uncertainty, the robust LP with 2 mm/s velocity uncertainty, and a non-robust LP with 2 mm/s velocity uncertainty. The simulation with no noise used $\Delta V \approx 0.5$ mm/s per orbit. Formation-keeping using the robust LP requires $\Delta V \approx 30$ mm/s per orbit for each vehicle, which is a significant increase. The non-robust control works well at times, but not always and results in an average $\Delta V \approx 90$ mm/s per orbit.

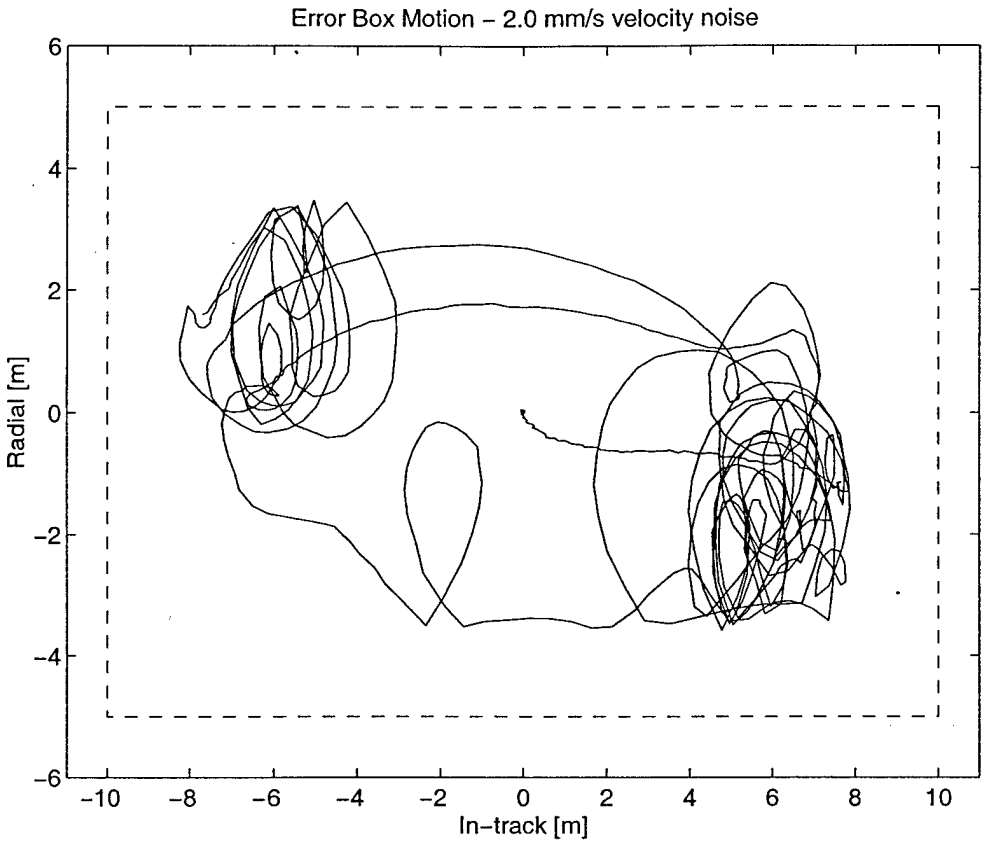

Figure 4-8: Typical motion for 2 mm/s velocity noise level.

4.2.3 Sensor Noise in Terminal Constraint Problems

Terminal constraint problems such as formation initialization and reconfiguration contain equality constraints as opposed to the inequality constraints in formation-keeping. As a result, the robust LP technique presented in the previous section does not apply. This section presents two methods to account for sensor noise in the formation maneuvers. One method is to use a feedback controller such as a Linear Quadratic Regulator (LQR) to track the original designed trajectory. The second method re-plans the trajectory when the true trajectory deviates from the designed path by a specified amount. Simulations are performed to compare the methods as well as the consequence of ignoring the initial condition uncertainty.

The simulations involve a three vehicle formation with a reference orbit represented by a virtual satellite with properties similar to the average of the fleet. The

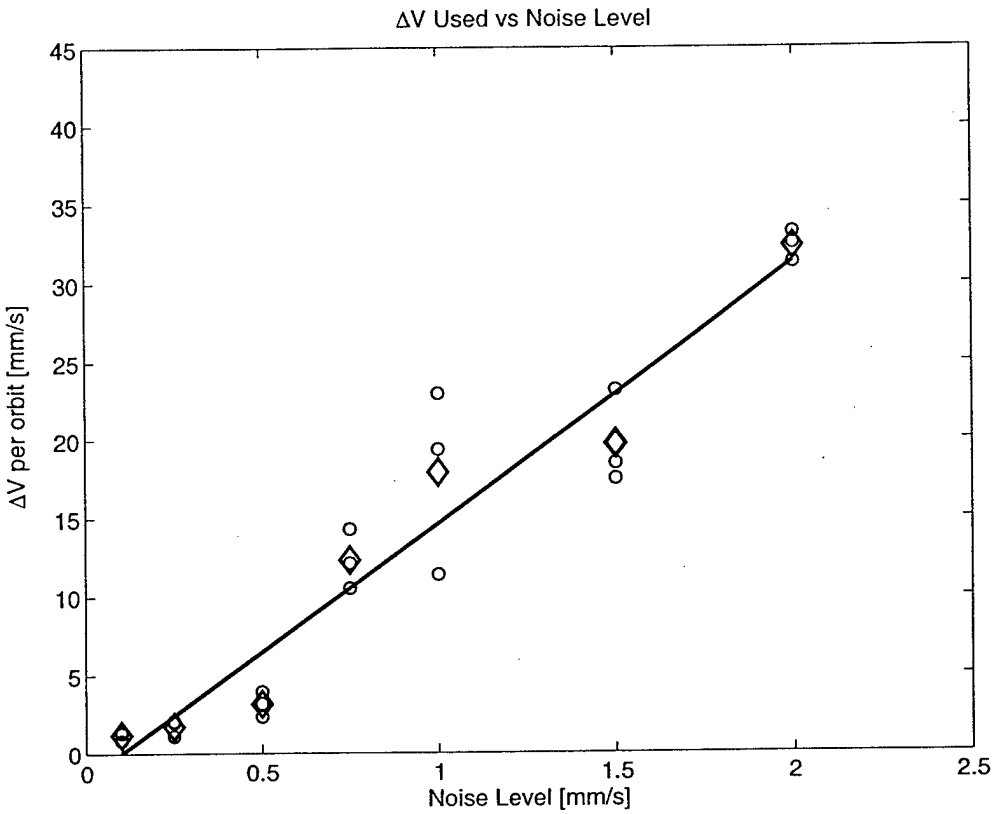

Figure 4-9: Average fuel use per orbit versus noise level. The circles represent individual simulation data and the diamonds are the mean values of the data.

reference orbit has a semi-major axis of 6900 km, inclination 35°, and eccentricity 0.005. The spacecraft begin with an initial in-track separation of 250 m. A formation initialization maneuver is executed to achieve a passive aperture formation that projects a 400 × 200 m ellipse on the orbital plane and oscillates with an amplitude of 100 m in the cross-track direction. This aperture is maintained through formation-keeping for two days then the formation reconfigures to a second passive aperture with a projected in-plane ellipse of 1200 × 600 m and cross-track amplitude of 300 m. The cross-track motion is phased by 90° which causes the plane of the formation to rotate 90° from the previous aperture. All disturbances (J_2, drag, solar radiation pressure, etc.) were included in all simulations, however, only differential drag was included in the LP control formulation.

Each vehicle is modeled as an Orion spacecraft based on the current specifications

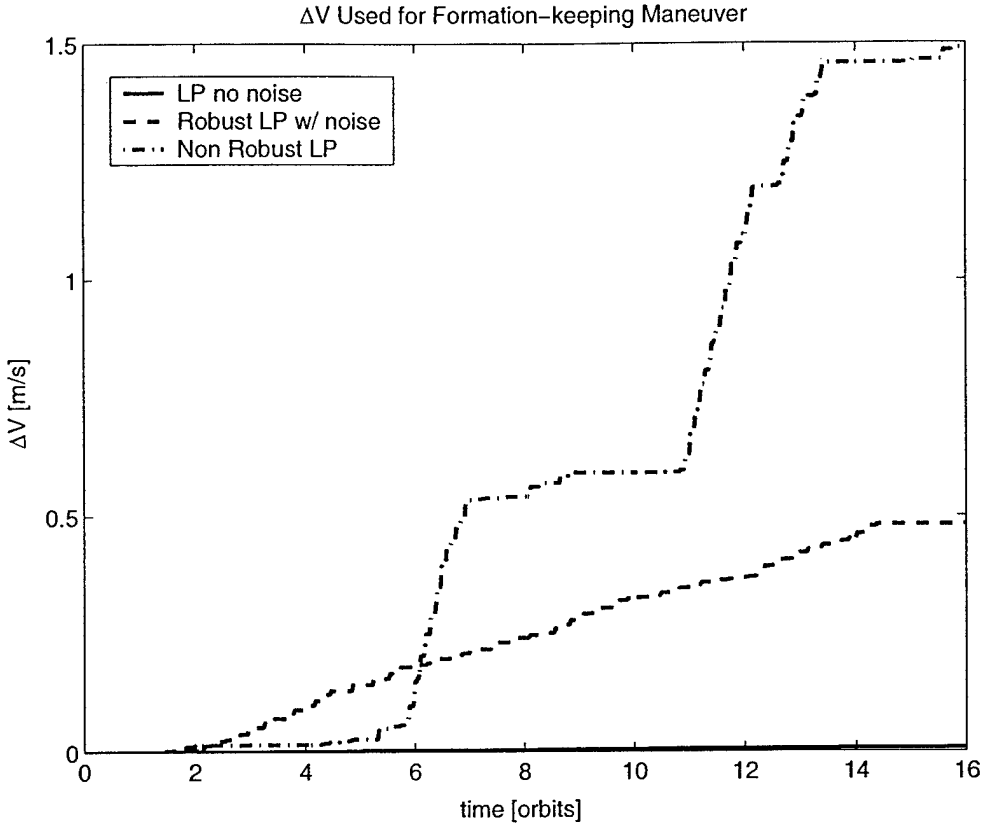

Figure 4-10: Comparison of fuel used for each type of formation-keeping control. Note that the "perfect case" LP fuel usage is very small on this scale.

for the Orion-Emerald mission [6, 56]. Each spacecraft has a mass of 45 kg, but they have slightly different ballistic coefficients, resulting in a differential drag disturbance. The spacecraft thrusters are restricted to provide a maximum acceleration of 0.003 m/s^2 and a minimum of 5×10^{-6} m/s^2. The maximum thrust corresponds to turning on the thruster for the full time-step. The minimum thrust is determined from a minimum impulse bit of 10 msec during the time-step. The relative dynamics for the vehicles are discretized on a 5.4 seconds time-step. Lawden's time-varying equations are used to determine the desired state for each spacecraft, however Hill's equations are used in LP problem.

No Measurement Noise

The first simulation implements the control scheme assuming knowledge of the spacecraft positions and velocities without noise/uncertainty. This corresponds to

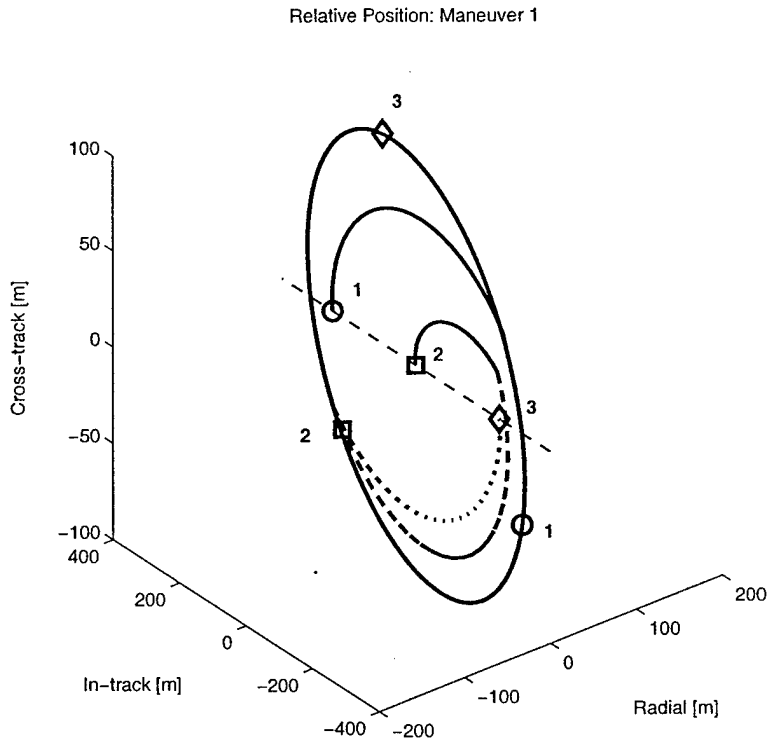

Figure 4-11: Formation initialization from a line (250 m separation) to an aperture (200 m semi-major axis) followed by four orbits of formation-keeping.

the ideal case and is used to demonstrate the extent to which LP can be used to generate fuel-optimal trajectories. Figures 4-11 and 4-12 show the initial maneuver to a closed-form ellipse and the second maneuver from one ellipse to another. The fuel used by each vehicle for the maneuvers are shown in Table 4.1. The actual fuel use in FreeFlyer™ agrees with the predictions by the coordinator for the initial maneuver (0.520 m/s), but differs slightly for the second maneuver (2.560 m/s). This small difference is a result of the spacecraft's deviation from the initial position and velocity that was used by the coordinator in the trajectory optimization.

Noise

A simulation was also performed to implement the control scheme with measurement noise included to add uncertainty in the knowledge of the relative positions and velocities of the vehicles. The noise is modeled in the simulations as the true state vector plus a white noise component. An estimator is currently not used. The noise

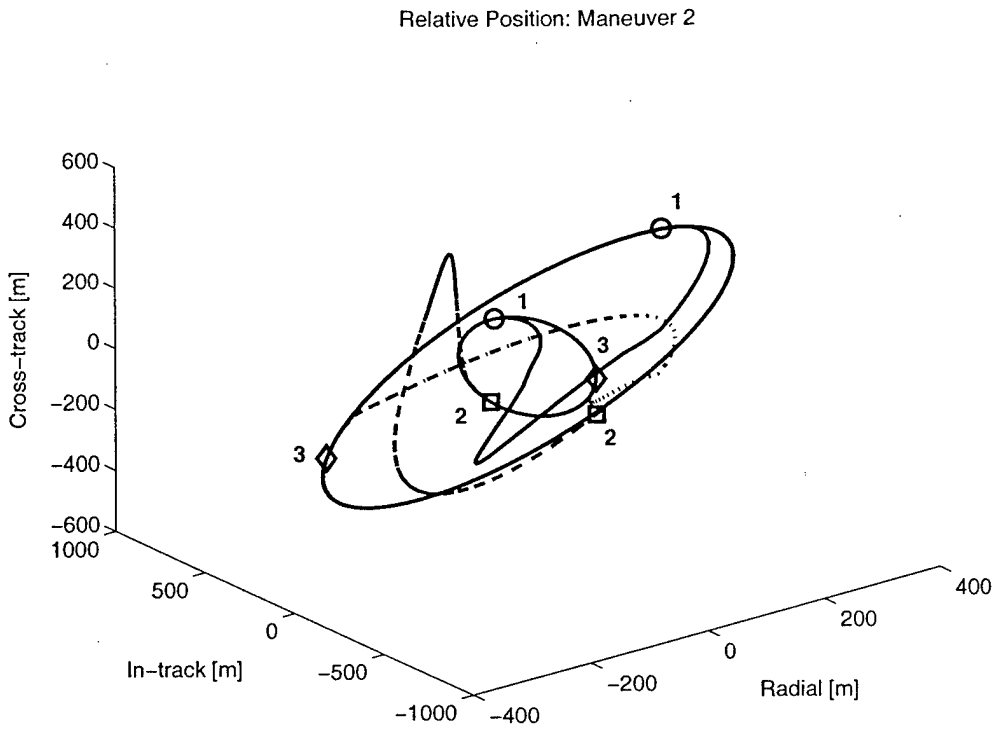

Figure 4-12: After 2 days (32 orbits) of formation-keeping, the fleet reconfigures to a new non-coplanar aperture (600 m semi-major axis). The fleet resumes formation-keeping at the new configuration.

is restricted to a maximum amplitude of 2 cm for position and 1 mm/s for velocity as per current studies in GPS measurement noise [50, 51]. Because the formation reconfiguration maneuvers are based on initial conditions that are uncertain, the spacecraft will not follow the desired trajectories.

Noise: LQR Feedback Control

One method of ensuring the vehicle continues on the trajectory is to use feedback control to force the spacecraft to track the desired trajectory for the maneuvers. The desired position and velocity during the formation maneuver is determined for each vehicle by simulating the response to the LP designed inputs using the same linearized dynamics used in the LP control algorithm. An error box is centered on the desired position for each spacecraft at each time-step during the maneuver. If the vehicle is within the error box, no feedback control is applied, otherwise a simple Linear Quadratic Regulator (LQR) is used to drive the state towards the desired state and

hence the vehicle position back into the error box. The LQR control is used until the position state returns back inside the error box. This feedback control is only applied when there are no scheduled feed-forward control inputs.

In this case, the results of the formation reconfiguration maneuvers are essentially the same as those shown in Figures 4-11 and 4-12. The fuel results are summarized in Table 4.1. With errors in the initial conditions, the initial maneuver requires a $\Delta V = 0.830$ m/s, which corresponds to an extra 0.310 m/s (60% increase) due to feedback control. The second maneuver requires an extra 0.360 m/s (15% increase) for feedback control.

Noise: Re-plan

Another method of completing the formation reconfiguration in the presence of measurement noise is by re-planning over a reduced horizon during the maneuver. For this method, the desired position for the spacecraft during the maneuver is simulated using the designed inputs from the LP problem. An error box is centered on the desired position at each time-step. However, now when the error in position of the vehicle exceeds the error box, a new plan is determined based on the current state using the terminal constraint LP. The new plan occurs over a plan length that is reduced by the number of time-steps executed up to that point. One advantage of this method is that, rather than tracking a trajectory based on incorrect initial conditions, a new trajectory is determined based on the current knowledge of the spacecraft state.

The simulations results for this method are summarized in Table 4.1. Using the re-planning method, the fuel cost with initial condition uncertainty for the initialization maneuver is only increased by 0.121 m/s (23% increase) from the no noise case (approximately one-third of the fuel increase using LQR). The fuel increase for the formation reconfiguration is 0.074 m/s (3% increases), which is again a significant improvement over the LQR result.

A comparison of combined formation fuel cost for the initialization maneuver with and without uncertainty using the two methods described above is shown in Figure 4-14. The simulation results clearly show that the re-plan method has a lower

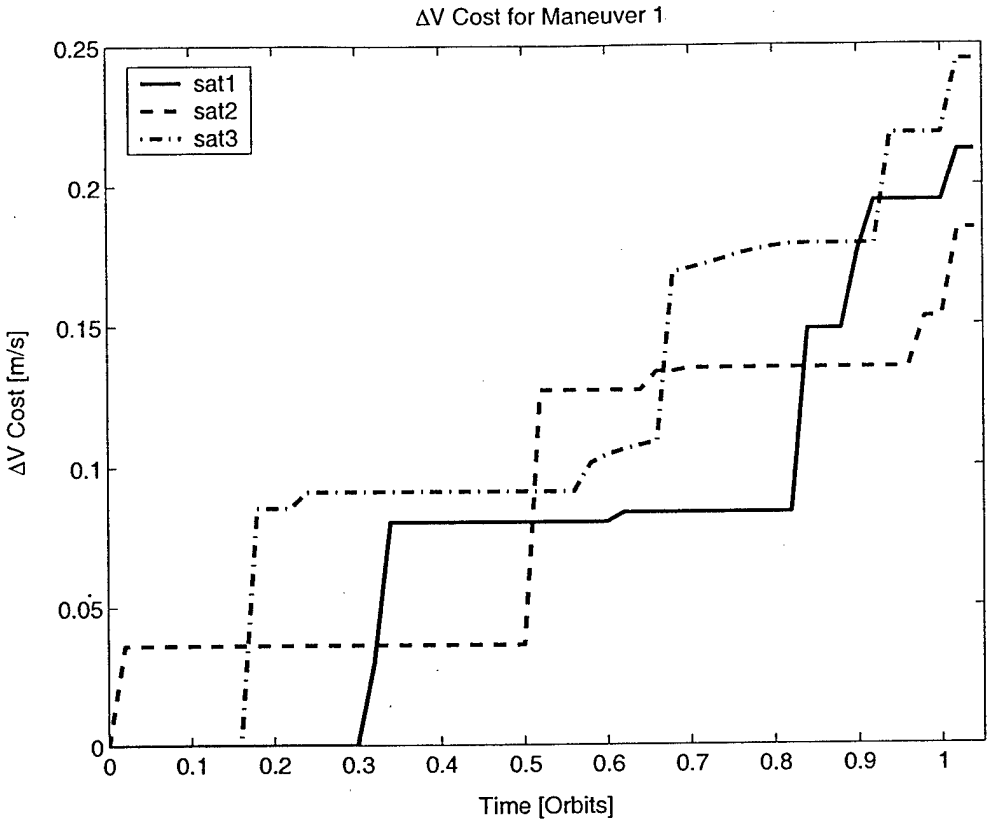

Figure 4-13: Total fuel (ΔV) used for the initialization maneuver. The total $\Delta V = 0.641$ m/s.

fuel cost than planning based on the erroneous initial conditions and then tracking the designed trajectory using either LQR or other feedback control methods.

4.2.4 Additional Model Uncertainty

Disturbances such as differential drag can be included in the dynamics model for the LP control problem, however the model of the disturbance forces will be uncertain and lead to errors in the control design. Disturbance forces such as differential drag and the out of plane J_2 disturbance in Equation 2.23 enter the LP problem as a disturbance input $w(k)$ as in Equation 2.36. The disturbance input enters the $b(k)$ part of the LP in the same manner as initial condition uncertainty, $x(0)$, in Equation 2.39. Therefore, the robust LP method described in Section 4.2.2 can be applied to increase robustness to disturbance input uncertainty.

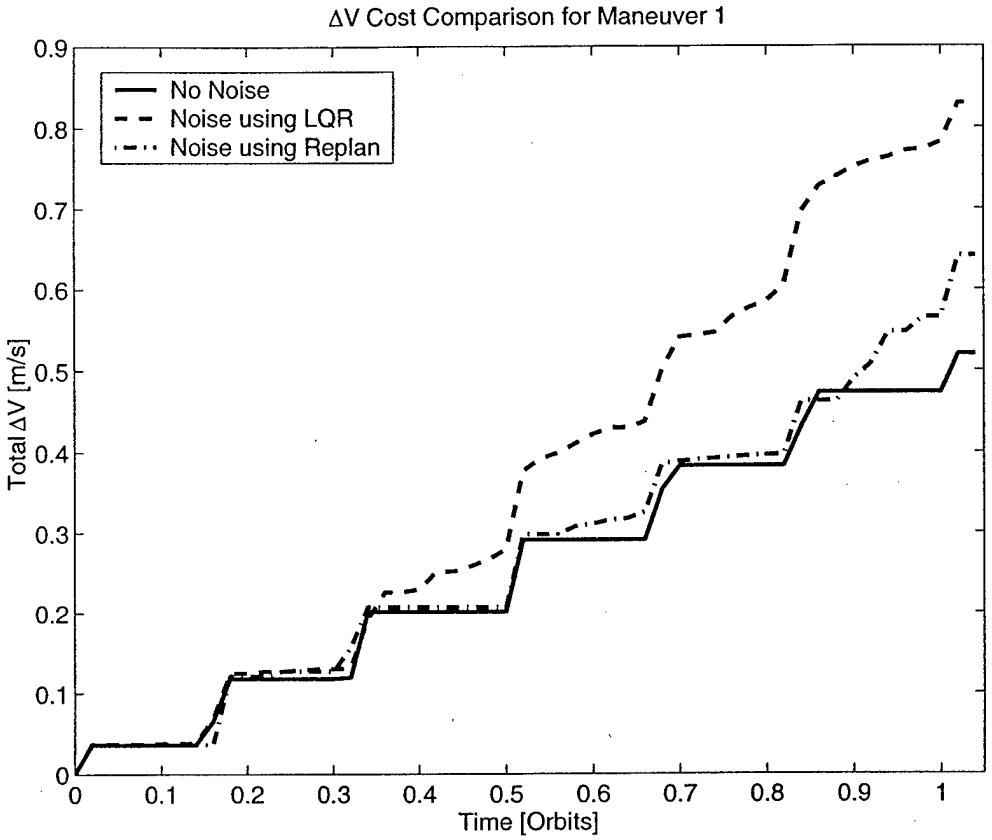

Figure 4-14: Total fuel (ΔV) comparison using feed-forward, feed-forward/feedback LQR, and re-planning for the initialization maneuver. Total change in $\Delta V = 0.310$ m/s for feedback LQR and $\Delta V = 0.121$ m/s for re-planning.

Another source of uncertainty is in the relative dynamics models in the LP. The relative dynamics models presented in Chapter 2 depend on reference orbit parameters such as mean motion, n, eccentricity, semi-major axis, and true anomaly. The reference orbit used to determine these parameters depends on the method of specifying the formation center. Three methods were described in Section 3.2.2. If the reference orbit method is used, then the parameters are specified in the mission plan. If a physical satellite is placed at the formation center as in the leader-follower method, then the parameters can be determined from the trajectory of the leader satellite. The virtual satellite state is formed by a weighted least squares of the states of the satellites in the formation and requires an estimation of the parameters for the virtual orbit. The last two methods will result in uncertainty in the orbital parameters

Table 4.1: Fuel summary for reconfiguration maneuvers.

Maneuver	Fuel Cost	Veh 1	Veh 2	Veh 3	Total
Initial Move	Predicted				0.520 m/s
	No Uncertainty	0.173 m/s	0.173 m/s	0.173 m/s	0.520 m/s
	Uncertainty-LQR	0.336 m/s	0.174 m/s	0.320 m/s	0.830 m/s
	Difference				0.310 m/s
	Uncertainty-Re-plan	0.212 m/s	0.184 m/s	0.244 m/s	0.641 m/s
	Difference				0.121 m/s
Second Move	Predicted				2.536 m/s
	No Uncertainty	0.917 m/s	0.820 m/s	0.821 m/s	2.559 m/s
	Uncertainty-LQR	1.004 m/s	0.881 m/s	0.945 m/s	2.862 m/s
	Difference				0.303 m/s
	Uncertainty-Re-plan	0.920 m/s	0.857 m/s	0.837 m/s	2.614 m/s
	Difference				0.055 m/s

used for the relative dynamics. This uncertain is contained in the discrete dynamics matrix Φ which appears in both A and b of the LP as in Equations 2.38 and 2.39. The uncertainty leads to perturbations in A and b, resulting in k perturbations, A_k, and b_k. Reference [57] presents solutions to this type of uncertainty problem. The uncertain problem can be solved as

$$\min_{x} \max_{i=1,\ldots,m} \|\tilde{A}_i x - \tilde{b}_i\|_1 \tag{4.5}$$

with $\tilde{A}_i$ and $\tilde{b}_i$ defined as

$$\tilde{A}_i^T = [a_{0,i}, \rho a_{1,i}, \ldots, \rho a_{L,i}] \tag{4.6}$$

$$\tilde{b}_i^T = [b_{0,i}, \rho b_{1,i}, \ldots, \rho b_{L,i}] \tag{4.7}$$

where $a_{k,i}^T$ is the i^{th} row of A_k and $b_{k,i}$ is the i^{th} component of b_k, and ρ is a measure of the degree of uncertainty. This problem is a convex optimization problem that can be solved as an LP [57].

4.3 Feasible Solutions

Any planned trajectory will rely heavily on the knowledge of the vehicle's initial conditions, but the initial relative positions and velocities must be measured and will be noisy. Investigation of the impact of sensor noise on the LP control technique and a method for making formation-keeping plans robust to sensor noise is presented in Section 4.2. By considering several different initial conditions, the result of the LP design is more robust to measurement errors, but due to the large effect of the initial velocity errors, obtaining a feasible solution is a difficult issue. One solution to this problem is to reduce the plan horizon until a solution is feasible. The plan horizon could be reduced iteratively, but this would require attempting to solve multiple LP problems until a solution is achieved.

An alternative approach is to include a scaling of the error box size as a variable in the LP problem. The error box scaling variable, $y_{\text{scale}} \geq 1$, is heavily weighted in the cost function to prevent increasing the error box to achieve a solution with zero control inputs. Thus y_{scale} would only be increased to scale the error box to achieve a feasible solution. This problem formulation is as follows

$$\begin{bmatrix} A(k) & -A(k) & -y_{\text{tol}} \\ -A(k) & A(k) & -y_{\text{tol}} \end{bmatrix} \begin{bmatrix} \hat{U}_k \\ y_{\text{scale}} \end{bmatrix} \leq \begin{bmatrix} y_{\text{des}}(k) - b(k) \\ -y_{\text{des}}(k) + b(k) \end{bmatrix} \tag{4.8}$$

The scaling variable is also constrained to be greater than one to prevent reducing the position tolerance below the original size in an attempt to minimize the heavily weighted scaling variable at the expense of increasing the control input.

4.4 LP Solution Times

The size of the LP problem is of interest in terms of both the solution time and data storage. LP solution time is important because if the LP controller is to be used in a real-time system, the solution must be available for execution by the next time-step in the discrete controller. If the solution takes several time-steps, the state must be

propagated far enough forward in time to ensure the solution does not determine control inputs for a time-step that is now in the past. This propagation increases the uncertainty of the state used as the initial condition to the LP. The propagation can either be performed by a nonlinear propagator or can be achieved by not allowing control inputs the first n time-steps of the LP. Decreasing the solution time reduces or eliminates the need to propagate the states, reducing the initial condition uncertainty.

The variables of the LP problem are the control inputs at each time-step. In fact, at each input step there are six variables, a positive and negative input for each of the three input directions. The LP also consists of various state constraints. In the terminal constraint problem, there are six constraints (final position and velocity). For the formation-keeping problem there are six constraints for each position tolerance, two constraints for each of the three positions as in Equation 3.17. Thus the size of the LP problem grows quite quickly with the length of the trajectory and the solution times can become unrealistic for real-time implementation. However, this difficulty can be significantly reduced by judiciously removing variables and constraints from the problem.

For example, variables can be eliminated from the problem by constraining when an actuator can be used. Assume that the system dynamics are discretized on a small time-step for high accuracy, but the inputs are restricted to every m_1 time-steps, thus reducing the number of variables. Since many of the optimal plans involve control inputs at the beginning and end of the maneuvers, another method is to constrain the inputs to only occur during the first and last m_2 number of steps and every m_3^{th} step in-between. Eliminating control inputs changes the form of Equation 2.38. The columns of matrix A are altered because the indices of Φ and Γ only correspond to time-steps when a control input is considered. The control input vector U_k in Equation 2.40 is also reduced to the new number of control inputs.

State constraints can also be applied only every m_4^{th} time-step to reduce the number of constraints. Removing constraints reduces the size of the problem, but allows the solution to exceed the position tolerance in-between the constraint checks, which reduces performance. Removing constraints eliminates rows in the A matrix for each

time-step no longer constrained. The disturbance inputs in the b vector, Equation 2.39 are still applied at all time-steps and must be summed accordingly for all discretized time-steps up to each constraint step considered.

The following simple example demonstrates the method of eliminating variables and constraints from an LP over 6 time-steps into the future. The dynamics considered are time invariant and $H = I, J = \Gamma$, and $P = M$ to simplify the notation from Equation 2.38. If no variables or constraints are removed, the A matrix and b vector would be of the form below

$$A = \begin{bmatrix} \Gamma & 0 & 0 & 0 & 0 & 0 & 0 \\ \Phi\Gamma & \Gamma & 0 & 0 & 0 & 0 & 0 \\ \Phi^2\Gamma & \Phi\Gamma & \Gamma & 0 & 0 & 0 & 0 \\ \Phi^3\Gamma & \Phi^2\Gamma & \Phi\Gamma & \Gamma & 0 & 0 & 0 \\ \Phi^4\Gamma & \Phi^3\Gamma & \Phi^2\Gamma & \Phi\Gamma & \Gamma & 0 & 0 \\ \Phi^5\Gamma & \Phi^4\Gamma & \Phi^3\Gamma & \Phi^2\Gamma & \Phi\Gamma & \Gamma & 0 \\ \Phi^6\Gamma & \Phi^5\Gamma & \Phi^4\Gamma & \Phi^3\Gamma & \Phi^2\Gamma & \Phi\Gamma & \Gamma \end{bmatrix} \tag{4.9}$$

$$b = \begin{bmatrix} Mw_0 + \Phi x_0 \\ Mw_1 + \Phi Mw_0 + \Phi^2 x_0 \\ Mw_2 + \Phi Mw_1 + \Phi^2 Mw_0 + \Phi^3 x_0 \\ Mw_3 + \Phi Mw_2 + \Phi^2 Mw_1 + \Phi^3 Mw_0 + \Phi^4 x_0 \\ Mw_4 + \Phi Mw_3 + \Phi^2 Mw_2 + \Phi^3 Mw_1 + \Phi^4 Mw_0 + \Phi^5 x_0 \\ Mw_5 + \Phi Mw_4 + \Phi^2 Mw_3 + \Phi^3 Mw_2 + \Phi^4 Mw_1 + \Phi^5 Mw_0 + \Phi^6 x_0 \\ Mw_6 + \Phi Mw_5 + \Phi^2 Mw_4 + \Phi^3 Mw_3 + \Phi^4 Mw_2 + \Phi^5 Mw_1 + \Phi^6 Mw_0 + \Phi^7 x_0 \end{bmatrix} \tag{4.10}$$

To reduce the size of the LP problem, control inputs are allowed only every two time-steps and constraints are applied every third time-step. The control inputs u_1, u_3, u_5 are removed, eliminating the corresponding columns of A and the second, third, fifth and sixth rows are removed to eliminate constraints. However, the disturbance input

contributes at all time-steps in the plan. The results are now as follows

$$A = \begin{bmatrix} \Gamma & 0 & 0 & 0 \\ \Phi^3\Gamma & \Phi\Gamma & 0 & 0 \\ \Phi^6\Gamma & \Phi^4\Gamma & \Phi^2\Gamma & \Gamma \end{bmatrix} \tag{4.11}$$

$$b = \begin{bmatrix} Mw_0 + \Phi x_0 \\ Mw_3 + \Phi Mw_2 + \Phi^2 Mw_1 + \Phi^3 Mw_0 + \Phi^4 x_0 \\ Mw_6 + \Phi Mw_5 + \Phi^2 Mw_4 + \Phi^3 Mw_3 + \Phi^4 Mw_2 + \Phi^5 Mw_1 + \Phi^6 Mw_0 + \Phi^7 x_0 \end{bmatrix} \tag{4.12}$$

If the above problem was a formation-keeping control problem for a single vehicle, the original problem would have 42 variables and 42 constraints. However, the reduced problem consists of 24 variables and 18 constraints. Note that the constraints and variables eliminated can be picked independently. The A matrix does not have to be square.

Removing variables and constraints from the LP problem can drastically reduce the LP problem size and achieve solution times on the order of seconds. However this is possibly accomplished at the expense of degraded performance and increased fuel. Including the parameters m_1–m_4 provides a direct means of exploring these trade-offs between desired position tolerance, fuel cost, and solution time.

4.5 Dynamics Models

In this section, the formation control problem is analyzed in terms of two key issues: 1) what dynamics model should be used to specify the desired state to maintain a passive aperture; and 2) what dynamics model should be used in the LP to represent the motion about this state. Several linearized models of the relative dynamics are considered in this analysis, including Hill's equations for circular orbits, modified linear dynamics that partially account for the J_2 effects, and Lawden's equations for eccentric orbits. Numerous simulations are performed to demonstrate the effects of

each dynamics model on the LP controller design.

4.5.1 Dynamics for Desired State

The first issue in the control problem is what relative dynamics and initialization procedure should be used to specify the desired state for obtaining or maintaining a passive aperture. For the formation initialization or reconfiguration maneuver, the desired state represents the terminal state constraint in the control problem. For the formation-keeping maneuver the desired state is the position and velocity the satellite must maintain within some tolerance. The desired state can be as simple as an in-track separation or a more complicated case such as a time-varying state on a passive aperture. Figure 3-6 shows an example of this second case – the desired state is given by the diamond and the reference position is shown as a circle. The reference point can be specified by a mathematical reference orbit, a satellite in the formation, or a virtual center as discussed in Section 3.2.2. Typical periodic relative motion for a passive aperture in the absence of disturbances is shown in Figure 3-6.

The desired state to form a passive aperture is determined from the closed form solutions of the linearized dynamics and the initial conditions. Note that the closed-form solutions and initial conditions for periodic motion are slightly different (see References [10, 17, 21] for details) for each type of relative dynamics discussed in Chapter 2.1. The conditions for periodic motion for each set of dynamics are

$$\text{Hill's Equations: } \frac{\dot{y}(0)}{x(0)} = -2n \tag{4.13}$$

$$\text{Lawden's Equations: } \frac{\dot{y}(0)}{x(0)} = -\frac{n(2+e)}{(1+e)^{1/2}(1-e)^{3/2}} \tag{4.14}$$

$$\text{J}_2 \text{ Equations: } \frac{\dot{y}(0)}{x(0)} = -2n\sqrt{1+s}\ ;\ \frac{\dot{x}(0)}{y(0)} = \frac{n(1-s)}{2\sqrt{1+s}} \tag{4.15}$$

These initial conditions are then used in the corresponding closed-form solutions to determine the desired state at any other time. Note that each model accounts for different aspects of the fleet reference orbital motion (eccentricity) and disturbances

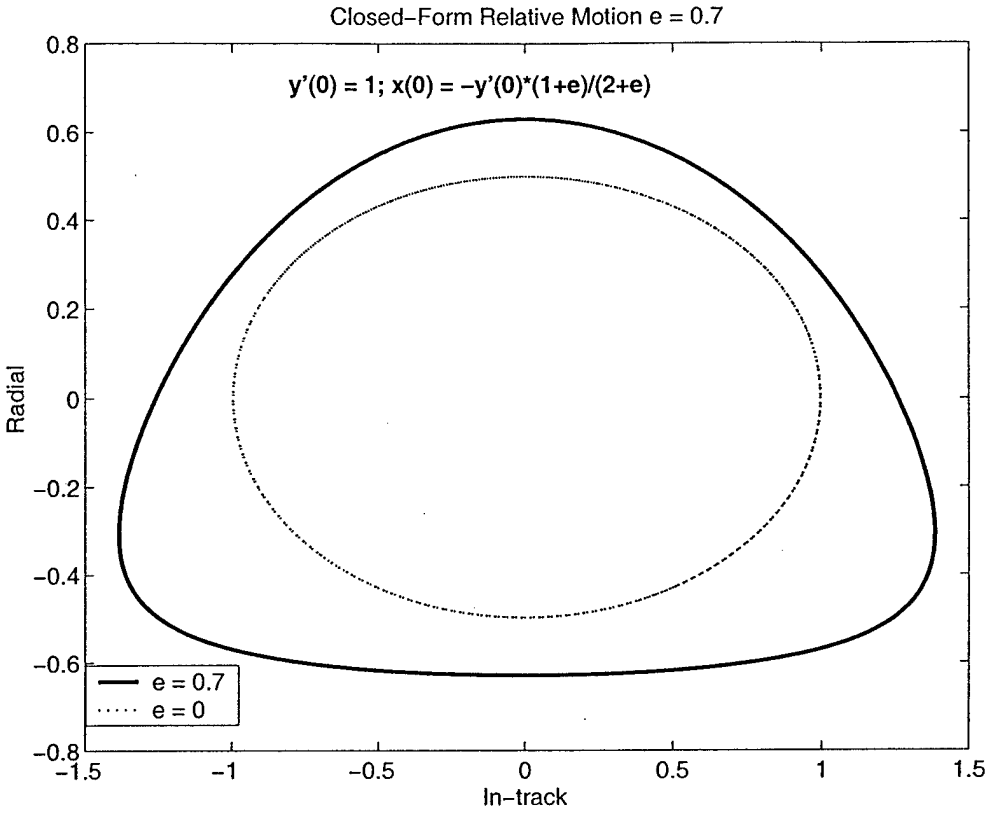

Figure 4-15: Comparison of closed-form in-plane motion for circular and $e = 0.7$

(J_2). Figure 4-15 shows the difference in the passive aperture formed for a circular orbit and when considering orbit eccentricity. This change in the specification of the desired state is critical to successful formation control. If the incorrect desired state is used, the formation is tracking a state that does not result in a natural periodic motion. As a result more control effort is required to maintain the formation. The simulations in Section 4.5.3 demonstrate the impact of using each of these models to predict the desired state used with the LP controller.

4.5.2 Dynamics for the Linear Program Controller

The second issue in the formation control problem is which relative dynamics to use in the linear programming formulation. For the formation initialization maneuver, the dynamics are relative to the reference orbit used to determine the desired terminal

state. The control problem is to determine the fuel-optimal control inputs and trajectory to achieve the desired terminal state at a fixed time. For formation-keeping, the dynamics are relative to a formation center. An error box represents the position tolerance constraints for the formation-keeping and is centered on the desired state for the satellite which is changing with time (see Figure 3-6). In the case of a passive aperture design, the desired state and error box revolve around the reference orbit on the elliptical shape defined by the periodic relative motion.

Each form of the relative dynamics presented in Section 2.1 model certain aspects of the relative motion. Hill's equations provide a representation for the motion using a circular reference orbit. The linearized J_2 model is also for a circular reference orbit but includes a model of the differential gravity gradient disturbances. Lawden's equations provide a model of the motion with an eccentric reference orbit. Lawden's equations are linear time varying, therefore, the discrete dynamics matrix, Φ used in the LP is different at each time-step in the LP. This will require a significant increase in the storage and computation for forming the matrices used in the LP. However, the number of variables and constraints in the LP problem is not increased when using the time-varying dynamics.

Sample trajectories generated using the LP controller for Lawden's Equations are shown in Figure 4-16 and Figure 4-17 for eccentricity values of $e = 0.001$ and $e = 0.005$. Some of the constraints included are: 1) the vehicle positions must remain within the error box at all times, 2) the final position must be within 1 m of the center of the box, and 3) the actuator inputs must not exceed the limits. The trajectories followed using inputs designed from Hill's equations are also plotted for comparison. For eccentricity of 0.001 the error in using a circular orbit reference (i.e., Hill's equations) results in a final position error of approximately 0.2 m. For eccentricity = 0.005 the final position error is $\approx$2 m. These trajectories demonstrate the effect of incorrectly modeling the relative dynamics in the LP formulation.

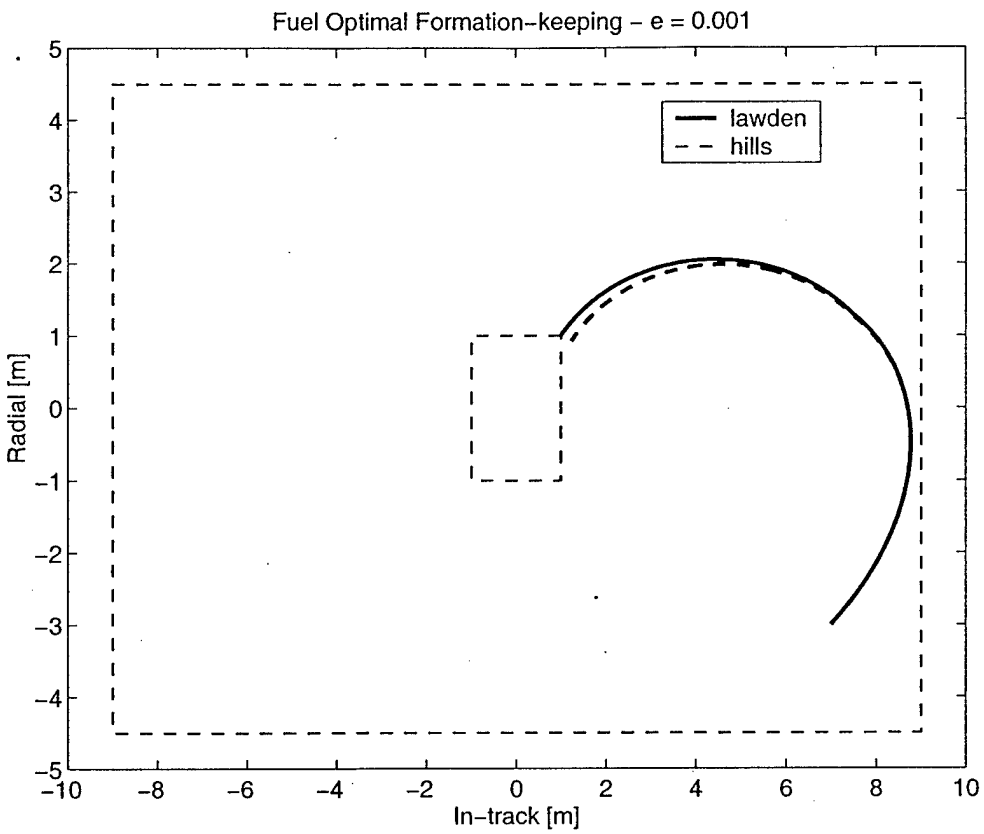

Figure 4-16: Trajectories designed using Lawden's and Hill's equations – reference orbit $e = 0.001$ and half-orbit plan time. Final position error ≈ 0.2 m.

4.5.3 Simulations

Several nonlinear simulations were performed using FreeFlyer™ orbit simulator [34] in order to demonstrate the effectiveness of the LP control method and determine the effect of dynamics models on controller performance. The simulations are separated into groups that focus on various aspects of the the dynamics and performance. The first group examines the effects of orbit eccentricity when Hill's dynamics and Lawden's dynamics are used in the specification of the desired state. The second section examines the effects of eccentricity specifically in the LP controller. The third group demonstrates the controller in eccentric orbits with all disturbances, while the fourth group compares all three forms of dynamics in nearly circular orbits and low eccentricity orbits in order to determine the appropriate combination of dynamics for

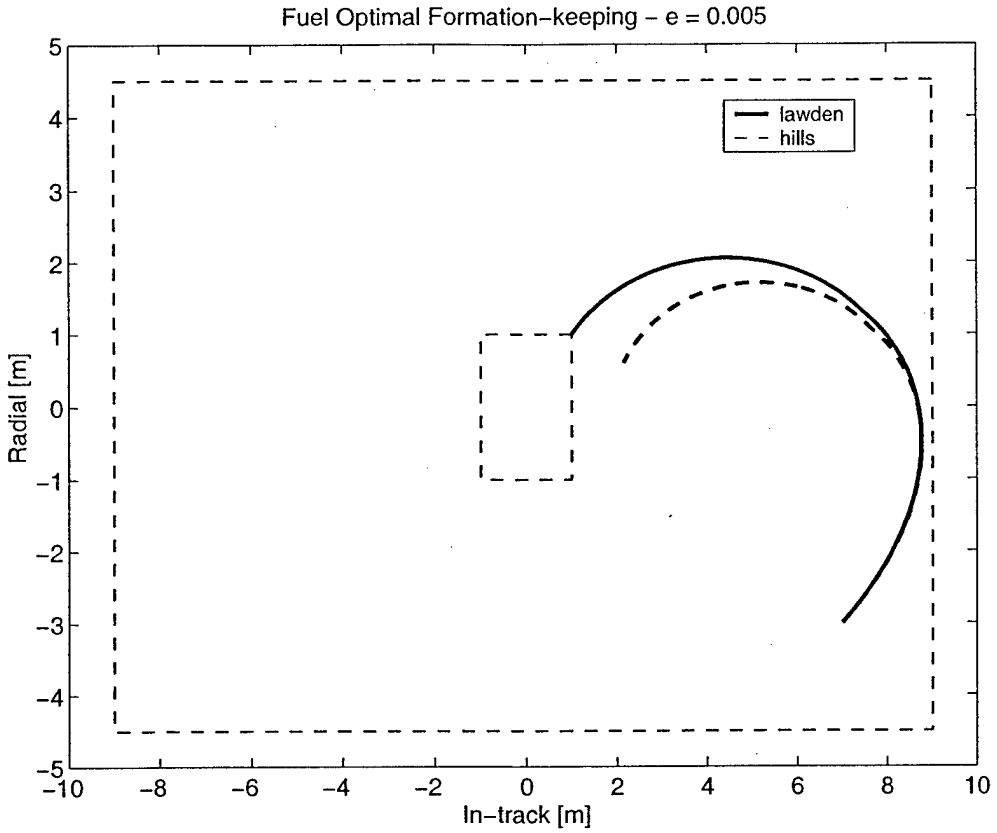

Figure 4-17: Trajectories designed using Lawden's and Hill's equations – reference orbit $e = 0.005$ and half-orbit plan time. Final position error $\approx$2.2 m.

specifying the desired state and for use in the LP controller.

Simulation #1 : Figures 4-18 through 4-22

The first group of simulations demonstrate the effectiveness of the control using Lawden's time-varying equations of motion and the corresponding conditions for periodic motion in eccentric orbits. The vehicles are in an approximately 90 minute orbit and the eccentricity is increased from 0 to 0.01. The same simulations were performed once using Hill's equations of motion and corresponding initial conditions and once using Lawden's equations of motion and initial conditions to show how the error in assuming a circular orbit affects the efficiency of the control and increases the fuel cost.

In order to clearly examine the effect of eccentricity modeling error on the LP control and fuel use for formation-keeping, only the differential drag disturbances

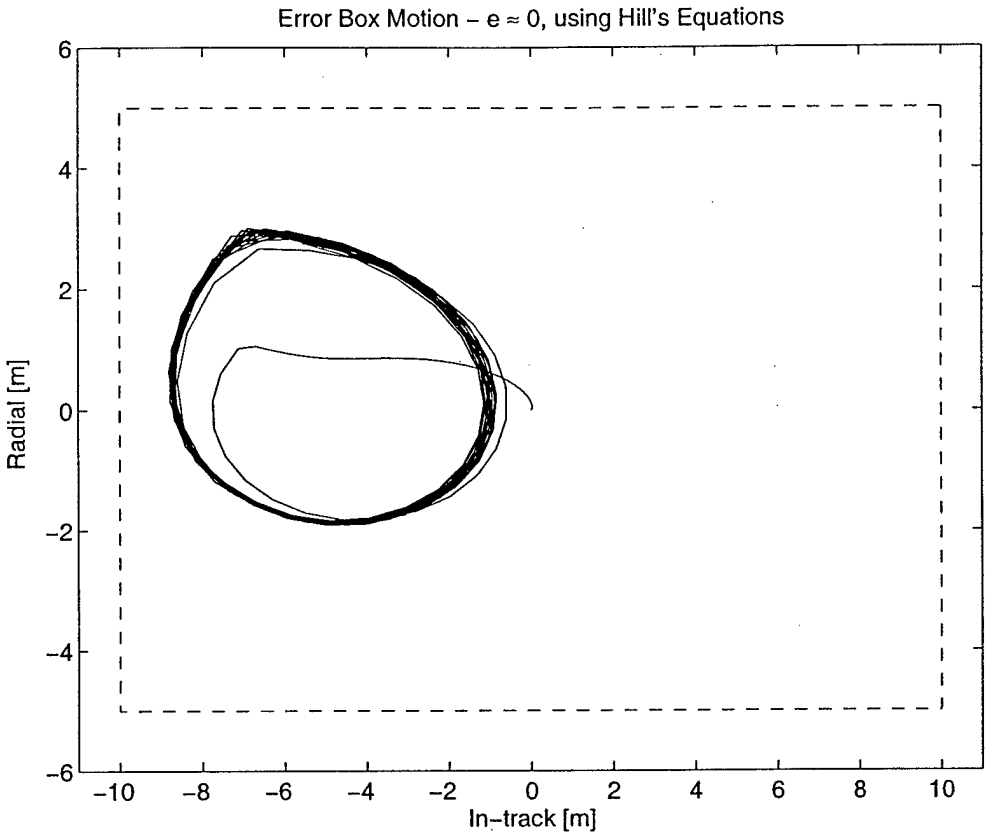

Figure 4-18: Error box motion for a reference orbit with $e \approx 0$, using Hill's equations. The average fuel cost was 6.548 mm/s/orbit.

are implemented in the FreeFlyer™ simulation, other disturbances such as J_2 effects and solar radiation pressure are not implemented. The J_2 and other disturbances are disabled in the FreeFlyer™ simulations because the dynamics in the LP do not account for these disturbances. J_2 also affects the eccentricity which would cause an additional disturbance to the controller which is not the focus of these simulations. For each simulation, the spacecraft begins in the center of the error box and drifts to the edge due to a differential drag. When the vehicle nears the edge, a series of control inputs are determined that move the spacecraft to within 1 m of the center of the error box and reduce the velocity error to within 0.5 mm/s. The LP plan interval is half an orbit (45 min) and the vehicle is constrained to remain inside the error box during the plan interval.

Figures 4-18 and 4-19 show the motion of the spacecraft within the error box for

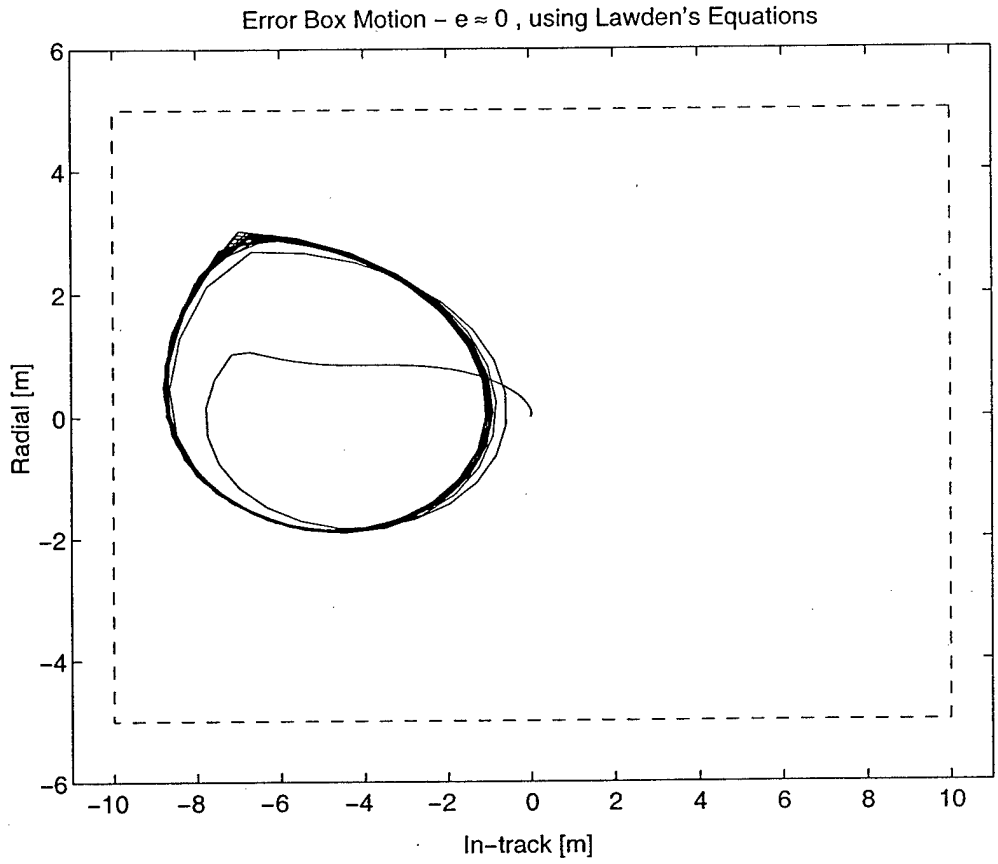

Figure 4-19: Error box motion for a reference orbit with $e \approx 0$, using Lawden's equations. The average fuel cost was 6.530 mm/s/orbit.

a reference orbit with $e \approx 0$. There is little difference between the two, which is as expected (in the limit as $e \rightarrow 0$, Lawden's equations return to Hill's equations). The fuel cost is also approximately the same (6.548 mm/s/orbit using Hill's and 6.530 mm/s/orbit using Lawden's). The fuel cost includes fuel used in the radial, in-track, and cross-track directions, however the cross-track fuel cost was zero for this simulation. Figures 4-20 and 4-21 show the error box motion for a reference orbit with $e = 0.01$. The fuel cost was 107.5 mm/s per orbit using Hill's and 9.481 mm/s per orbit using Lawden's equations, which is a drastic difference. Again, the cross-track fuel cost was zero. Clearly, Hill's equations are no longer appropriate because the orbit is not circular, and this is confirmed by the inability of the control to return the vehicle to the center of the error box. However, Lawden's equations are still effective. The difference in motion between Figure 4-19 and Figure 4-21 is due to the difference

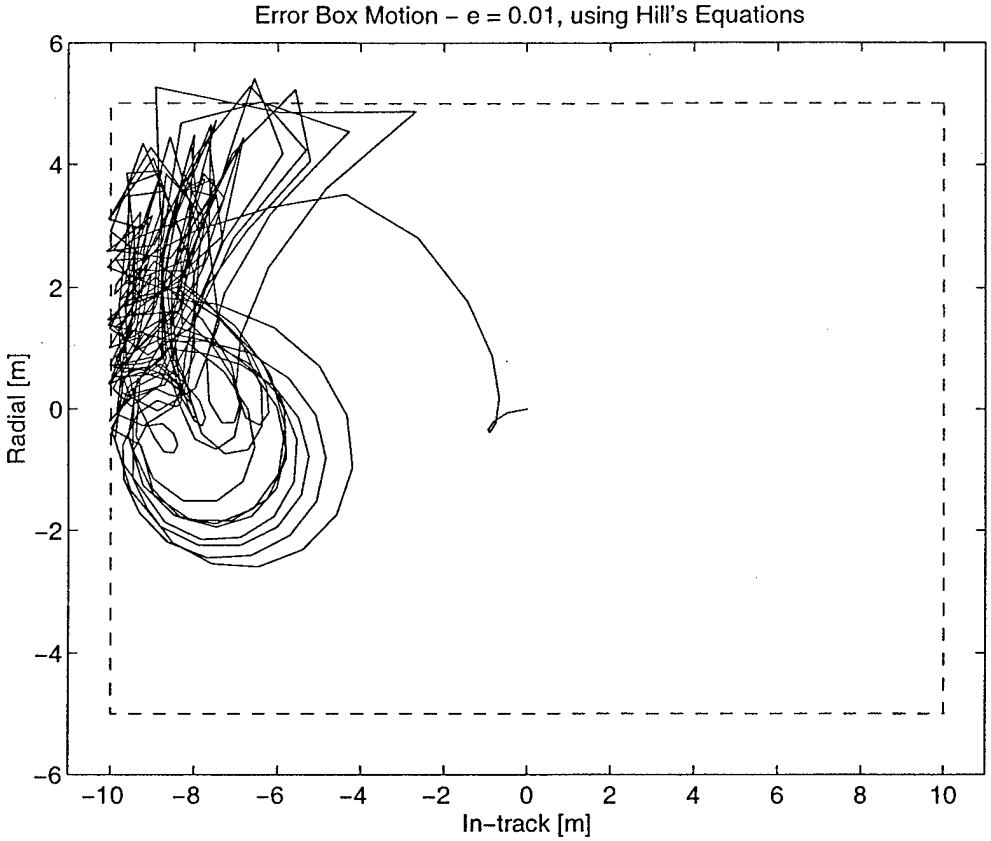

Figure 4-20: Error box motion for a reference orbit with $e = 0.01$, using Hill's equations. The average fuel cost was 107.5 mm/s/orbit.

in drag in an elliptical orbit. For the case $e = 0$, a constant model for the drag is reasonable because the altitude of the spacecraft does not vary much. For $e > 0$ the altitude varies, so the drag in the simulation is not constant. An improved model of the drag could be implemented in the LP to correct this error. The fuel cost versus eccentricity is summarized in Figure 4-22. The three cases included in the plot are:

1. Use Hill's initial conditions to determine the desired state for periodic motion and Hill's equations of motion for the LP.
2. Use Lawden's initial conditions to determine the desired state, but use Hill's equations of motion in the LP, and
3. Use Lawden's initial conditions to determine desired state and Lawden's equations of motion for the LP.

As shown in the Figure 4-22, using Hill's initial conditions to determine the desired

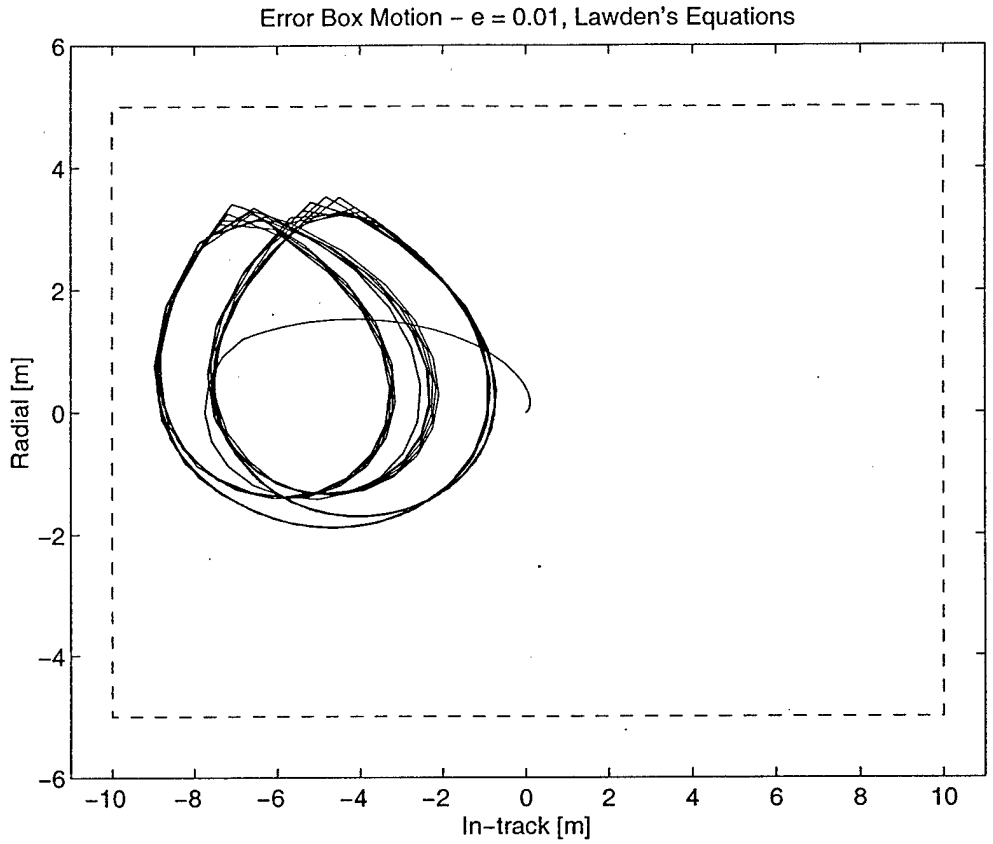

Figure 4-21: Error box motion for a reference orbit with $e = 0.01$, using Lawden's equations. The average fuel cost was 9.481 mm/s/orbit.

state leads to an increased fuel cost, even for very small values of the reference orbit eccentricity. However, these results also indicate that using Hill's equations in the LP does not significantly increase the fuel cost much if e is small ($e < 0.01$). This observation is important because the LP using Lawden's equations requires a discretization of the time-varying dynamics at every step in true anomaly considered in the LP. This tends to dramatically increase the amount of computation required to set up the LP optimization, although the LP size does not change, therefore computation time for solving the LP does not increase. With Hill's equations, the matrices are constant and need only be formed once. As the eccentricity becomes larger, the trajectories designed using Hill's in the LP becomes less effective and the fuel cost will be larger than the LP using Lawden's dynamics. The error in the resulting trajectory is demonstrated in Figures 4-16 and 4-17.

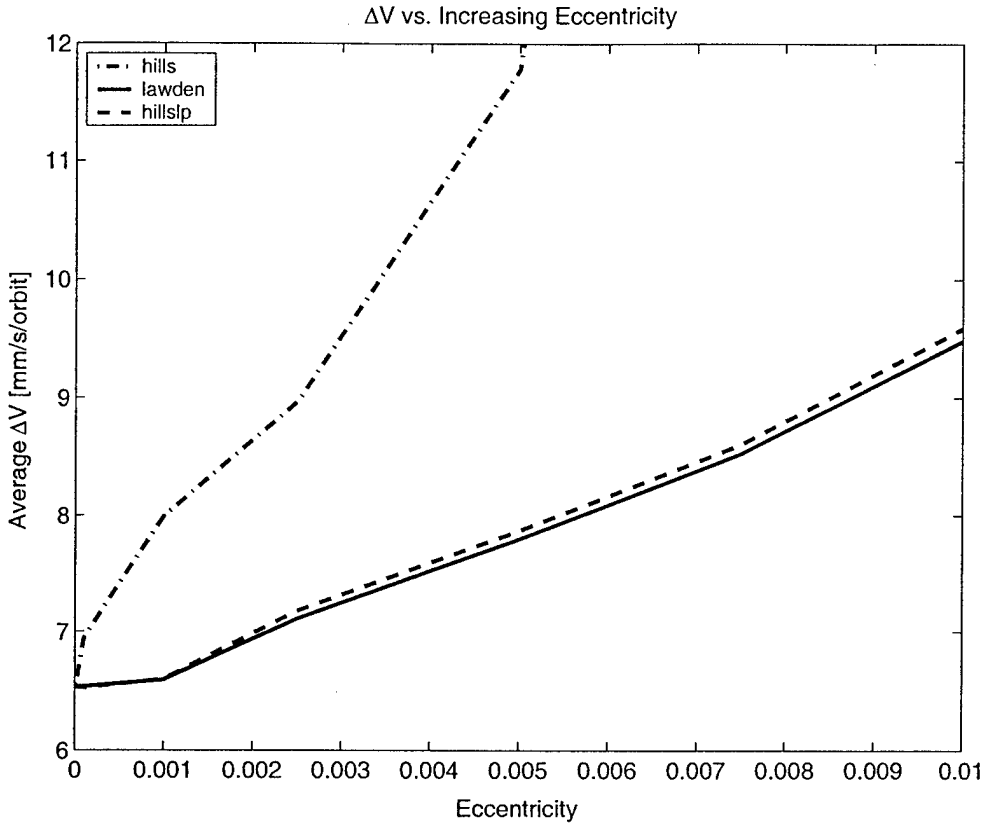

Figure 4-22: ΔV fuel cost versus increasing eccentricity for control using the three (IC and model) cases described in the text.

Simulation #2 : Table 4.2

To further examine the difference between using Lawden's versus Hill's dynamics in the LP, simulations were performed with increasing plan horizon in the LP. A reference orbit with $e = 0.005$ was used in these simulations. Table 4.2 contains average fuel costs for increasing plan horizons using Lawden's and Hill's equations. The fuel cost using either form of dynamics decreases with increasing plan horizon because the longer plan time allows smaller control inputs and takes advantage of the nonlinear motion to increase "drift" time between control inputs. Using Hill's equations rather than Lawden's results in only a slight increase in fuel cost as the plan horizon increases. The time-invariant Hill's equations, however, result in decreased computation time in the LP formulation as mentioned before. The increase in fuel cost for Hill's is due to planning control inputs based on a propagated state using

Table 4.2: ΔV for increasing plan horizon.

Vel Noise (mm/s)	0.1	0.75	1.0	1.25
Hill's	7.969	3.723	2.109	1.701
Lawden's	7.746	3.416	1.751	1.543

dynamics with errors that add up at each time-step.

Simulation #3 : Figures 4-23–4-26

To test the true performance of the controller in eccentric orbits, the following simulations include all disturbances, differential drag, lift, solar radiation pressure, J_2, etc. The duration of the simulation is two days which is long enough to observe the effects of J_2 on the controller. The disturbance effects are set for what is believed to be a worst case scenario in that the drift due to differential drag and the drift due to J_2 are in the same direction. The differential drag could be set such that the drift partially or completely cancels the drift due to J_2, however this was not done in the following simulations. The controller uses Lawden's equations for desired state determination as well as for the dynamics in the LP. The first simulation is for a reference orbit with $e = 0.005$. The average fuel cost is 8.241 mm/s/orbit. This fuel cost includes the cost to control the cross-track perturbations caused by J_2. Using Lawden's equations results in only a slight increase in fuel cost with all disturbances included. The motion of the spacecraft within the error box is shown in Figure 4-23 and the fuel cost is shown in Figure 4-24. For comparison, control using Hill's equations results in a fuel cost of $\approx$ 300 mm/s/orbit, which is clearly not acceptable.

A simulation with $e = 0.5$ was also performed. For the orbit to be feasible the semi-major axis was increased to 14000 km, which results in $\approx$ 275 minute orbit. The error box motion is shown in Figure 4-25 and the average fuel cost was 11.812 mm/s per orbit. The fuel cost is plotted in Figure 4-26.

These simulations show that even in the presence of J_2, the control is effective. J_2 causes short and long period oscillations in the eccentricity [11]. For low eccentricity these oscillations dominate and are on the order of 0.001 which was shown earlier to cause an increase in fuel cost when using Hill's instead of Lawden's equations of mo-

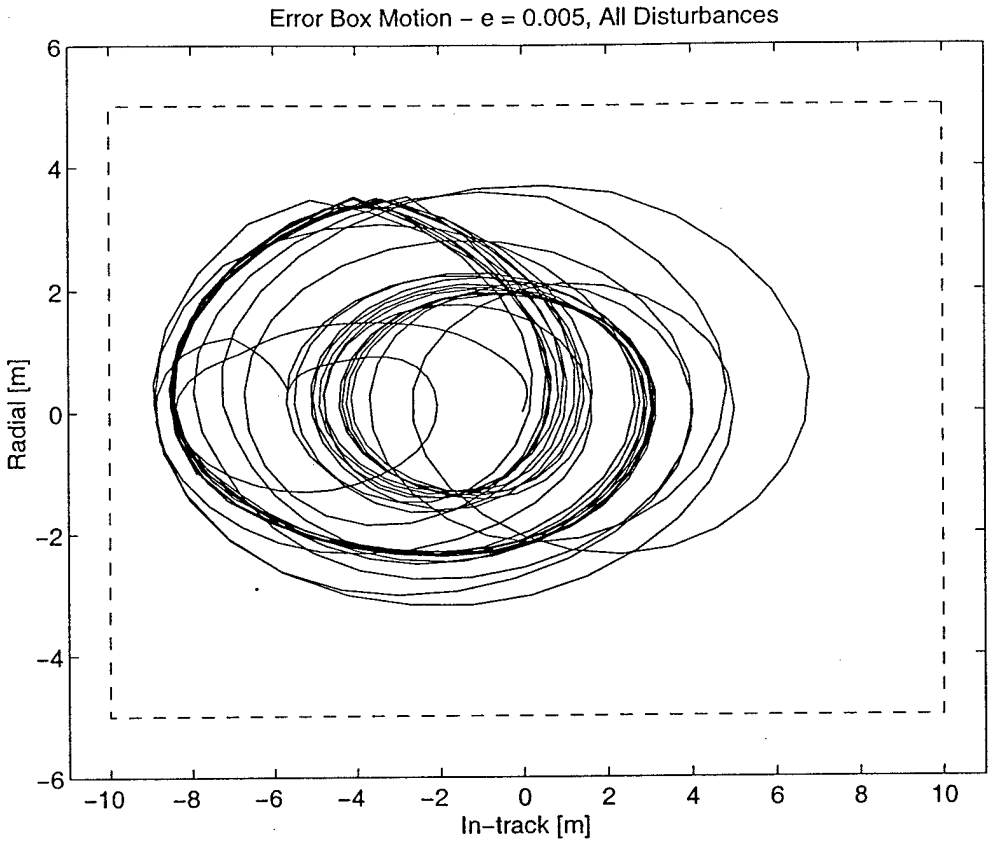

Figure 4-23: Error box motion with all disturbances included for a reference orbit $e = 0.005$.

tion. By using Lawden's equations in the LP formulation, the osculating eccentricity could easily be included in the dynamics for the trajectory planning, capturing some of the effects of J_2 in the dynamics.

Simulation #4 : Dynamics Comparison

Several nonlinear simulations were performed using the FreeFlyer™ orbit simulator [34] in order to compare the effectiveness of the LP control method based on different forms of the dynamics. The simulations involve two similar vehicles. One spacecraft acts as the formation center and serves as the reference orbit and the other vehicle is initialized on a passive aperture. The reference orbit has a semi-major axis of 6900 km and inclination 35°. Simulations were performed for eccentricity $e \approx 0$ and $e = 0.005$. The passive aperture formed projects a 400×200 m ellipse on the orbital plane and oscillates with an amplitude of 100 m in the cross-track direction,

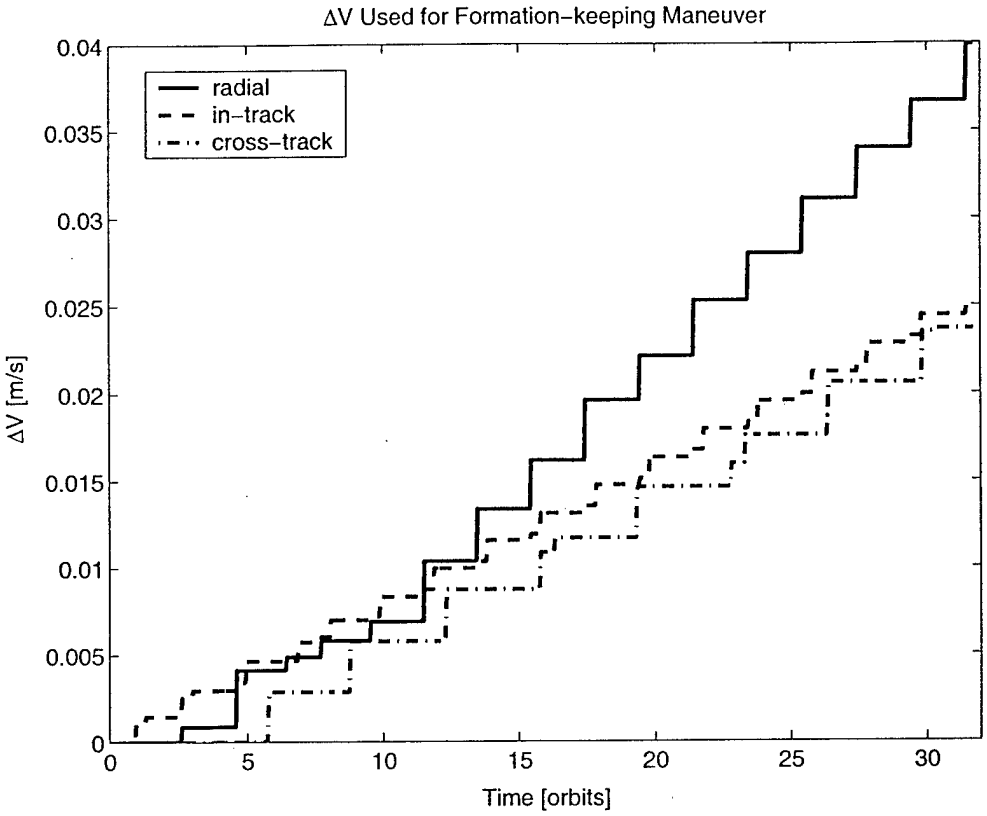

Figure 4-24: ΔV fuel cost with all disturbances included for a reference orbit $e = 0.005$. The average fuel cost is 8.241 mm/s/orbit.

achieved through an inclination difference between the two satellites. This aperture is maintained through formation-keeping over two days. Each satellite is modeled as an Orion spacecraft based on current specifications for the Orion-Emerald mission [56].

Each vehicle has a mass of 45 kg, but have slightly different ballistic coefficients, resulting in a differential drag disturbance. The differential drag is modeled as a constant 5×10^{-8} m/s^2 disturbance acceleration in the LP. The spacecraft thrusters are restricted to provide a maximum acceleration of 0.003 m/s^2. The maximum thrust corresponds to turning on the thruster for the full time-step. Sensor noise was also included as a true state plus white noise component. The noise is restricted to values less than 2 cm on position and 0.5 mm/s on velocity. These values are consistent with currently predicted noise levels using carrier phase differential GPS as the relative navigation sensor [51]. All disturbances (J_2, drag, solar radiation pressure, *etc.*)

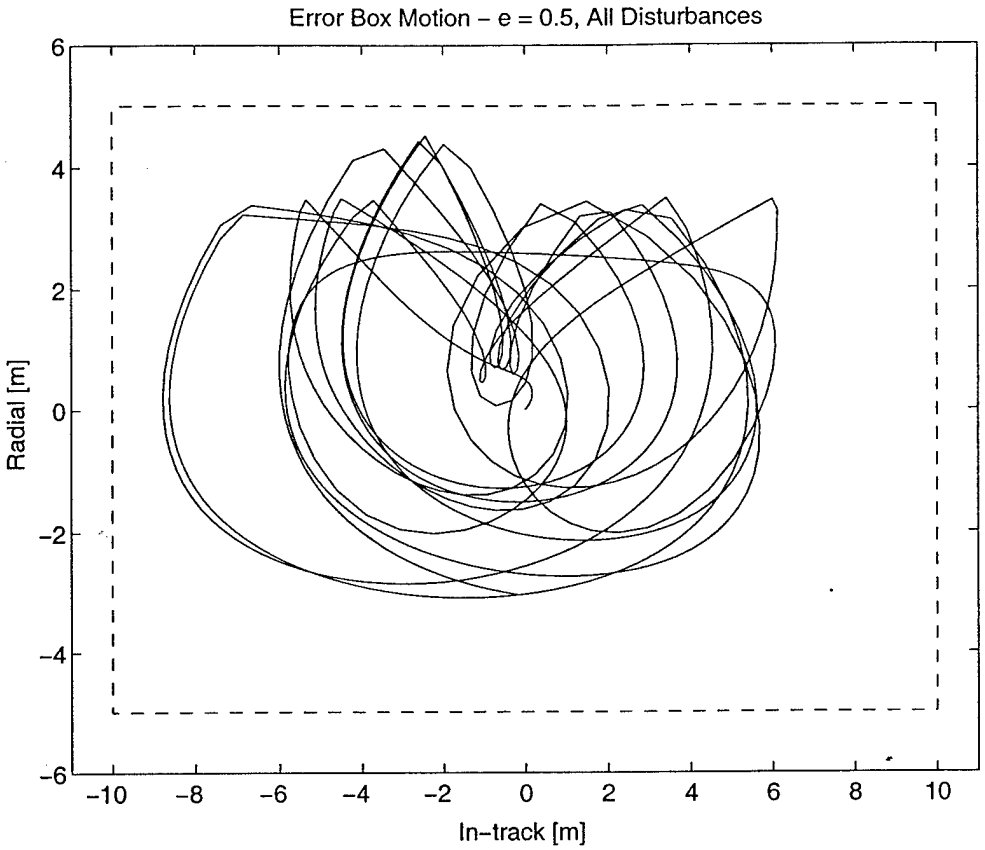

Figure 4-25: Error box motion with all disturbances included for a reference orbit $e = 0.5$. Semi-major axis 14000 km.

were included in all simulations, but the dynamics used in the controller are varied for comparison. The relative dynamics for the spacecraft are discretized on a 10.8 second time-step and the LP plan horizon is half an orbit (approximately 45 minutes). Control inputs are allowed and state constraints are applied every 108 seconds in the LP design. This reduces the LP size and decreases the solution time to 1–5 seconds.

Due to the stochastic nature of the simulations resulting from the sensor noise, each specific simulation in the following discussion was run three times, for a total of 24, two day simulations. There are two main parts that were varied for the simulations. The first part is the dynamics and resulting closed form-solutions used for initialization and to determine the desired state, labeled in the Table as **Rel Dyn**. Only Lawden's and the J_2 dynamics are varied in this part because Hill's does not provide a fuel efficient desired state in the presence of J_2. In fact, using Hill's results

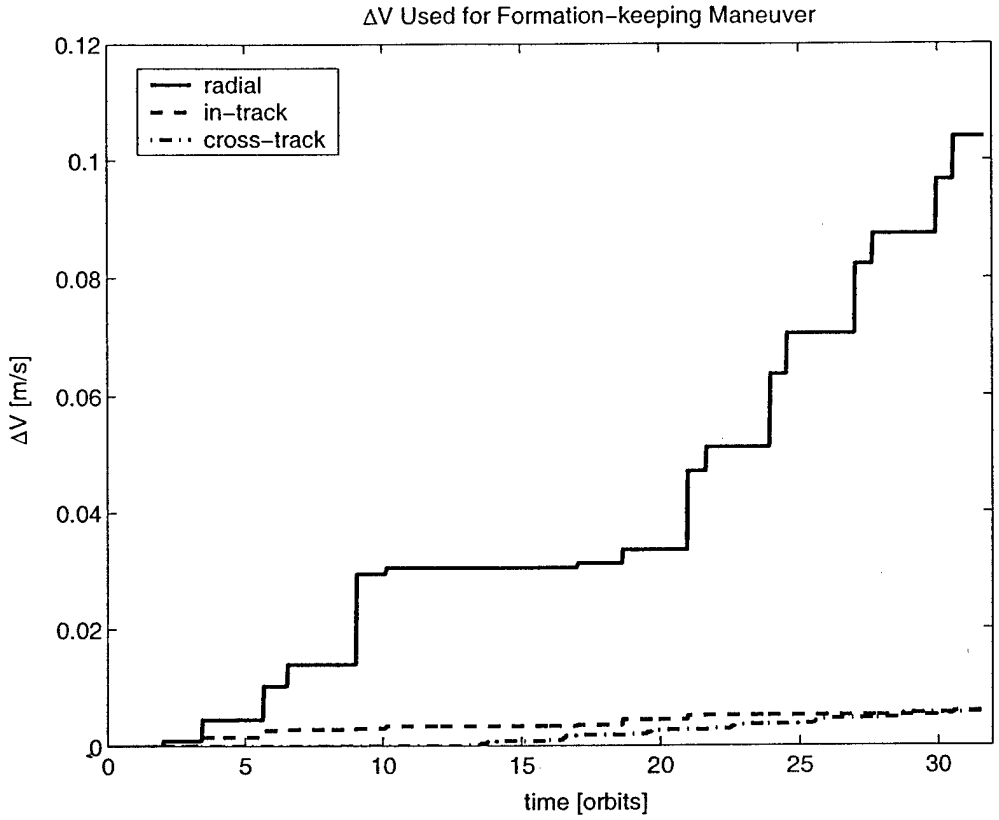

Figure 4-26: ΔV fuel cost with all disturbances included for a reference orbit $e = 0.5$. Semi-major axis 14000 km. The average fuel cost is 11.812 mm/s/orbit.

in a fuel cost of approximately 300 mm/s per orbit in the presence of J_2. The second part varied is the dynamics used in the LP, labeled **LP Dyn**. All three forms of dynamics are used in the LP.

Table 4.3 summarizes the average fuel cost for formation-keeping using the various forms of the dynamics. The simulation results show that for nearly circular orbits, the J_2 dynamics provide the most fuel efficient results, with the other combinations of dynamics resulting in only a minimal increase in fuel cost. The correction of the mean motion with the parameter c in the dynamics with linearized J_2 effects or the inclusion of eccentricity in both the relative dynamics and periodicity conditions lead to similar results and similar fuel cost savings. The improvement in using J_2 dynamics arises mostly from the inclusion of the secular cross-track disturbance, which is unmodeled in the other dynamics.

Table 4.3: Fuel comparison for formation-keeping using each set of dynamics.

Rel Dyn	LP Dyn	$e \approx 0$ mm/s/orbit	$e = 0.005$ mm/s/orbit
J_2	J_2	5.65 $\pm$ 0.5	8.31 $\pm$ 2
Lawden's	Hill's	7.65 $\pm$ 0.5	4.82 $\pm$ 1
Lawden's	Lawden's	7.64 $\pm$ 0.5	4.80 $\pm$ 1
Lawden's	J_2	6.12 $\pm$ 0.5	4.01 $\pm$ 0.5

However, for a slightly eccentric reference orbit, the J_2 dynamics no longer provide an accurate description of the dynamics for determining the desired state. This degradation is a result of the fact that the J_2 dynamics still assume a circular reference orbit. References [19, 21] have shown the significance of ignoring eccentricity. These simulations also confirm the results in Reference [19] that using Hill's in the LP formulation does not significantly increase fuel cost. For the eccentric orbit, using Lawden's equations to specify the desired state and using the J_2 dynamics for the LP provides approximately 50% fuel cost reduction. This combination captures the orbit eccentricity in the prediction of the desired state and knowledge of the J_2 disturbance in the LP.

A single simulation for each case discussed above was performed over a two week period to verify the control effectiveness over long time periods. The fuel cost numbers are within the uncertainty bounds of those presented in Table 4.3. An example simulation over two weeks with $e = 0.005$ and using Lawden's equations to specify the desired state and the J_2 dynamics in the LP is shown in Figures 4-27 and 4-28. Figure 4-27 shows the relative motion between the two vehicles while Figure 4-28 shows the error box motion for a one day period during the simulation in order to observe the motion inside the error box. Figure 4-29 shows the error box motion over the entire two week simulation. Figure 4-30 shows the fuel cost during the simulation in the radial, in-track, and cross-track directions. The average fuel cost for this simulations was 4.0 mm/s per orbit.

The fuel cost for formation-keeping has been significantly reduced from the simulations in Section 4.2.2 and simulations earlier in this section through advancements

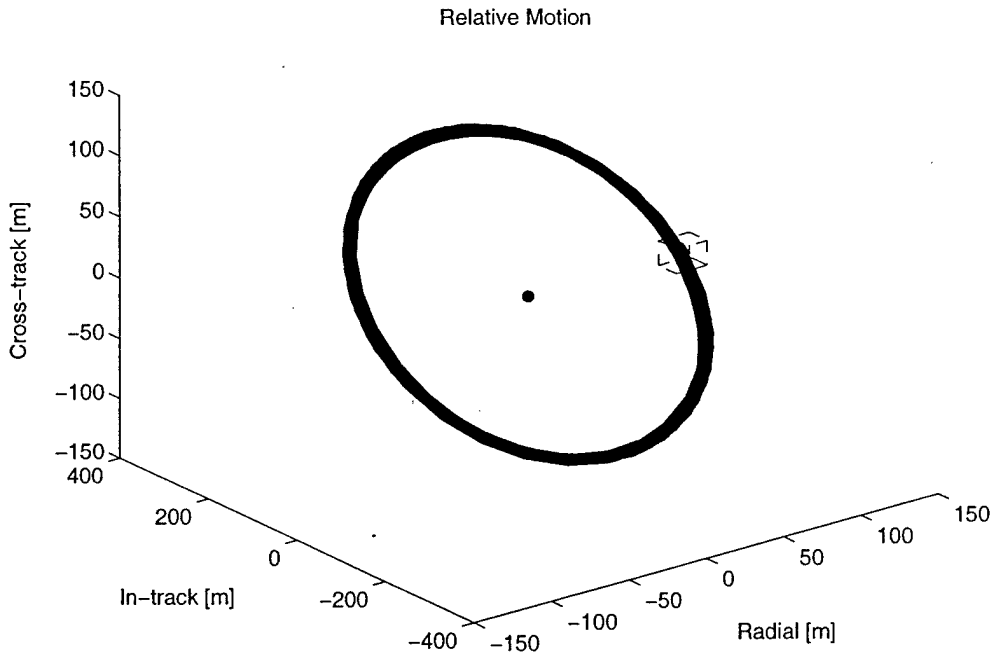

Figure 4-27: Relative motion of spacecraft during the two week simulation. The circle represents the formation center and the diamond enclosed in the box represents an example of the desired state and error box.

in the guidance algorithm and reduction in sensor noise. Specific improvements are: 1) selection of the best dynamics to determine the desired state to maintain a passive aperture, 2) inclusion of the linearized J_2 effects in LP dynamics model, and 3) relaxation of the position tolerance variable to always allow feasible solutions. The inclusion of J_2 effects in the dynamics increases the accuracy of the model for developing trajectories. This means less replanning due to deviations from the designed trajectory, which also reduces fuel cost. The reduction in the sensor noise level and reformulating the problem for an always feasible solution allow longer plan horizons, which also reduces fuel cost. Further examination of the error box shape and size could lead to even further fuel savings.

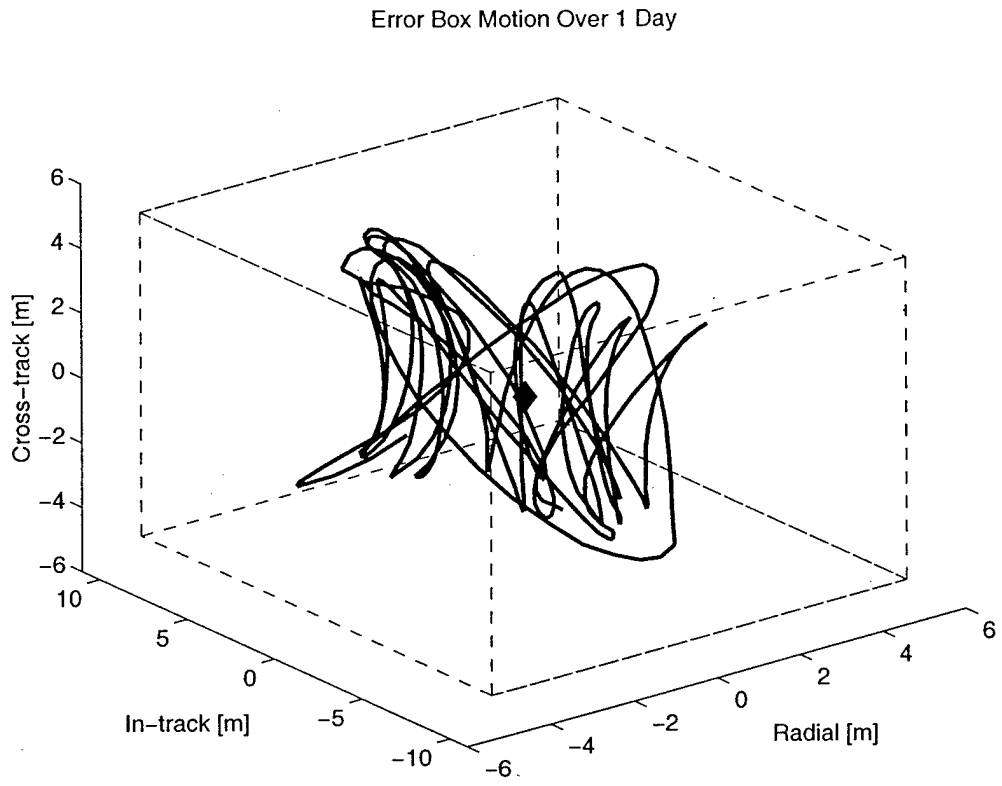

Figure 4-28: Error box motion of spacecraft during simulation over a one day period. The diamond in the center of the box represents the desired state for maintaining the aperture.

4.6 Additional Actuator Constraints

Another implementation issue is a method of modeling actuator constraints in the control algorithm. Actuator constraints can be added to the LP problem by using binary variables and solving a Mixed Integer Linear Program (MILP) problem. The binary variables are used as ON/OFF switches for the control inputs in the LP problem. This work applies the MILP techniques that have been developed for the collision avoidance and plume impingement of formation flying spacecraft [58, 59]. Note that software, such as CPLEX, is available to solve these MILP problems [39, 60, 61].

The binary variables, d, are linked to the control inputs through the expression

$$-d_i(k) + u_i(k) \leq 0 \tag{4.16}$$

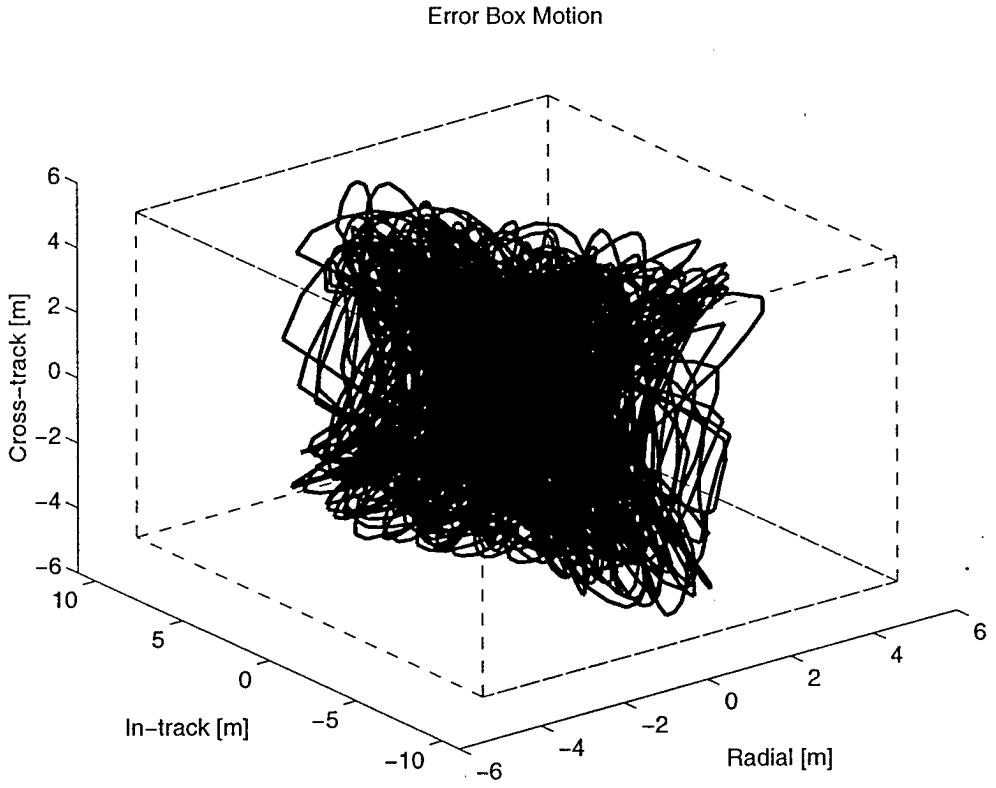

Figure 4-29: Error box motion of spacecraft during the two week simulation.

where $u_i(k)$ is the control input and $d_i(k)$ is the associated binary variable in the i^{th} direction at time-step k. This expression restricts the control input to 0 if the binary is 0 (OFF) and the control input is restricted to $u_i(k) \in [0, 1]$ when $d_i(k) = 1$ (ON).

4.6.1 Minimum Impulse Bit

Maximum limits can be placed on the actuator in a standard LP by defining the input variable $u_i(k) \leq u_{\max}$, however, a lower limit cannot be specified in this form. A lower limit would require the thruster to be on at all times because $u_i(k)$ cannot simultaneously satisfy the lower limit constraint and be equal to zero unless the lower limit is zero. Binary variables allow the formulation of a lower limit actuator constraint of the form

$$u_i(k) - (d_i(k) - 1)u_{\min} \geq u_{\min} \tag{4.17}$$

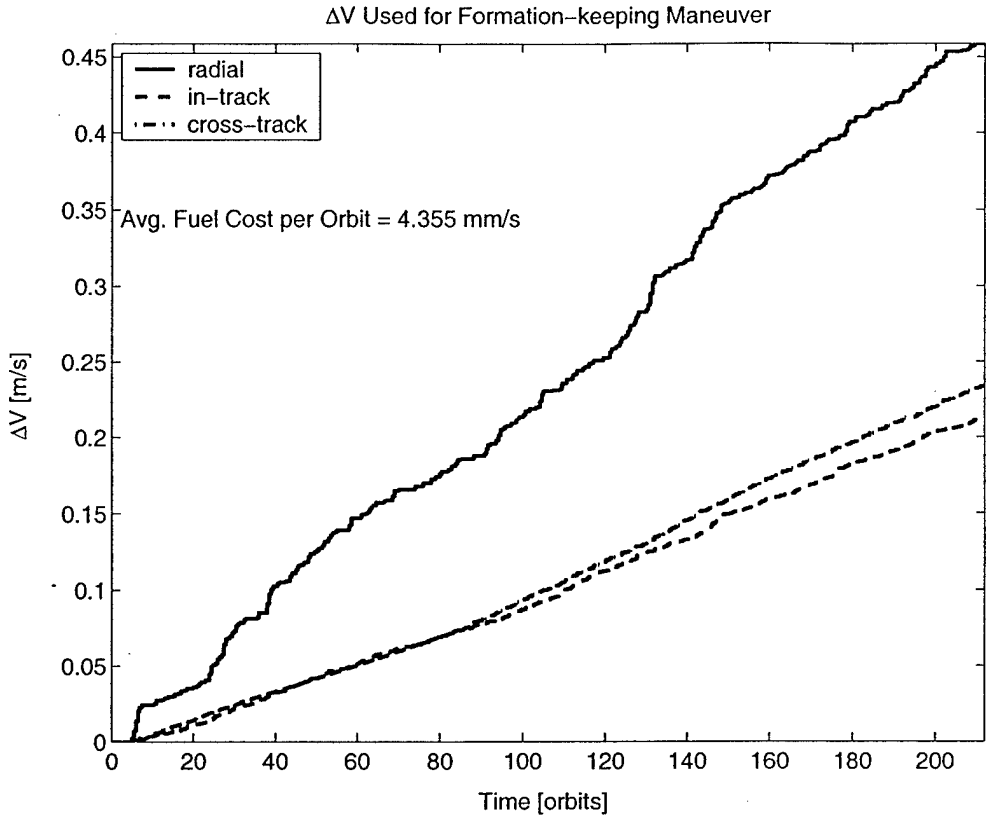

Figure 4-30: ΔV fuel cost during simulation.

When $d_i(k) = 0$, the control input is constrained to equal zero through Equation 4.16, but if $d_i(k) = 1$ then $u_i(k)$ must be greater than $u_{\min}$.

4.6.2 Sequence Constraints

Additional constraints can be placed on the actuators such as limits on the number of actuators that are active at any time for power concerns or constraints on actuation sequences. For example, the TechSat21 satellite currently only has one large thruster for orbital maneuvers (*i.e.,* formation reconfiguration). As a result, a thrust can only be applied in one direction at one time-step and a delay is required for an attitude maneuver to re-align the thruster before actuation can occur in a new direction. This constraint could also arise due to an actuator failure on a spacecraft. In the event one or multiple thrusters fail on a spacecraft, the original LP problem is no longer applicable, but the problem can be modified to include these constraints and a fuel-optimal

solution is obtainable. Binary variables allow constraints on the number of actuators activated over a particular interval through a summation. The following constraint restricts actuation in any direction other than the previous actuation direction over the next t_{delay} number of control input steps

$$5TS_{\text{delay}}d_i(k) + \sum_{m=k}^{m=t_{\text{delay}}} d_j(m) \leq 5t_{\text{delay}}, \forall j \neq i \tag{4.18}$$

By including the delay, an attitude maneuver could be performed to reorient the available actuators to continue to provide actuation in all directions at a reduced overall performance. The parameter t_{delay} is multiplied by five because there are five additional actuation directions.

An alternative to solving the MILP problem is to create a buffer that applies the designed control inputs from the original LP as soon as possible by placing the inputs in a buffer to be processed according to the constraints. This however creates errors in the implementation of the plan and need not result in the desired performance.

Two simulations are performed to demonstrate the effect of the MILP and buffered control. The spacecraft begins in a 100 m in-track separation and ends on a passive aperture. The reference orbit has a semi-major axis of 6900 km and inclination 35°. The passive aperture formed projects a 400 × 200 m ellipse on the orbital plane and oscillates with an amplitude of 100 m in the cross-track direction, achieved through an inclination difference between the two vehicles. For the simulation, the dynamics were discretized with a 30 second time-step, the input-step was every two minutes, and the actuator delay between firing in each direction was ten minutes. Figure 4-31 shows the resulting motion from using a buffer to enforce the constraints (top plot) and using MILP to include the constraints in the planning process. The results show that, with the inputs buffered to satisfy the constraint, the periodic motion is not centered about the reference orbit as originally planned. Other simulations using the buffer resulted in non-periodic motion.

The bottom plot is for the simulation using MILP to include the constraints in the plan. The final motion of the MILP simulations is the same as the desired

motion without actuator constraints, but the fuel cost increased from 34.56 mm/s to 36.66 mm/s due to the additional constraints. The LP problem with no actuator constraints requires a total of six control inputs, however, two of these occured at the same time, which would be a violation of the actuator constraints. The MILP problem resolved the violation but required a total of seven inputs. Note the error in final relative motion using the buffer was a result of incorrectly applying a single control input.

Formation-keeping simulations show that, for actuation constraints similar to the previous simulations, violations of the constraints can occur for $\approx$20% of all actuation inputs. The buffer control was implemented with little loss of performance and only a slight increase in fuel cost for formation-keeping. This is because the control inputs are much smaller in magnitude. The terminal constraint is also not as critical to the future motion of the spacecraft because the control is designed to maintain the satellite within a box rather than meet a specific terminal state. Solving the MILP problem with actuator constraints results in a slight increase in fuel cost.

The optimization problems shown here can be easily translated into the AMPL modeling language [61]. An AMPL model file contains the constraint forms for all cases, while the data is written to an AMPL data file by a MATLAB™ script. CPLEX optimization software is used to solve the problem [60]. A series of scripts in MATLAB™ and AMPL allow the entire path-planning problem to be invoked by a single command. The problems were solved in 5-15 seconds on a 1GHz PC with 256MB RAM.

4.7 Chapter Summary

This chapter addresses several aspects of implementing the LP controller in a real-time control system. Because the control algorithm is a planning controller rather than reactive controller, an algorithm initiation and execution verification method is required. This is achieved by introducing an error box centered on the desired state for the spacecraft. The error box acts as a trigger to start the control algorithm

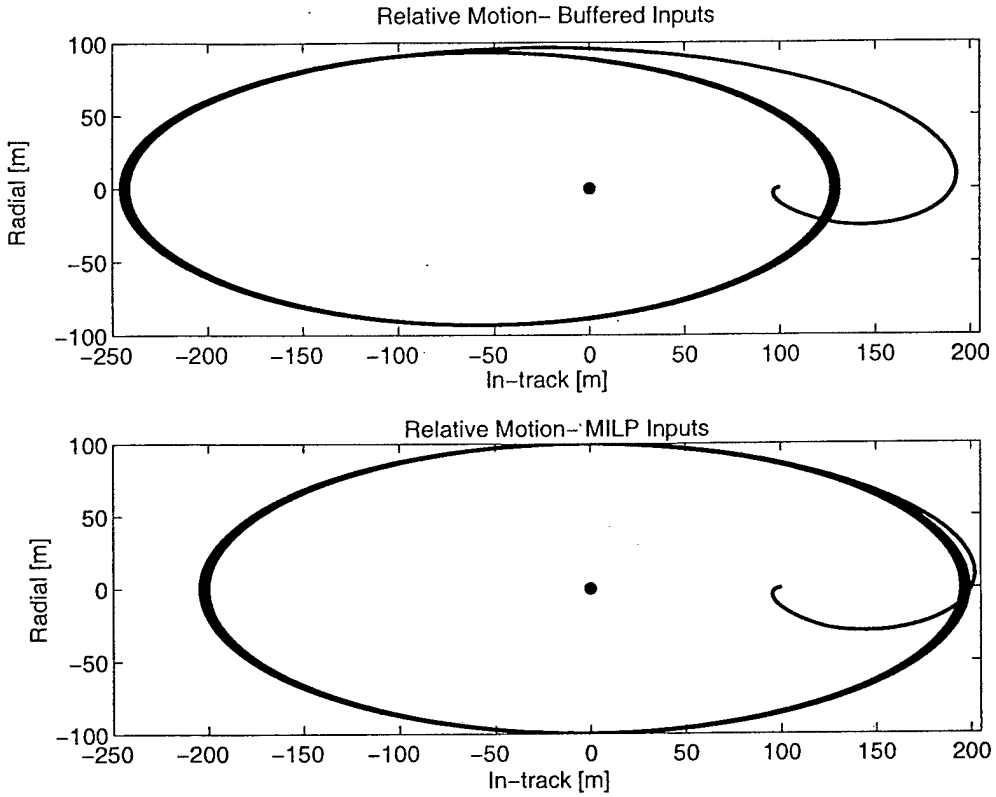

Figure 4-31: In-plane view of the relative motion for simulations with actuator constraints. The top graph shows the resulting motion if the inputs are buffered to meet the constraints. The motion is no longer centered about the reference orbit. The bottom plot is the relative motion achieved when using MILP to plan with the actuator constraints.

as well as a means to incorporate state feedback checking. The current state of the spacecraft is compared with the designed state and a decision is made whether to continue using the existing plan or make a new plan. Sensor noise is also addressed by modifying the LP algorithm to add robustness to initial condition uncertainty created by the noise on the state measurements. The robust solution can lead to feasibility issues which are resolved by introducing a new variable to relax the constraints in the problem such that a feasible solution is always obtained. The solution time for the LP problem is also reduced by selectively removing variables and constraints from the LP control problem. The relative dynamics are also investigated in terms of specifying the desired state and modeling the spacecraft motion relative to the desired state.

Numerous nonlinear simulations are performed to determine which dynamics models should be used in the LP controller design. The chapter concludes with methods of including additional actuator constraints such as minimum impulse bit and sequence constraints by introducing binary switching variables and solving a mixed integer linear programming problem.

Chapter 5

Complete Formation Control Algorithm

Chapter 3 described a linear programming method to determine fuel-optimal trajectories for both formation maneuvers such as aperture reconfiguration and formation-keeping maneuvers. Methods of including fleet cooperation were also discussed for both types of maneuvers. Chapter 4 discussed and presented solutions to several issues that must be addressed in order to implement the LP controller in a formation control system. This chapter presents the complete formation control algorithm. The chapter begins with the high-level coordination algorithm and then moves to the low-level control algorithms which exist in each vehicle. The algorithms are discussed in terms of procedure and required information flow throughout the fleet. The chapter concludes with a final simulation demonstrating the control system in a typical spacecraft formation flying mission. The performance of the control system is discussed in detail.

5.1 High-Level Coordination Algorithm

The high-level coordination algorithm is performed on a single vehicle in the fleet acting as the coordinator. Assuming the coordination algorithm is programmed on multiple vehicles, the coordinator vehicle can change during the mission, eliminating

a single point failure for the fleet. The high-level coordination algorithm performs two main functions. The first function calculates the reference point state based on the current states of the fleet. The reference point is used to specify the formation center and the desired formation geometry in the low-level control. The second function coordinates the formation maneuvers for a fleet initialization or reconfiguration.

5.1.1 Reference Point Coordination Algorithm

Three types of reference point representations are discussed in Section 3.2.2, each with advantages and disadvantages. This section describes the information flow required between the high-level coordination and low-level controllers for the algorithms as well as the sequence of calculations that must occur to specify the reference point for the low-level controllers. The reference point coordination algorithm calculates the reference point state for the fleet. The reference point is used to determine the formation center state, position and velocity, which is used to specify the desired state for each vehicle. The formation center state is specified relative to the reference spacecraft, which is the origin of the reference frame for all measurement of relative states in the fleet. The reference spacecraft is not necessarily the same vehicle that performs the coordinating algorithms.

If the reference orbit method is used to specify the reference point, then the coordinator acts as the reference orbit propagator and determines the location of the reference point relative to the reference spacecraft. The formation center is then fixed to the reference point. At each time-step, the coordinator propagates the absolute state of the reference orbit to the current time. The formation center state relative to the reference spacecraft is then transmitted to the rest of the fleet for use in the low-level control. The reference orbit dynamics model used in the propagation can be updated using a time history of the states of the fleet to adjust disturbance or dynamics properties in the propagator. This, however, will require the states of all vehicles in the fleet to be sent to and recorded by the coordinator. The coordinator will also need an estimator to determine the values of parameters used for the dynamics and disturbance models in the propagator, increasing computational load. The

reference orbit propagator can also be placed on each vehicle, eliminating any fleet communication requirements. However, ensuring that all vehicles in the fleet obtain the same location for the formation center will be difficult.

If the reference point is determined through the leader-follower approach, then no propagator is required for the reference point. The reference point moves with the leader vehicle. The states of the other vehicles in the fleet are also not required by the leader, therefore information flow across the fleet is reduced. If the leader spacecraft is placed at the center of the formation, then the formation center state is the leader spacecraft state. If the leader spacecraft is on the aperture, then the formation center is specified using the desired state for the leader spacecraft. The coordinator only needs to transmit the formation center state and the orbital elements used for the dynamics and desired state calculations by the other vehicles in the fleet. The desired states of the follower vehicles are calculated in the low-level controller.

If the reference point is determined using the virtual center method, the coordinator algorithm calculates the location of the virtual center relative to the reference spacecraft that minimizes the difference between the actual vehicle states and desired vehicle states of the total fleet. The details of the virtual center calculation are shown in Section 3.2.2. The information flow between the high-level coordinator and low-level controller for the virtual center calculation is shown in Figure 5-1. The low-level controller must send the current estimated state, y_{err}, and the current desired state, y_{des}, to the coordinator to calculate the reference point. The desired state is either the current state required to maintain a passive aperture during formation-keeping or the current state from the designed trajectory plan for a formation maneuver. If a fuel weighting is used to adjust the virtual center, then the current fuel state must also be transmitted. In addition, if the control actions of the other vehicles are considered in the low-level controller, then the current control input plan, u, must be broadcast for use by other vehicles. The coordinator returns the center state, y_c, and any parameters used in the low-level LP controller such as orbital elements and disturbance parameters. Figure 5-1 will be discussed in further detail for the low-level controller in Section 5.2.

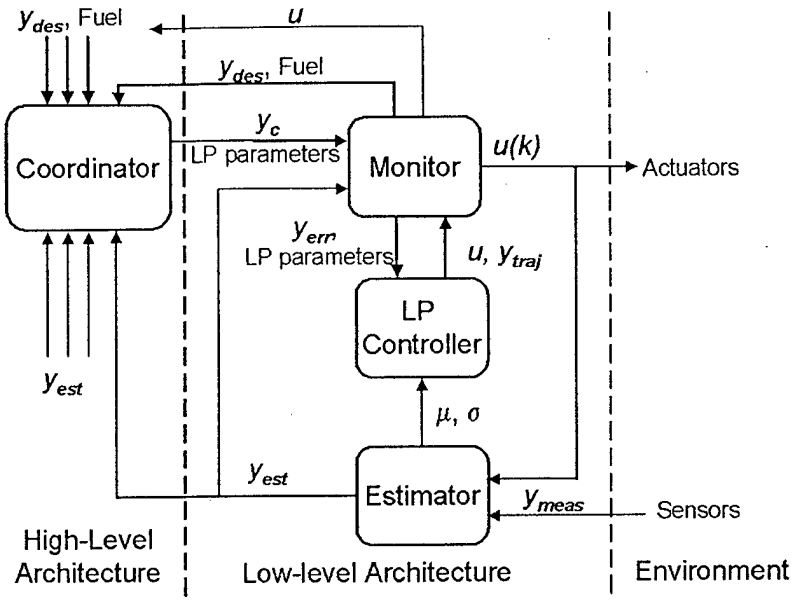

Figure 5-1: Low-level control diagram.

Although the three methods require different coordination calculations, the output of the reference point coordinator is always the position and velocity of the formation center relative to the reference spacecraft and the orbital elements required for the relative dynamics in the low-level controller. The method used for determining the reference point and formation center state only affects the amount of information required by the coordinator to calculate the center.

5.1.2 Formation Maneuver Coordination Algorithm

The second type of coordination algorithm is for the formation maneuvers. The coordinator first determines the possible final states on the new aperture and the time length for the maneuver. The ordered list of possible final states and time length as well as the orbital elements required for the dynamics are sent to each vehicle in the fleet. The low-level controller uses this information to calculate the ΔV fuel cost maps for each vehicle in the fleet to achieve each possible final state configuration on the new formation geometry.

Each vehicle in the fleet computes the fuel cost to achieve each possible final state

by solving terminal constraint LP problems for the minimum fuel with the plan length specified by the coordinator. The plan length is chosen to minimize a combination of maneuver time and fuel costs. The plan length can be increased to reduce fuel cost, but plan horizons greater than one orbit do not further reduce the fuel costs as demonstrated in [62]. The costs for each final position are grouped in the same order as the final states and returned to the coordinator. The current fuel state for each vehicle can also be sent to the coordinator to adjust the final position assignment based on the past fuel use for each vehicle.

The coordinator receives the fuel cost maps from each vehicle and groups them together to solve the formation assignment problem discussed in Section 3.2.1. The result of the assignment problem is a final state for each vehicle. This state is transmitted to the corresponding vehicle where a final terminal constraint LP is solved and the control inputs and trajectory is stored for use in the low-level control in the formation maneuver mode as described in Section 5.2.1.

5.2 Low-Level Control Algorithm

The low-level control algorithm exists on each spacecraft in the formation and consists of the spacecraft monitor, the LP control algorithm, and estimation algorithms. Figure 5-1 shows the low-level controller and the interaction with the high-level coordinator and environment. The following section describes the sequence of events in the low-level controller for a single spacecraft.

The algorithm description begins with the measurements taken by sensors. The sensors are in the lower right corner of Figure 5-1. The raw sensor measurements enter an estimation algorithm [51, 63]. The LP controller designed in this thesis will work with any estimation algorithm provided the estimator outputs the relative position and velocity as well as the statistical properties, mean (μ) and standard deviation (σ). The statistical information is passed to the LP controller for use in the robust LP design discussed in Section 4.2.2. The estimated state, y_{est}, is the state relative to the reference spacecraft as described in Section 3.2.2. This relative state is transmitted

to the coordinator to calculate the formation center state.

The next step in the low-level control is for the control monitor to receive information from the coordinator spacecraft as discussed in Section 5.1.1. The position of the formation center relative to the reference spacecraft is received by the vehicles as well as various data required for formulating the LP problem. These parameters include: 1) orbital elements $(a, e, i, \Omega, \theta)$ for the relative dynamics and desired state calculations, 2) weighting used in the virtual center calculation, which adjust disturbance models, 3) plan horizon (length), and 4) error box parameters. If the control inputs from other vehicles are included in the LP formulation, then control input plans for all other vehicles in the fleet must also be received from either the coordinator or the other vehicles directly.

The information from the coordinator enters the spacecraft monitor on the individual vehicles. The spacecraft monitor decides when control action is required and implements the control inputs for the current time-step. The spacecraft monitor operates in two modes: 1) formation maneuver mode and 2) formation-keeping mode. These two modes are similar but will be discussed separately. The formation maneuver mode will be discussed first followed by the formation-keeping mode.

5.2.1 Formation Maneuver Mode

In the formation maneuver mode, the monitor uses the location of the formation center and the current state of the spacecraft relative to the reference spacecraft to calculate the spacecraft state relative to the center. If no control plan exists, then a new formation maneuver has been requested by the coordinator and the formation coordination algorithm discussed in Section 5.1.2 is initiated. When a plan does exist, an error box is fixed to the current designed position obtained from the LP designed trajectory stored on-board the spacecraft. The current state relative to the center is differenced with the current designed state to produce an error state, y_{err}. If the error state exceeds the tolerance specified by the error box, the monitor requests a re-plan of the control inputs based on the current vehicle state. A more detailed discussion of the re-plan decision and method is given in Section 4.2.3.

If a re-plan is requested in the formation maneuver mode, the plan length for the LP is calculated to terminate the plan at the original time specified for the formation maneuver. The length reduction is calculated using the original plan length and current step in the plan which are both available to the monitor. The monitor passes the adjusted plan length, current state relative to the center, and other parameters needed for the algorithm to the LP controller. The LP controller solves the resulting terminal constraint LP and returns the new list of control inputs and the resulting trajectory. The current step is also reset to the start of the new plan. Reducing the plan length can result in an infeasible solution if the terminal state cannot be reached in the specified time. If the LP solution is infeasible, the plan length is increased and the LP is solved again to generate a feasible trajectory.

When the new plan is completed or if the monitor decides to continue with an existing plan, the control inputs for the current step in the plan are selected from the stored plan and implemented through the actuators. The current step in the plan is then updated for the next time sequence through the controller. If the end of the plan is reached, the formation maneuver is completed and the monitor switches to formation-keeping mode.

5.2.2 Formation-keeping Mode

In formation-keeping mode, the spacecraft monitor calculates the spacecraft state relative to the formation center using the same method described in the formation maneuver mode. This state is now differenced with the desired state required to maintain the aperture to produce an error state. The error state is used to determine the appropriate control action. The monitor determines: 1) if control action is needed when a plan does not exist; 2) if the controller should continue to use the existing plan; or 3) make a new plan. The action taken depends on the error state and the definitions of the three levels of the error box specifying the tolerance.

The error box and decision process is discussed in Section 4.1. A decision tree for the spacecraft monitor is shown in Figure 5-2. The error state, y_{err}, is compared to each level in the error box description. If the error state is inside the trigger box

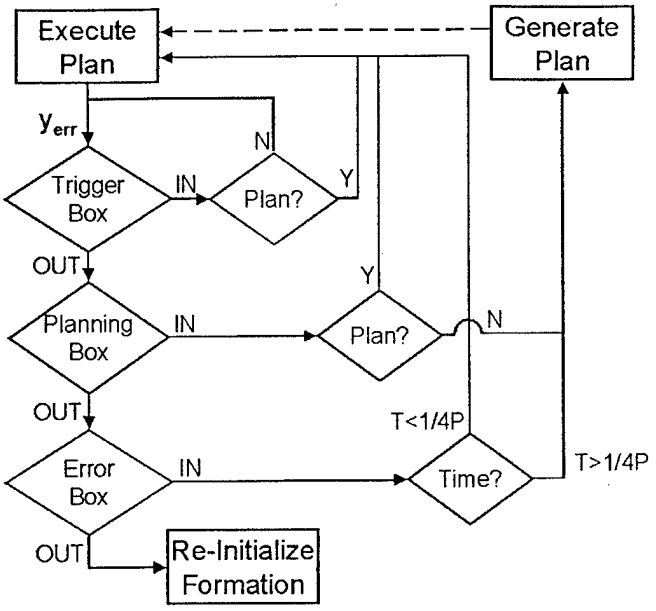

Figure 5-2: Decision tree for the spacecraft monitor in Figure 5-1. At each error box level, the monitor determines if the error state is inside or outside the box. For the first two boxes, the next step is to determine if a plan exists. For the last box, the first quarter of the plan is implemented and if the state remains outside the box, a new plan is generated. If the error state exceeds all boxes, a corrective action must be taken. One possible action is to re-initialize the formation using a formation maneuver.

and no plan exists, the control system remains idle. If a plan does exist, the monitor continues to execute the current plan. If the monitor decides to continue with an existing plan, the control inputs for the current step in the plan are selected from the stored plan and implemented through the actuators. The current step in the plan is then updated for the next time sequence through the control. If the error state is outside the trigger box, inside the planning box, and a plan exists, then the monitor will continue to execute the plan. If no plan exists, the monitor will request a new plan by activating the LP controller to generate a new set of control inputs and trajectories. If the error state is outside the planning box and inside the error box a plan will exist. Now the decision process is based on the current step within the plan. If less than one-quarter of the plan has been executed, the monitor will continue to use the current plan. If more than one-quarter of the plan has been executed, the

monitor will request a re-plan and a new set of inputs is generated through the LP algorithm. A portion of the plan is executed even if the error state is outside the planning box to allow the plan to attempt to control the spacecraft back inside the box. If a portion of the plan was not allowed to execute, the monitor would request a re-plan every time-step and the plan would never get executed. If the monitor allows the plan to be fully executed without checking the state, then the control actions are being executed for a state that does not matched the design state and the resulting motion can be quite different from the designed response. If the error state exceeds the error box, the position tolerance has been violated. The always feasible solution will continue to allow formation-keeping control sequences to be generated, but the formation could be re-initialized with a formation maneuver to correct the large error.

To produce a new plan for formation-keeping, the monitor must pass the current error state of the spacecraft, the length of the plan, and other parameters needed for the formation-keeping algorithm to the LP controller. If the LP controller uses the control inputs from other spacecraft in the development of the LP, then this information and a vehicle weighting must also be provided by the monitor. The monitor will also broadcast the spacecraft's control input sequence and current step in the plan to other vehicles for use in the LP controllers on-board other spacecraft. The method of including external control inputs is discussed in Section 3.2.2. The LP controller uses this information and the sensor noise parameters from the estimator to develop control inputs to maintain the vehicle within the tolerances over the plan length. The robust LP is discussed in detail in Section 4.2.2. The resulting plans are returned and stored by the monitor and the current step in the plan is reset to the beginning of the plan. The first control inputs in the new plan are implemented through the actuators and the current plan step is updated for the next control cycle. The control action results in a response in the spacecraft motion, which is observed by the sensors, completing the low-level control loop.

The high-level coordinator and low-level controller combine to provide a flexible architecture to provide real-time control using linear programming to solve for fuel optimal control input sequences for a fleet of spacecraft. The architecture allows the

controller to easily transition between formation maneuvers and formation-keeping during a mission.

5.3 Final Simulation

A final simulation was performed to demonstrate the effectiveness of the control system design presented in this thesis. Several formation maneuvers were performed during the simulation with formation-keeping maneuvers used to maintain the formation geometry over extended periods of time. FreeFlyer™ orbit simulation software is used as the nonlinear propagator for each satellite. MATLAB™ mathematical software is used to perform the calculations for the controller. The entire control system is executed without human intervention during the simulation. This section describes the details of the simulation and analyzes the performance of the control system presented in this thesis.

5.3.1 Simulation Description

The final simulation consists of three vehicles, each modeled as an Orion spacecraft [56]. It is assumed that each 45 kg spacecraft has a slightly different drag coefficient resulting in a differential drag between vehicles. All other disturbances such as gravity perturbations, solar radiation pressure, atmospheric lift, and third body effects are also activated in the FreeFlyer™ propagator. Sensor noise is included in the simulation as a white noise component added to the true relative state. The magnitude of the sensor noise is restricted to less than 2 cm for position and 0.5 mm/s for velocity. These values are based on current estimates of sensor noise using carrier phase differential GPS as the relative navigation sensor [51]. The spacecraft thrusters are restricted to provide a maximum acceleration of 0.003 m/s^2. The maximum thrust corresponds to activating a thruster for the full time-step. The spacecraft attitude is neglected in the simulation. All control inputs are specified in a local-vertical local-horizontal frame and can be mapped to the thruster directions based on the current spacecraft attitude. This step is separate from the control al-

gorithm and is not considered in the simulation. The formation is initialized on a reference orbit with semi-major axis 6900 km and eccentricity of 0.005, similar to a space shuttle orbit. This results in an orbital period of about 95 minutes. The inclination of the reference orbit is 35°, introducing a significant differential gravity disturbance for spacecraft with differences in inclination.

The high-level coordinator calculates the reference point using the virtual center procedure described in Section 3.2.2. The virtual center is updated at every time-step, eliminating the need to propagate the reference point. The formation center is fixed to the virtual center for the fleet. The low-level controller for each spacecraft utilizes Lawden's equations to determine the desired state for any passive apertures in the simulation. Lawden's dynamics were selected based on the simulation results in Section 4.5.3, which shows a significant fuel cost reduction over the J_2 dynamics for orbits with significant eccentricity (e=0.005). The J_2 relative dynamics are selected for the LP controller. The J_2 dynamics are linear time-invariant, which reduces the computational complexity in the formulation of the LP problem when compared to the time-varying Lawden's dynamics. The simulations in Section 4.5.3 also show some fuel cost savings that results primarily from the cross-track disturbance model provided in the J_2 dynamics. The differential drag is modeled as a constant in-track disturbance acceleration in the LP controller. The magnitude of the disturbance is calculated based on the difference between the drag for the particular vehicle and the weighted fleet average drag. The relative dynamics are discretized on a 10.8 second time-step to match the propagation step-size in FreeFlyer™. The formation-keeping problems are planned over a half orbit time horizon. The LP formation-keeping formulation restricts the control inputs and applies the position constraints to every sixth time-step through the method presented in Section 4.4, which reduces the LP solution time to about 1–3 seconds. The robust LP approach in Section 4.2.2 is implemented to account for the sensor noise and the always feasible solution approach presented in Section 4.3 is also included in the LP controller. The size of the error box for position tolerance is 10 m in-track, 5 m radial, and 5 m cross-track, which meets the tolerance requirement of 10% of the baseline [5] for all the formations in the simulation.

The simulation consists of several maneuvers that are typical in a formation flying mission. The maneuvers demonstrate the formation-keeping and formation maneuver ability of the control system. The time for each maneuver and formation geometry is specified by the user. Once the simulation starts, the control system is completely autonomous, transitioning between control modes without user intervention. The simulation begins with the formation in an off-center in-track separation. The first spacecraft trails the reference point by 150 m, the second leads the reference point by 50 m, and the third leads by 250 m. The purpose of the off-center formation is to demonstrate that the virtual center is not the geometric center of the formation. The in-track separation is maintained for 1/4 day (about 4 orbits) before a formation maneuver occurs to place the fleet on a passive aperture. The passive aperture is shown in Figure 5-3. The aperture projects a 400×200 m ellipse in the in-track–radial plane and a circle with a 100 m radius in the radial–cross-track plane. This aperture would provide a convenient geometry for viewing objects away from the earth. The coordinator assigns the spacecraft to the aperture through the procedure described in Section 3.2.1 with a plan horizon of one orbit. At the end of the formation maneuver the control system automatically transitions to formation-keeping and the formation is maintained for about seven days.

After seven days have elapsed, a second formation maneuver reconfigures the formation to a larger aperture that faces a different direction. The second passive aperture is shown in Figure 5-4. Again the maneuver is coordinated over a one orbit plan horizon. The new aperture projects a 600×300 m ellipse in the in-track–radial plane and now projects a 300 m radius circle in the in-track–cross-track plane. In order to project a circle in the in-track–cross-track plane, the phasing between the in-track oscillation and cross-track oscillation must be adjusted. This aperture provides a good geometry for Earth imaging. The aperture is maintained through formation-keeping for about six days. On the thirteenth day of the simulation the formation transitions back to an in-track separation. The separation from the reference point is 100 m, 0 m and -100 m in the in-track direction. The assignment of each vehicle to a position in the in-track separation is performed by the coordinator. The in-

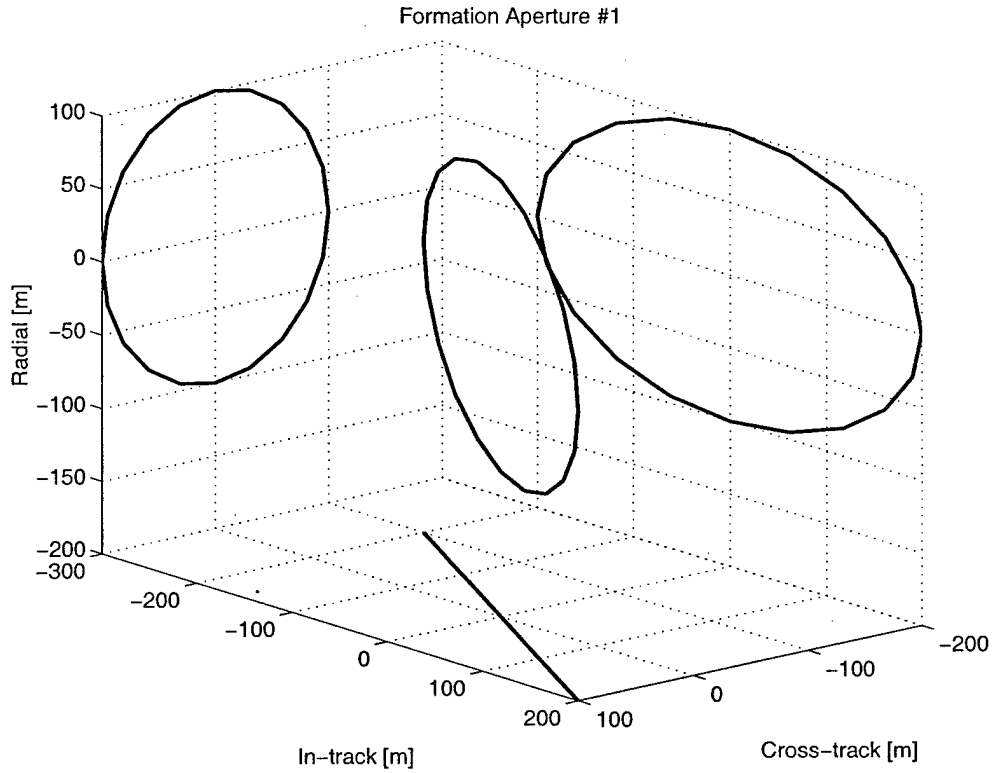

Figure 5-3: First formation aperture with motion projected in each plane.

track separation is maintained through formation-keeping until the conclusion of the simulation at the end of the fourteenth day.

The total simulation contains three formation maneuvers with formation-keeping at each formation configuration. The formation-keeping for the passive apertures occurs over a significant time period (about a week) to observe any long and short term effects of the disturbances, particularly the gravity perturbation effects. This simulation successfully demonstrates the control system presented in this thesis for all aspects of a spacecraft formation flying mission.

5.3.2 Analysis of Controller Performance

The simulation was performed for three different levels of cooperation between the fleet. The first simulation calculates the virtual center in the formation with equal weights on each vehicle in the fleet. The low-level control is also performed independent of any control actions taken by other members of the fleet. The second

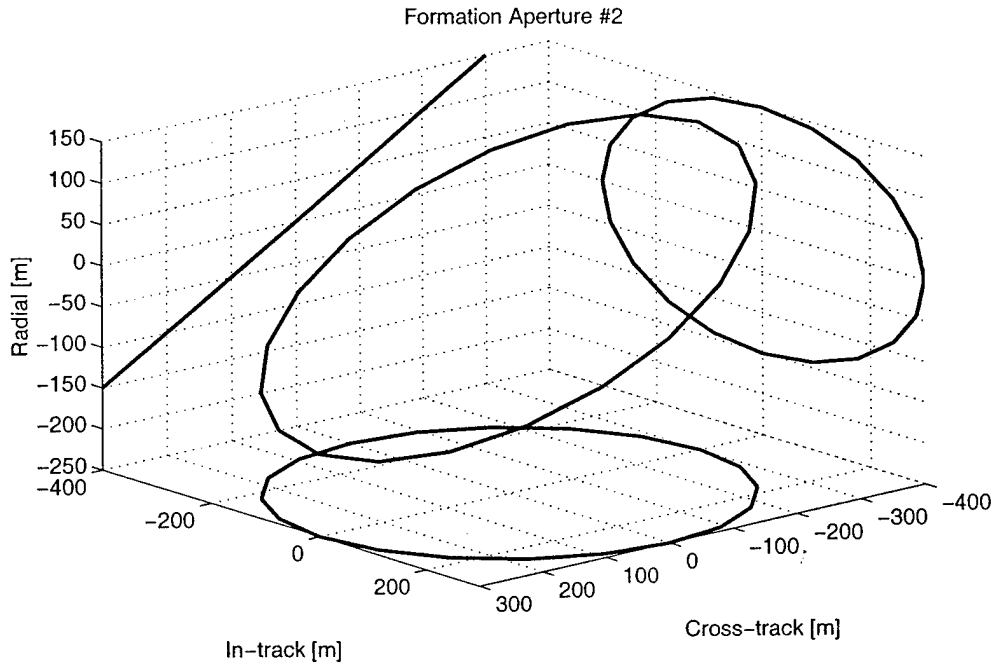

Figure 5-4: Second formation aperture with motion projected in each plane.

simulation includes the control actions by other spacecraft in the low-level control determination, but the high-level control remains unchanged. The third simulation includes the external control inputs as in the second simulation and also adjusts the weighting of the vehicles in the high-level coordinator based on fuel use. A vehicle that uses more fuel will receive a higher weight. The fuel weighting forces the virtual center calculation to reduce errors in this particular vehicle over other errors, thereby reducing the future fuel use for the vehicle that has used the most fuel in the past. The goal of the fuel weighting scheme is to lengthen the fleet mission by spreading the fuel cost across the fleet.

All three methods successfully achieve and maintain the specified configurations during the formation flying mission. The motion of the fleet as viewed from the reference point is shown in Figure 5-5. The fuel cost over time for one of the simulations is shown in Figure 5-6. The fuel cost figure clearly shows the three formation maneuvers, which take large amounts of fuel over a short period of time. The long, constant slope segments are the formation-keeping maneuvers. The total fuel cost data for each of the simulations is contained in Table 5.1. The fuel data for formation-keeping

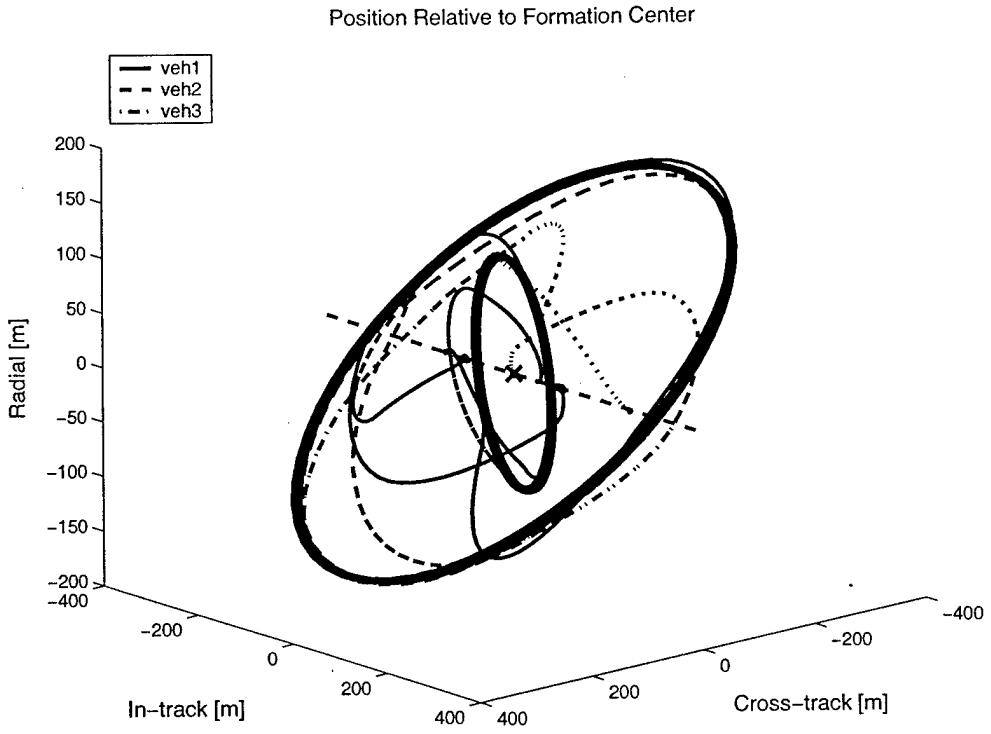

Figure 5-5: Relative motion of the three vehicle formation throughout the simulation. The fleet begins and ends in an in-track separation along the dashed line. The fleet moves from the dashed line to the smaller ellipse first and then transitions to the larger ellipse before returning to the dashed in-track line.

maneuvers is displayed as a fuel cost per orbit. The fuel for formation maneuvers is shown as a total fuel, which can also be interpreted as a fuel cost per orbit because each maneuver occurs over one orbit. The controller performance for each level of co-operation will now be discussed for the formation maneuvers and formation-keeping.

Formation Maneuver Analysis

The formation maneuver controller coordinates each maneuver to minimize fleet fuel, but the fuel weighting for each vehicle is adjusted based on current fuel state to equalize the fuel use across the fleet. Vehicles that have used more fuel will be assigned final states that require less fuel to achieve, equalizing fuel use across the fleet. During the simulations performed in this chapter, the fuel weighting in the coordinator does not alter the assignment. This is because with only three vehicles and one orbit to perform the maneuver, there is an asymmetry in the fuel cost maps

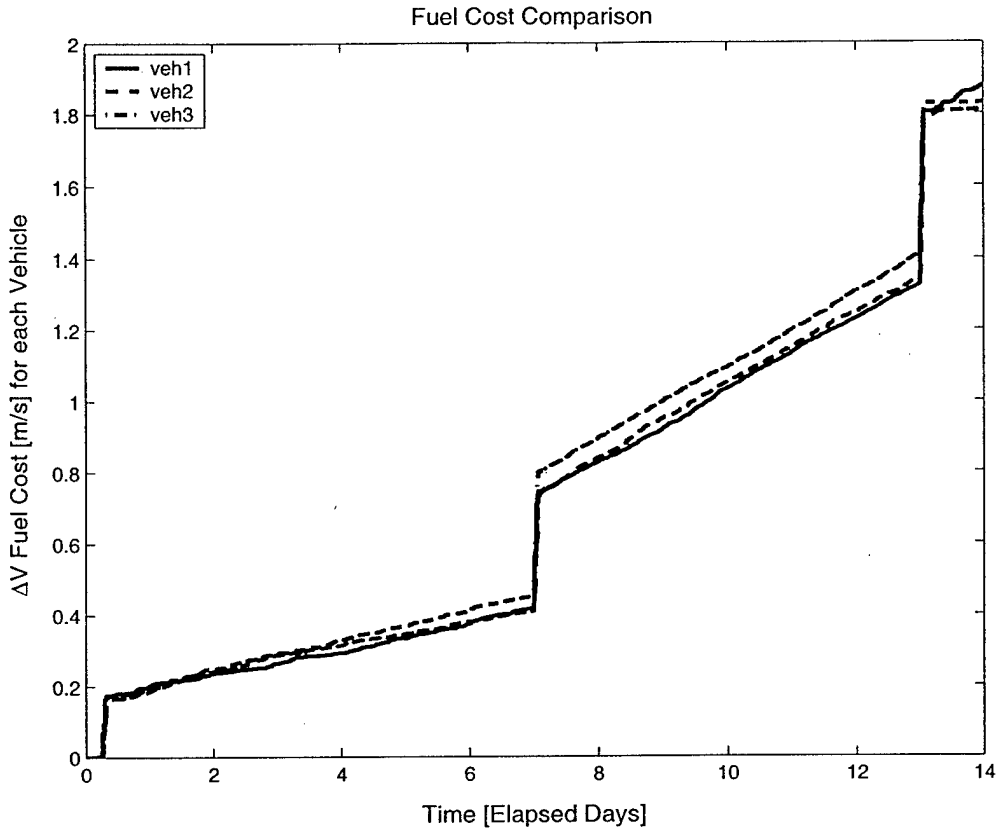

Figure 5-6: ΔV fuel cost for each of the three vehicles in the fleet during the complete simulation. The sharp rises indicate the formation maneuvers and the constant slope parts result from the formation-keeping maneuvers.

such that there is one "good" assignment that minimizes the fuel cost for each vehicle and any other configuration results in a large increase in total fuel for each vehicle. Assigning the vehicle that has used the most fuel the best possible final state results in the same assignment that also minimizes fuel cost for the fleet if no fuel weighting is considered. The coordinator minimizes the total fuel cost for the fleet which will be increased for any assignment other than the one that is the minimum for each vehicle. For larger fleets, the cost map is more complex, such as the cost map in Figure 3-4, and there is not a single configuration that will minimize the fuel for all members of the fleet. As a result, the fuel weighting will assign those vehicles that have used more fuel to final states that are closer to the minimum fuel cost position for that particular vehicle.

Table 5.1: Table of fuel costs for various aspects of the simulation. The simulation number corresponds to the level of coordination in the controller for each simulation. The spacecraft in the feet is indicated by SC#. The maneuver types are followed by the number of orbits the maneuver was performed for. FK indicates formation-keeping maneuvers and FM represents formation maneuvers.

Maneuver Type	Sim 1 SC 1	Sim 1 SC 2	Sim 1 SC 3	Sim 2 SC 1	Sim 2 SC 2	Sim 2 SC 3	Sim 3 SC 1	Sim 3 SC 2	Sim 3 SC 3
FK #1 (4) mm/s/orbit	0.509	0	0.523	0.652	0	0.112	0.542	0	0.341
FM #1 (1) mm/s	163	150	171	160	148	168	169	157	165
FK #2 (101) mm/s/orbit	3.07	2.82	2.43	2.70	2.54	2.26	2.39	2.48	2.51
FM #2 (1) mm/s	315	291	315	339	291	320	275	306	314
FK #3 (90) mm/s/orbit	8.14	6.90	6.18	7.42	6.57	6.59	6.59	6.73	6.82
FM #3 (1) mm/s	415	440	391	408	410	374	404	392	393
FK #4 (14) mm/s/orbit	2.64	4.69	2.30	1.71	0.696	1.45	3.90	2.25	0.541
FM Total mm/s (3)	893	881	877	907	849	862	848	855	872
FK Total mm/s (209)	1141	1040	899	1019	920	931	979	1004	964
Total Fuel mm/s (212)	2034	1921	1776	1926	1769	1793	1827	1859	1836

Because the plans are based on uncertain initial conditions, the re-planning method is required to correct the plan during execution, which can lead to increased fuel use over the predicted value used in the coordination. This re-planning method can eliminate any benefit of assigning a vehicle that has used a large amount of fuel to the lower fuel cost final state. Therefore, unless the cost for a maneuver is drastically different for each vehicle, the benefit of altering the assignment in the maneuver based on previous fuel use may not be observable in the final results.

The results in Table 5.1 show that there is no appreciable difference in fuel cost

between the three different controllers for the formation maneuvers; however, this is not unexpected. The difference between the first two simulations is the inclusion of the control inputs of other vehicles in the low-level controller for formation-keeping. Therefore, there is no expected improvement in the formation maneuvers from this change. The last simulation adds fuel weighting to the calculation of the formation center. The fuel weighting is only updated once every two orbits, whereas the formation maneuvers occur over a single orbit. Some benefit can be expected because the fuel weighting will reduce the differential disturbances of vehicles that have used large amounts of fuel, however, this change will be minimal over the course of one orbit.

Formation-keeping Maneuver Analysis

In the formation-keeping mode, the vehicles are maintained approximately within the specified position tolerance. The always feasible solution does allow some flexibility in the tolerance. This flexibility allowed the vehicles to exceed the position tolerance from time to time, particularly in the larger passive aperture where the cross-track disturbance is much larger due to a greater inclination difference between vehicles in the fleet. An example of the motion within an error box for one vehicle is shown in Figure 5-7. Although the original position tolerance (10 m in-track, 5 m radial, 5 m cross-track) was exceeded, the maximum deviation from the desired state for any of the simulations was less than 11 m in-track, 5 m radial, and 7 m cross-track.

For the two passive aperture formation-keeping maneuvers, the rate at which fuel is expended for each vehicle is heavily dependent on the cross-track disturbance. The in-track and radial control effort is about the same for each vehicle in the formation, regardless of the spacecraft location in the aperture; however, the cross-track fuel use varies significantly for each vehicle. The cross-track disturbance, shown in Equation 2.23, results in a secular increase in the amplitude of the cross-track oscillatory motion. The magnitude of this increase is dependent on the cross-track phasing, $\cos\alpha$. If $\cos\alpha$ equals one, the disturbance is largest because the inclination difference between the particular vehicle and the inclination of the reference orbit is greatest. Conversely, if $\cos\alpha$ equals zero, the disturbance is eliminated. This case

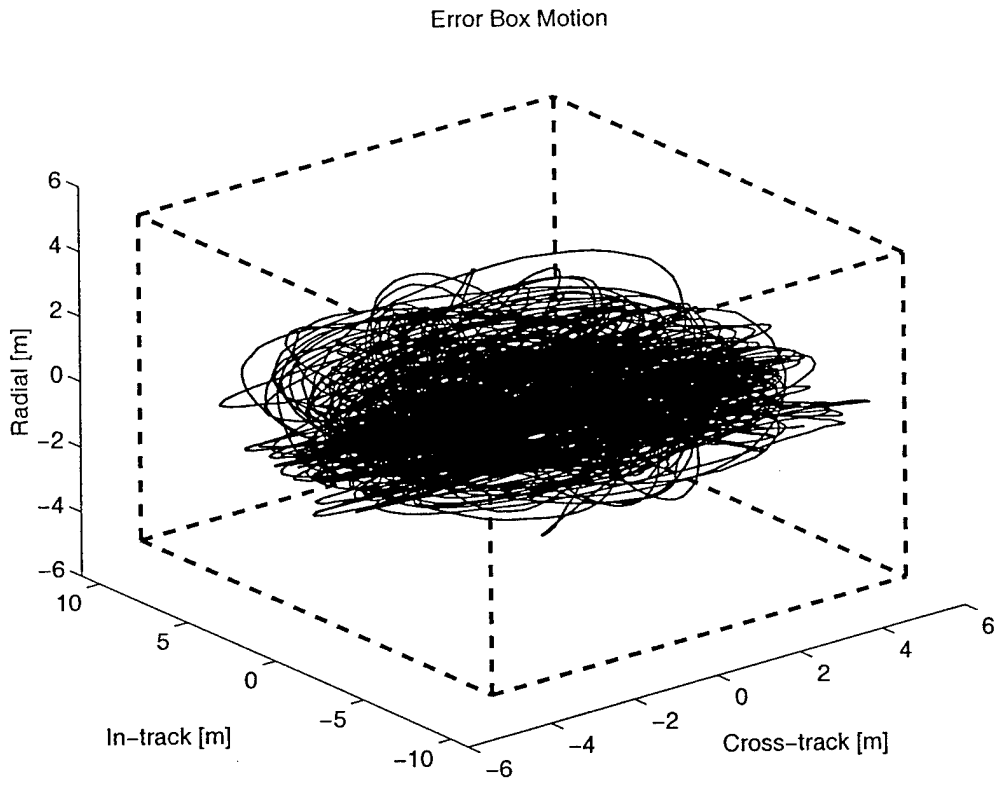

Figure 5-7: Example of the motion inside the error box for one vehicle over the entire simulation. The dashed lines represent the position tolerances in each dimension.

corresponds to two vehicles in the same orbit around the earth with only a change in argument of latitude. With a three vehicle formation it is impossible to eliminate the disturbance completely for every vehicle, thus at least two vehicles will experience a cross-track disturbance and will expend more control effort than the other in response to the cross-track disturbance. Reference [24] presents a method to distribute the cross-track disturbance force across the fleet by slowly changing the cross-track phasing angle, α_c, described in Section 2.1.3. By altering the phasing over time, the cross-track disturbance for each vehicle changes such that each vehicle experiences the same average disturbance over the mission life. This method can be included in the control system presented in this thesis, however, the coordinated virtual center also equalizes the fuel cost due to the cross-track disturbance through the fuel-weighted virtual center calculation.

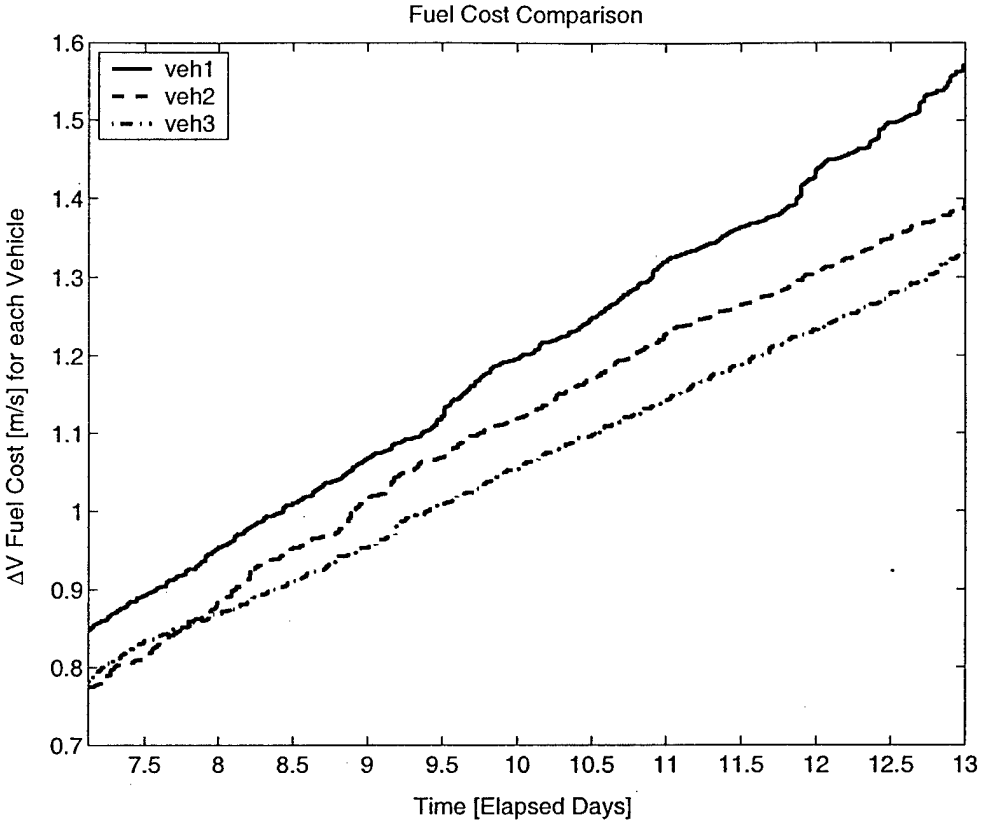

Figure 5-8: Fuel cost during the formation-keeping maneuver for the second aperture. The slope of the fuel cost for each vehicle is different due mainly to the difference cross-track disturbance for each vehicle.

Figure 5-8 shows the fuel cost for the three vehicles during the time period for the first formation-keeping maneuvers. Notice the slope of each line corresponding to a different vehicle is slightly different. The fuel cost for the second aperture is also increased over the first aperture because the amplitude of the disturbance force is greater in the larger aperture. The increase in fuel use is shown by the increased slope from day seven to thirteen as compared to day one to seven in Figure 5-6. The slope is also tabulated in Table 5.1 for the FK #2 and FK #3 maneuvers. There is an increase in fuel for the larger aperture for all three simulations.

The choice of controller type for each simulation has the most effect on the fuel cost during formation-keeping maneuvers. This is expected because the controllers for the fleet are in formation-keeping mode the majority of the simulation time. Table 5.1

shows a decrease in the fuel use per orbit for each level of increased cooperation in the simulations.

The decrease between the first and second simulation is due to the increased knowledge of the control inputs of the other vehicles. The control actions of the other vehicles in the fleet will result in a change in the error states for those vehicles, which will ultimately lead to a change in the virtual center state. Without the knowledge of the other spacecraft control inputs, the low-level controller cannot predict the motion of the center due to the other vehicles in the fleet. Including a weighted average of the control inputs from the other vehicles allows the LP controller to solve the formation-keeping problem such that the controlling spacecraft is not correcting an error that will be corrected by the already planned motion of the other vehicles. The net result is a decrease in fuel cost because: 1) the control inputs of other vehicles indirectly reduce the error of the acting vehicle; 2) the control inputs designed do not negate the control efforts of the other vehicles; and 3) the LP model more accurately represents the motion of the spacecraft relative to the moving virtual center. The external inputs control scheme is not perfect because the LP plans are solved based on current knowledge of the other vehicles' future actions, which may or may not be executed depending on the spacecraft monitor decisions for each vehicle. However, including the external inputs is shown to reduce the fuel costs for the vehicles.

The decrease in fuel use between the second and third simulation is due to the use of fuel weighting in the calculation of the virtual center. The fuel weighting will reduce the errors of vehicles that have used more fuel more than the other vehicles. As a result, the virtual center will behave more like the high fuel use vehicle, therefore the differential disturbances will decrease and the control effort to resist the disturbances will be less. Not all of the fuel numbers for the formation-keeping maneuvers in Table 5.1 for simulation #3 are less than the numbers for simulation #2, but the largest value is decreased at the expense of a slight increase in the fuel use for the other two vehicles. For example, consider the formation-keeping maneuver for the first passive aperture, FK #2. The highest fuel cost for simulation #2 is 2.70 mm/s per orbit followed by 2.54 and 2.26. In simulation three, the highest fuel cost is reduced

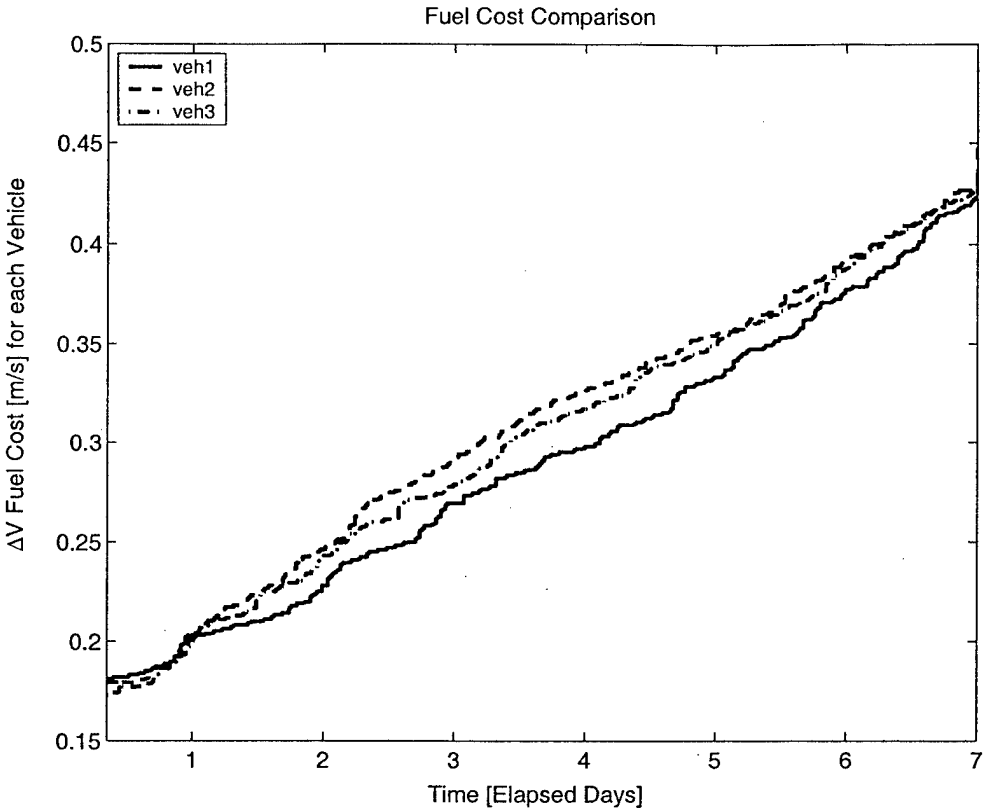

Figure 5-9: Fuel cost during the formation-keeping maneuver for the first aperture with fuel weighting in the formation center calculation. The fuel weighting equalizes the fuel cost for the fleet.

to 2.56 mm/s per orbit, but the other vehicle fuel costs are now to 2.48 and 2.39. The effect of the fuel weighting can be seen in Figure 5-9 for the formation-keeping for the smaller aperture. The fuel costs diverge initially, but the fuel weighting drives them back together by reducing the differential disturbances on the vehicle using the most fuel. For the larger aperture, the fuel weighting does not overcome the disturbance effect to drive the fuel costs together, but the slopes of the lines are made more equal. The rate of fuel use for each vehicle with fuel weighting is shown in Figure 5-10. Compared to Figure 5-8, the slopes of the lines are more equal.

Total Fuel Cost Analysis

The net effect for the improvements in each controller can also be observed in the total fuel cost for the mission. If a formation flying mission is dependent on all vehicles in the fleet, then the mission life is limited by the vehicle with the greatest fuel use

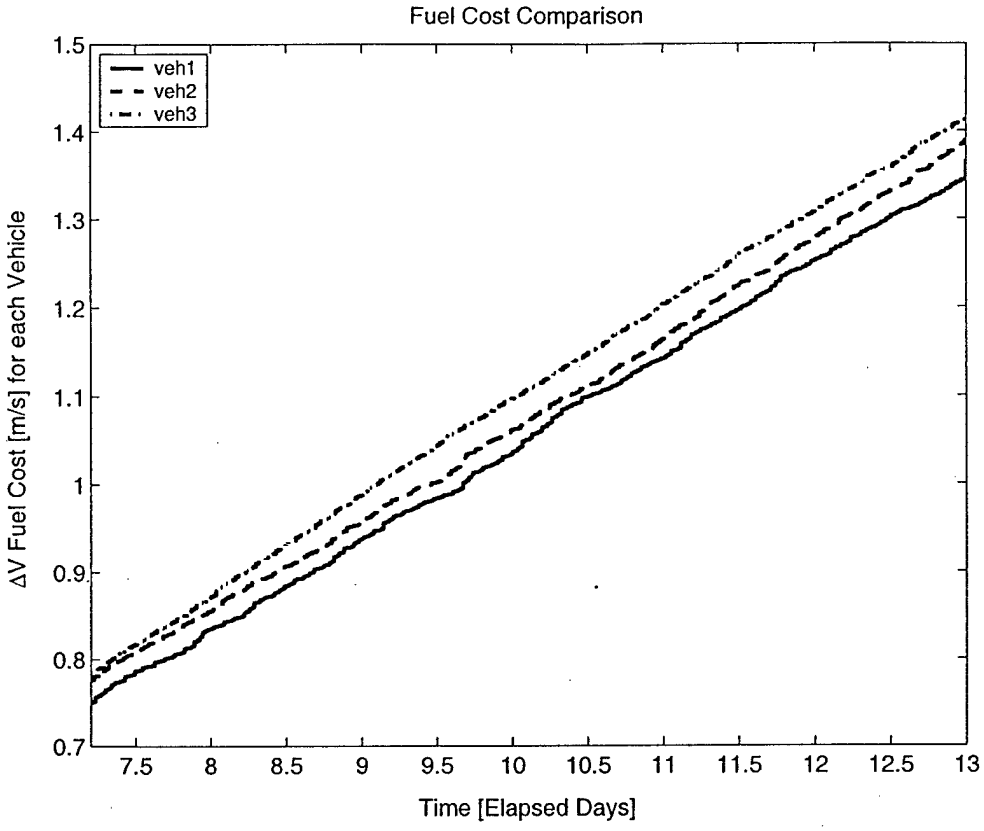

Figure 5-10: Fuel cost during the formation-keeping maneuver for the second aperture with fuel weighting in the formation center calculation. The slopes of the fuel cost for all vehicles is about the same because the fuel weighting equalizes the cross-track disturbance across the fleet.

in the fleet assuming no other critical spacecraft failures. The total fuel expenditure for each vehicle during the mission is summarized in the bottom row of Table 5.1. The maximum fuel cost is reduced from 2.03 m/s for the first simulation to 1.93 m/s for the second simulation. However, the fuel costs for the other two vehicles in the fleet are much lower than the maximum for both simulations. The third simulation utilizes the fuel weighting scheme to reduce the maximum fuel use by shifting some of the control effort to the lower fuel cost vehicles. The result is a reduction in the maximum fuel cost to 1.86 m/s for simulation #3.

The simulations in this section demonstrate the effectiveness of the control system presented in this thesis for a spacecraft formation flying mission. Several aspects of

a typical mission are addressed in the simulations. The two types of maneuvers for formation flying are implemented using the terminal constraint LP for the formation maneuvers and the formation-keeping LP to maintain the formation in both an in-track separation configuration and multiple passive aperture formations. The robust LP formulation is implemented to address sensor noise within the control system. The LP controller is placed in a hierarchical control architecture. The high-level coordinator performs the centralized calculations for determining the virtual center in the formation as well as the coordination for formation maneuvers. The low-level controller includes the LP algorithm within a state feedback monitor system that determines when the LP controller is activated to solve for new control input plans for the spacecraft. The entire control system is operated autonomously throughout the mission given user inputs for formation descriptions and execution times to perform the maneuvers. The result is an efficient real-time control system using the benefits of a fuel-optimal controller to plan control actions and coordination between the fleet to further reduce fuel effort. The fuel costs from the simulation indicate that this control system can adequately maintain a formation at a fuel cost of 2–8 mm/s per orbit.

5.4 Chapter Summary

Chapter 5 begins with a discussion of the complete algorithm procedure. The discussion is separated into the high-level coordination procedures and low-level control development and execution. Each level of the algorithm is further discussed by the type of maneuver: 1) formation maneuvers such as formation initialization or reconfiguration and 2) formation-keeping maneuvers. The chapter concludes with a final simulation that demonstrates several aspects of a typical formation flying spacecraft mission. The simulation demonstrates the effectiveness of the controller presented in the thesis as well as the improvements made through the modifications in implementation discussed in Chapter 4 and through the increased coordination between vehicles in the fleet.

Chapter 6

Conclusions

This thesis presents coordination and control algorithms as well as a control system design for spacecraft formation flying. The control system design is constructed based on a control algorithm using convex optimization to determine fuel optimal control inputs over a fixed time horizon. Several additional challenges were encountered and solved in order to implement the control algorithm in a control system architecture that is viable for a spacecraft formation flying mission. This chapter concludes the thesis with a discussion of the major contribution from the work performed in developing the control system. The chapter also includes a discussion of avenues for further improvements and study in the design and implementation of the control system. The areas of future work include methods of further improving the control algorithm as well as further areas of study in implementation such as model estimation for the dynamics models used in the controller.

6.1 Thesis Contributions

In developing the control system presented in the thesis, several key insights and contributions were made in the analysis of the spacecraft formation flying control problem. The contributions include advancement in passive aperture initialization, control algorithm generation, coordination algorithms, dynamics models analysis and a complete control system design for formation flying control. The complete control

system design is successfully demonstrated in a detailed nonlinear simulation typical of a spacecraft formation flying mission. This section discusses the major contribution from the work in this thesis.

6.1.1 General Passive Aperture Initialization for Eccentric Orbits

Previous work in the design of passive aperture developed initial conditions required for periodic relative motion between two spacecraft in the absence of disturbances. The initial conditions for a reference orbit with eccentricity were developed for the case with zero true anomaly. The work in this thesis developed a generalized initialization procedure for any true anomaly. The procedure involves the in-plane spacecraft states for the radial and in-track direction. The cross-track motion is naturally periodic because the secular growth caused by the differential J_2 effect is ignored in Lawden's relative dynamics for eccentric orbits.

The homogeneous solutions to Lawden's Equations in Equations 2.16 and 2.18 are a function of the integration constants, b_i's. The goal of the initialization procedure is to solve for the integration constants that meet the constraints of problem. The current position of the vehicle and periodicity constraint can be written in terms of the b_i's to provide three constraints on the solution, however the fourth constraint is still free to choose. This thesis presents three methods of initializing the fleet at any true anomaly. The first method introduces a fourth constraint to make the relative motion symmetric about the origin of the reference frame. The constraint results in a linear system with four equations and four unknowns. The initialization procedure is also posed as a linear programming problem that solves for the integration constants resulting in the minimum velocity change, or minimum fuel, for the spacecraft to meet the constraints for periodic motion. The solution to the LP always results in a change in in-track velocity and no change in radial velocity. From this observation, a third initialization was presented with the fourth constraint being that the radial velocity is also fixed to the current velocity. This again results in a linear system

with four equations and four unknowns. The solution is the same as the minimum fuel solution from the linear program formulation but can be solved much faster.

The general initialization procedure provided by this thesis allows the conditions for periodic relative motion to be determined at any true anomaly in the spacecraft orbit. This is an improvement because the formation maneuvers for achieving a passive aperture are no longer constrained to occur at true anomaly equal to zero. In addition the desired state to maintain the aperture in a formation-keeping maneuver must be specified at all points in the orbit. The homogeneous solutions can be used to specify the desired state at any time, but the initialization procedures allow the additional input of the fourth constraint to further design the aperture shape.

6.1.2 Fuel-Optimal Control Algorithms

There are two main types of control problems in a formation flying mission. The first problem is a formation maneuver used to control the spacecraft to reach some terminal state. The terminal state is a position in the formation geometry either on a passive aperture or an in-track separation. The formation maneuver is used to initialize or reconfigure the formation geometry. Once the formation geometry is achieved, disturbances will disperse the spacecraft from the desired formation configuration. As a result a second control scheme is required for formation-keeping or maintaining the formation geometry. The major contribution of this thesis is the development of fuel optimal control algorithms using convex optimization techniques for each of these control problems. The thesis presents a control algorithm using linear programming to solve for the fuel optimal control inputs and trajectories over a fixed time interval. An LP formulation is presented for 1) the terminal constraint problem required for formation initialization and reconfiguration maneuvers, and 2) the formation-keeping problem to maintain the formation geometry over extended time periods.

The linear programming approach provides a flexible control problem formulation structure. The thesis presents several types of constraints that can be included in the control problem. In addition, the linear program structure easily allows several different types of spacecraft dynamics models. All three relative dynamics models

presented in the thesis are used in the LP formulation for comparison. Although the linear time varying dynamics increase the computation complexity during the LP formulation, the actual LP problem is not increased in size and therefore the solution time is not increased. The structure of the LP formulation also allows variables and constraints to be selectively removed to reduce the problem size and decrease solution times. Several more complicated constraints such as collision avoidance, plume impingement, and additional actuator constraints can also be easily implemented with the introduction of binary variables and extending the algorithm structure to mixed integer linear programming.

6.1.3 Coordination Algorithms

In addition to the control algorithms, coordination algorithms for both formation maneuvers and formation-keeping are presented. A distributed coordination scheme for formation maneuvers uses the low-level controllers to create fuel cost maps for possible final states on a new formation geometry. The coordinator solves the assignment problem as a linear program and returns the best final state to each vehicle to implement in the low-level controller. This coordination method allows much of the computation which occurs in creating the cost maps for each vehicle to be distributed across the fleet. Only the assignment problem is solved centrally on a single vehicle. The distributed coordination method decreases the computational load across the fleet.

The coordination in the formation-keeping maneuvers occurs in the description of the reference point for the relative dynamics and specification of the desired state for each vehicle. The thesis presents three methods of determining the reference point for the fleet. The virtual center is particularly attractive because the calculation allows the highest level of coordination in the fleet. The virtual center is formed based on a weighted average of the fleet motion, therefore disturbances are reduced. In addition, a fuel weighting scheme can be used with the virtual center calculation to help equalize the fuel use across the fleet. The virtual center can also eliminate the need for an on-board orbit propagator by recalculating the center at every time-step.

6.1.4 Initial Condition Uncertainty in Controller

The relative states of each vehicle in the fleet must be measured using some sort of sensor. The sensor noise will introduce uncertainty in the current state of the vehicle, which is critical to the solution to the LP control problem. The analysis in the thesis indicates that velocity uncertainty, particularly in-track velocity uncertainty, is most critical to the response of the spacecraft. Modifications to the LP formulation for formation-keeping are presented to add robustness to initial condition uncertainty by including several possible initial conditions and planning for the worst case. The robust solution will maintain all possible solutions within the position tolerance over the plan horizon. The robust solution can lead to infeasible solutions if the state of the solution can not be guaranteed to meet the position constraints. As a result, an always feasible solution technique is introduced that allows a penalized increase in the position tolerance to ensure a feasible solution. The position constraints are relaxed to allow a feasible solution. Sensor noise is addressed in formation maneuvers through a re-planning method that repeats the terminal constraint LP problem over a reduced time horizon so that the plan will terminate at the original time in the future. Simulation results show significant fuel cost reduction in using the re-planning method as opposed to a trajectory tracking method using LQR to follow the originally planned trajectory based on incorrect initial conditions.

6.1.5 Relative Dynamics Analysis

The relative dynamics in the formation control problem are analyzed in terms of two key issues: 1) which dynamics to use to represent the relative motion of the spacecraft to determine the desired state for passive aperture, and 2) which dynamics to use in the LP controller. Three linearized models of the relative dynamics are considered in the analysis, including Hill's equations for circular orbits, modified linear dynamics that partially account for the J_2 effects, and Lawden's equations for eccentric orbits. The key analytic result is the importance of reference orbit eccentricity in specifying the desired state. If Hill's equations, which assume a circular reference orbit, are

used to specify the desired state for eccentricities even as low as 0.001, then the spacecraft will be controlling to the incorrect state for periodic motion and the control effort will be drastically increased. However, if Lawden's equations of motion for eccentric orbits are implemented, the periodic motion is achieved and the control effort is reduced. The analysis also indicates that including the differential gravity perturbation, J_2 results in some small reference orbit eccentricity which can be capture by the linearized J_2 model or Lawden's equations.

The investigation of the dynamics used in the LP controller indicates that for short plans, about half an orbit, the type of dynamics included in the controller does not significantly affect performance. Although the time-varying dynamics for eccentric orbits are more accurate, the time-invariant dynamics can be used with little loss of performance. The time-invariant dynamics reduce the computation required to formulate the LP. Another reason that dynamics modeling errors are not critical to the controller is the sensor noise. The robust LP plans for the worst case based on initial condition uncertainty. The uncertainty in the response due to sensor noise is much greater than that due to dynamics modeling errors. If the sensor noise is decreased or the plan horizons increased, the dynamics modeling error can become significant enough to effect the controller performance.

6.1.6 Complete Control System for Spacecraft Formation

The work in the thesis incorporated the coordination and control algorithms in a hierarchical control system architecture for a fleet of spacecraft. A contribution to the architecture is the creation of a spacecraft monitor in the low-level architecture. The spacecraft monitor determines when control actions are needed and initiates the LP controller algorithm. The monitor provides the spacecraft level decision making on-board each vehicle. The coordination algorithms are implemented by a coordinator which is placed on a single vehicle. The form of the algorithms makes the location of coordinator arbitrary. Any vehicle can contain the coordinator, therefore if one vehicle fails, the coordinator can easily be activated on another vehicle provided the software exists.

The complete control system is demonstrated in a large simulation that contains several aspects of a typical spacecraft formation flying mission. The control system autonomously transitions between formation maneuvers and formation-keeping to achieve four different formation geometries. Two passive aperture geometries are maintained for about a week each to demonstrate the effectiveness of the formation-keeping control algorithm. The simulation results indicate a formation-keeping fuel cost of 2-8 mm/s per orbit depending on the formation geometry.

6.2 Areas of Future Work

Although this thesis presents a successful control system for formation flying spacecraft, areas of further improvement do exist. The areas range from algorithm improvements to changes in architecture design. This section discusses some possible areas of study that would improve the implementation of the control algorithms presented in the thesis and possibly reduce the fuel cost associated with spacecraft formation flying.

The primary concern with formation flying spacecraft is the fuel consumption to maintain the formation. The fuel cost depends on several factors in the control system design. The analysis of the sensor noise effect on the fuel cost in this thesis shows an approximate linear decrease in fuel cost with decreasing velocity noise level. The fuel cost savings are due to two main effects. With lower uncertainty, the LP controller can make plans over longer time horizons while still satisfying the position constraint. The longer plans allow the controller to make more use of the relative dynamics to drift within the error box without using control effort. The reduced cost also results from the spacecraft following the designed trajectory more closely, resulting in fewer re-plans. In other words, the vehicles actual trajectory more closely resembles the optimal trajectory.

With lower initial condition uncertainty the robust LP could also be reformulated with a loose terminal constraint. The terminal constraint would make the controller attempt to return the vehicle to the desired state, the center, rather than just remain-

ing inside the error box. The terminal constraint could be formulated with the same method presented for the always feasible solution method. The terminal constraint box would have a scaling variable that would be penalized in the cost. The goal is then to design a plan that allows the final position tolerance constraint to be as close to the center as possible while maintaining a feasible solution.

Another option for further decreasing fuel use could be to investigate the error box geometry. The error box geometry consists of the basic shape, the relative sizes of the trigger box and planning box, and the ultimate position tolerance. The basic shape of the box could be changed into an oblate sphere. The oblate sphere would have to be approximated as a polytope with N sides and a linear set of constraints would be imposed for each side. The sphere shape of the error box will eliminate poor initial conditions such as starting in a corner of the box with little maneuvering room. However, this method will increase the number of constraints and possibly increase the computation for the LP formulation and solution.

The actual sizes of the error box could also be increased. A larger error box will allow the LP to create longer plans regardless of the noise level. Initial investigations not included in this thesis do not, however, indicate that increasing the size will always decrease fuel consumption. One reason is due to spacecraft orbit energy levels. The periodic motion of the satellites is the result of the equal energy orbits. As the vehicle is perturbed from the desired state, the energy level is changing. For larger error box sizes, this energy level is allowed to change even more without correction. As a result, more effort will be required to match the energy levels and restore the formation. The larger error box size does allow for longer plans, but there is a limit to the accuracy of the dynamics model used to make the plan. For longer plans, several orbits, the control inputs are no longer near the beginning of the plan. The control inputs further into the future are designed assuming the true state of the vehicle will be the designed state from the LP. Due to inaccuracies in the dynamics and disturbance models this will not be true and the control input will not have the desired effect as planed by the optimization. This indicates that at some point the effectiveness of the controller for large plan lengths will be reduced and the expected fuel cost savings

will also be less. However, if the dynamics model are improved, then the long plans, accurately executed, could result in large fuel savings. If the dynamics models are very accurate, then the long plans could also be implemented without increasing the position tolerance, in the absence of noise effects.

Clearly, the fuel cost is a function of several parameters in the control system. The LP controller develops the optimal control inputs over a fixed time horizon, but the execution of the designed plan will not result in the optimal trajectory and therefore the fuel cost will be greater.

To further improve the relative dynamics models used in the LP controller, an estimation scheme can be implemented to adjust parameters in the dynamics and disturbance models to match the true motion of the fleet. The model updating through the estimation is a necessity because the spacecraft parameters, such as mass, will change during the mission, affecting the resulting motion. The estimation problem would be very complex because it is difficult to distinguish which parameter causes the change observed by the estimator. The research would first require a detailed analysis of the dynamics and disturbances to determine if and how an observed motion can be translated into a change in model parameters. The complexity of the estimation process is further increased through the use of a virtual center. The estimation process now must account for not only the motion of an individual spacecraft but the motion of the virtual center which is a function of the entire fleet. The disturbance models are now differential with respect to the virtual center whose dynamic properties are constantly changing with the fleet.

A final area of study involves the communication of information across the fleet. In order to coordinate the fleet, information will need to be gathered in a central location to make decisions. For the virtual center calculation, the current true and desired state of each vehicle must be sent to the coordinator and the resulting center must be returned to all vehicles. For a large fleet, the time required to transmit and receive all the required data may exceed the time-step for the controllers. The controller will then have to operate using either outdated information or run at a lower frequency, degrading the reaction time and performance of the controller. The forma-

tion maneuvers are also designed to be a synchronized motion of the fleet. Therefore stringent timing requirements for executing the maneuver will put demands on the communication system to ensure all information is received before the execution time. The large amount of information and time critical demands present an interesting communications problem for spacecraft formation flying.

6.3 Final Comments

The coordination and control algorithms presented in this thesis provide an analysis tool that can be used for mission planning. The control algorithms can also be included in a control system architecture to provide an efficient real-time control system for a fleet of spacecraft. One possible control system design is presented in this thesis that has been proven through simulations to provide effective control and general operation throughout all aspects of a typical formation flying mission. The formation-keeping maneuvers, which will occur for the majority of the mission time, have been predicted to require 2-8 mm/s per orbit ΔV fuel cost.

Bibliography

[1] F. Bauer, K. Hartman, J. Bristow, D. Weidow, J. How, F. Busse, "Enabling Spacecraft Formation Flying Through Spaceborne GPS and Enhanced Autonomy Technologies," *ION-GPS '99*, Proceedings of the 12th International Technical Meeting of the Satellite Division of the Institute of Navigation, Nashville, TN, Sept. 14-17, 1999 (A01-27218 06-32), Alexandria, VA, Institute of Navigation, 1999, p.369-383.

[2] A. Das, R. Cobb, "TechSat 21 - Space Missions Using Collaborating Constellations of Satellites," *Proceedings of AIAA/USU Annual Conference on Small Satellites*, 12th, Utah State University, Logan, Aug. 31-Sept. 3, 1998, Proceedings (A99-10826 01-20), Logan, UT, Utah State University, 1998.

[3] C. Beichman, "The Terrestrial Planet Finder - The search for life-bearing planets around other stars," *Proceedings of Astronomical Interferometry Meeting*, Kona, HI, Mar. 20-24, 1998. Pt. 2 (A98-40801 11-35), Bellingham, WA, Society of Photo-Optical Instrumentation Engineers (SPIE Proceedings. Vol. 3350), 1998, p. 719-723.

[4] F. Bauer, J. Bristow, D. Folta, K. Hartman, D. Quinn, J. How, " Satellite Formation Flying Using an Innovative Autonomous Control System (AutoCon) Environment," *Proceedings of AIAA Guidance, Navigation, and Control Conference*, New Orleans, LA, Aug. 11-13, 1997, Collection of Technical Papers. Pt. 2 (A97-37001 10-63), Reston, VA, American Institute of Aeronautics and Astronautics, 1997, p. 657-666.

[5] Air Force Research Laboratory Space Vehicles Directorate, "TechSat 21 factsheet page." http://www.vs.afrl.af.mil/factsheets/TechSat21.html.

[6] J. How, R. Twiggs, D. Weidow, K. Hartman, F. Bauer, "Orion - A low-cost demonstration of formation flying in space using GPS," *Proceedings of AIAA/AAS Astrodynamics Specialist Conference and Exhibit*, Boston, MA, Aug. 10-12, 1998, Collection of Technical Papers (A98-37348 10-13), Reston, VA, American Institute of Aeronautics and Astronautics, 1998, p. 276-286.

[7] J. Leitner, F. Bauer, D. Folta, M. Moreau, R. Carpenter, J. How, "Distributed Spacecraft Systems Develop New GPS Capabilities," in *GPS World: Formation Flight in Space* Feb. 2002.

[8] R. Sedwick, D. Miller, E. Kong, "Mitigation of Differential Perturbations in Clusters of Formation Flying Satellites," *Proceedings of the AAS/AIAA Space Flight Mechanics Meeting*, Breckenridge, CO, Feb. 7-10, 1999. Pt. 1 (A99-39751 10-12), San Diego, CA, Univelt, Inc. (Advances in the Astronautical Sciences. Vol. 102, pt.1), 1999, p. 323-342.

[9] P. Bainum, "Breakwell Memorial Lecture: Review of astrodynamics, 1958-2001 - A personal perspective," IAF, International Astronautical Congress, 52nd, Toulouse, France, Oct. 1-5, 2001. IAF Paper 01-A201.

[10] M. Kaplan. *Modern Spacecraft Dynamics and Control.* Wiley, 1976.

[11] D. Vallado. *Fundamentals of Astrodynamics and Applications.* McGraw-Hill, 1997.

[12] D. Lawden, *Optimal Trajectories for Space Navigation,* Butterworths, London, 1963.

[13] T. Carter, M. Humi, "Fuel-Optimal Rendezvous Near a Point in General Keplerian Orbit," AIAA Journal of Guidance, Control, and Dynamics , vol. 10, Nov.-Dec. 1987, p. 567-573.

[14] T. Carter, "New Form for the Optimal Rendezvous Equations Near a Keplerian Orbit," AIAA Journal of Guidance, Control, and Dynamics , vol. 13, Jan.- Feb. 1990, p. 183-186.

[15] J. Marec, *Optimal Space Trajectories,* Elsevier Scientific, NY 1979.

[16] H. Schaub, K. Alfriend, "J_2 Invariant Relative Orbits for Spacecraft Formations," in manuscript form, 1999.

[17] S. Schweighart, *Developement and Analysis of a High Fidelity Linearized J2 Model for Satellite Formation Flying,*" S.M. Thesis, Massachusetts Institute of Technology, Dept. Aeronautics and Astronautics, June 2001.

[18] G. Inalhan, J. How, "Relative Dynamics and Control of Spacecraft Formations in Eccentric Orbits," *Proceedings of the AIAA Guidance, Navigation, and Control Conference and Exhibit*, Denver, CO, Aug. 14-17, 2000, Collection of Technical Papers, Reston, VA, American Institute of Aeronautics and Astronautics, 2000. AIAA Paper 2000-4443.

[19] M. Tillerson, J. How, "Formation Flying Control in Eccentric Orbits," *Proceedings of the AIAA Guidance, Navigation, and Control Conference*, Montreal, Canada, Aug. 6-9, 2001, Collection of Technical Papers, Reston, VA, American Institute of Aeronautics and Astronautics, 2001.

[20] H. Yeh, A. Sparks, "Geometry and Control of Satellite Formations," *Proceedings of the 2000 American Control Conference*, Chicago, IL, June 28-30, 2000. Vol. 1 (A01-12703 01-63), Piscataway, NJ, Institute of Electrical and Electronics Engineers, 2000, p. 384-388.

[21] G. Inalhan, M. Tillerson, J. How, "Relative Dynamics & Control of Spacecraft Formations in Eccentric Orbits," AIAA Journal of Guidance, Control, and Dynamics (0731-5090), vol. 25, no. 1, Jan.-Feb. 2002, p. 48-59.

[22] Q. Yan, G. Yang, V. Kapila, M. de Queiroz, "Nonlinear Dynamics and Output Feedback Control of Multiple Spacecraft in Elliptical Orbits," *Proceedings of 2000 American Control Conference*, Chicago, IL, June 28-30, 2000. Vol. 2 (A01-12740 01-63), Piscataway, NJ, Institute of Electrical and Electronics Engineers, 2000, p. 839-843.

[23] M. deQueiroz, Q. Yan, G. Yang, V. Kapila, "Global Output Feedback Tracking Control of Spacecraft Formation Flying with Parametric Uncertainty," IEEE

Conference on Decision and Control, 38th, Phoenix, AZ, Dec. 7-10, 1999, Proceedings. Vol. 1 (A00-4816014-63), Piscataway, NJ, Institute of Electrical and Electronics Engineers, Inc., 1999, p. 584-589.

[24] S. Vadali, S. Vaddi, K. Naik, K. Alfriend, "Control of Satellite Formations," *Proceedings of the AIAA Guidance, Navigation, and Control Conference*, Montreal, Canada, Aug. 6-9, 2001. AIAA Paper 2001-4028.

[25] A. Sparks, "Satellite Formationkeeping Control in the Presence of Gravity Perturbations," *Proceedings of the 2000 American Control Conference*, Chicago, IL, June 28-30, 2000. Vol. 2 (A01-12740 01-63), Piscataway, NJ, Institute of Electrical and Electronics Engineers, 2000, p. 844-848.

[26] D. Redding, N. Adams, E. Kubiak, "Linear-Quadratic Stationkeeping for STS Orbiter," Astrodynamics Conference, Williamsburg, VA, Aug. 18-20, 1986, Technical Papers, p. 329-340), AIAA Journal of Guidance, Control, and Dynamics , vol. 12, Mar.-Apr. 1989, p. 248-255. Previously cited in issue 23, p. 3428, Accession no. A86-47936.

[27] H. Schaub, K. Alfriend, "Impulsive Feedback Control to Establish Specific Mean Orbit Elements of Spacecraft Formations," AIAA Journal of Guidance, Control, and Dynamics (0731-5090), vol. 24, no. 4, July-Aug. 2001, p. 739-745.

[28] J. Smith, R. Proulx, P. Cefola, J. Draim, "An Operational Approach for Generating Near-Optimal Station Keeping Strategies via Parallel Genetic Algorithms," Astrodynamics 1999; *Proceedings of the AAS/AIAA Astrodynamics Conference*, Girdwood, AK, Aug. 16-19, 1999 (A00-35089 09-12), San Diego, CA, Univelt, Inc. (Advances in the Astronautical Sciences. Vol. 103, pt. 2), 2000, p.1349-1369.

[29] A. Robertson, G. Inalhan, J. How, "Formation Control Strategies for a Separated Spacecraft Interferometer," *Proceedings of the 1999 American Control Conference*, San Diego, CA, June 2-4, 1999, Proceedings. Vol. 6 (A00-15511 02-63), Piscataway, NJ, Institute of Electrical and Electronics Engineers, 1999, p. 4142-4147.

[30] R. Beard, F. Hadaegh, "Constellation Templates: An Approach to Autonomous Formation Flying," 1998 World Automation Conference, Anchorage, AK.

[31] R. Beard, J. Lawton, F. Hadaegh, "A Coordination Architecture for Spacecraft Formation Control," IEEE Transactions on Control System Technology, vol 9., no 6., November 2001.

[32] R. Bate, D. Mueller, J. White, *Fundamentals of Astrodynamics,* Dover Publications Inc., NY, 1971.

[33] V. Chobotov, *Orbital Mechanics,* Second Edition, AIAA Educational Series, 1996.

[34] A.I. Solutions, "FreeFlyer User's Guide",Version 4.0, March 1999.

[35] G. Franklin, J. Powell, M. Workman, "Digital Control of Dynamic Systems," Third Edition,Addison-Wesley, 1998.

[36] S. Boyd, L. El Ghaoui, E. Feron, V. Balakrishnan, "Linear Matrix Inequalities in System and Control Theory," Studies in Applied Mathematics, Vol. 15, SIAM, 1994.

[37] S. Boyd, L. Vanderberghe, "Convex Optimization," *in manuscript form,* **http://www.stanford.edu/class/ee364/reader.ps**, 1999.

[38] T. Coleman, M. Branch, A. Grace, "Optimization Toolbox for use with Matlab," Published by The Mathworks Inc., Jan 1999.

[39] See **www.cplex.com**

[40] See **http://www-fp.mcs.anl.gov/otc/Tools/PCx/**

[41] S. Clearwater, "Market-based control, a paradigm for distributed resource allocation," *World Scientific,* 1996.

[42] R. Sedwick, T. Hacker, D. Miller, "Optimum Aperture Placement for a Space-Based Radar System Using Separated Spacecraft Interferometry," *Proceedings of the AIAA Guidance, Navigation, and Control Conference*, Portland, OR, Aug. 9-11, 1999. AIAA Paper 99-4271.

[43] C. Floudas, "Nonlinear and Mixed-Integer Programming – Fundamentals and Applications," Oxford University Press, 1995.

[44] H. Williams, S. Brailsford, "Computational Logic and Integer Programming," in *Advances in Linear and Integer Programming,* Editor J. E. Beasley, Clarendon Press, Oxford, 1996, pp. 249–281.

[45] T. Schouwenaars, B. DeMoor, E. Feron, J. How, "Mixed integer programming for safe multi-vehicle cooperative path planning," presented at the 2001 *European Control Conference.*

[46] A. Richards, T. Schouwenaars, J. How, E. Feron, "Spacecraft Trajectory Planning With Collision and Plume Avoidance Using Mixed Integer Linear Programming," submitted to the *AIAA Journal of Guidance, Control and Dynamics,* October, 2001.

[47] M. Kay, "Logistics and Facilities Planning Toolbox," Version 1.3, Aug. 2000. Available at **www.ie.ncsu.edu/kay/matlog/Contents.htm**

[48] R. Burkard, E. Çela, "Linear Assignment Problems and Extensions," In Z. Du and P. Pardalos, editors, *Handbook of Combinatorial Optimization,* pp. 75-149. Kluwer Academic Publishers, 1999.

[49] R. Yedavalli, A. Sparks,"Satellite Formation Keeping Control Design Based on Ultimate Bounded Analysis of Switched Systems," *Proceedings of the AIAA Guidance, Navigation, and Control Conference*, Montreal, Canada, Aug. 6-9, 2001. AIAA Paper 2001-4027.

[50] F. Busse, G. Inalhan, How, J. P., "Project ORION: Carrier Phase Differential GPS Navigation For Formation Flying," *Proceedings of the Annual AAS Rocky Mountain Conference*, Breckenridge, CO, Feb. 2-6, 2000 (A00-41276 11-12), San Diego, CA, Univelt, Inc. (Advances in the Astronautical Sciences. Vol. 104), 2000, p.197-212.

[51] F. Busse, J. How, J. Simpson, and J. Leitner, "PROJECT ORION-EMERALD: Carrier Differential GPS Techniques and Simulation for Low Earth Orbit Formation Flying," presented at the *IEEE Aerospace Conference*, Mar 10-17, 2001.

[52] S. Grocott, J. How, D. Miller, D. MacMartin, K. Liu", "Robust Control Design and Implementation on the Middeck Active Control Experiment (MACE)", AIAA Journal of Guidance, Control and Dynamics, Vol. 17, no. 6, Nov.–Dec., 1994, pp. 1163-1170.

[53] Bryson, A., Mills, R., "Linear-Quadratic-Gaussian Controllers with Specified Parameter Robustness," *Proceedings of the AIAA Aerospace Sciences Meeting and Exhibit*, 32nd, Reno, NV, Jan. 10-13, 1994, AIAA Paper 94-0002, AIAA Journal of Guidance, Control, and Dynamics (0731-5090), vol. 21, no. 1, Jan.-Feb. 1998, p. 11-18.

[54] Y. Miyazawa, "Robust Flight Control System Design with Multiple Model Approach," *Proceedings of the AIAA Guidance, Navigation and Control Conference*, Portland, OR, Aug. 20-22, 1990, Technical Papers. Part 1, p.874-882, AIAA Journal of Guidance, Control, and Dynamics , vol. 15, no. 3, May-June 1992, p. 785-788. Previously cited in issue 21, p. 3316, Accession no. A90-47666.

[55] A. Ben-Tal, A. Nemirovski, "Robust Solutions of Uncertain Linear Programs via Convex Programming," Technical Report, Faculty of Industrial Engineering and Management, Technion, **iew3.technion.ac.il/Labs/Opt/** 1997.

[56] P. Ferguson, F. Busse, B. Engberg, J. How, M. Tillerson, N. Pohlman, A. Richards, R. Twiggs, "Formation Flying Experiments on the Orion-Emerald Mission," *Proceedings of the AIAA Space 2001 - Conference and Exposition*, Albuquerque, NM, Aug. 28-30, 2001. AIAA Paper 2001-4688.

[57] H. Hindi, S. Boyd, "Robust Solution to l_1, l_2, and l_∞ Uncertain Linear Approximation Problems using Convex Optimization," *Proceedings of the 1998 American Control Conference*, Philadelphia, PA, June 24-26, 1998, Proceedings. Vol. 6 (A99-20203 04-63), Piscataway, NJ, Institute of Electrical and Electronics Engineers, 1998, p. 3487-3491.

[58] A. Richards, J. How, T. Schouwenaars and E. Feron, "Plume Avoidance Maneuver Planning Using Mixed Integer Linear Programming," *Proceedings of the*

AIAA Guidance, Navigation, and Control Conference, Montreal, Canada, Aug. 6-9, 2001. AIAA Paper 2001-4091.

[59] T. Schouwenaars, B. DeMoor, E. Feron, J. How, "Mixed integer programming for safe multi-vehicle cooperative path planning," *ECC*, 2001.

[60] *ILOG CPLEX 7.0 Reference Manual*, ILOG, 2000.

[61] R. Fourer, D. Gay, B. Kernighar, "AMPL: A Modeling Language for Mathematical Programming," Scientific Press, International Thomson Publishing, 1993.

[62] M. Tillerson, G. Inalhan, and J. How, "Coordination and Control of Distributed Spacecraft Systems Using Convex Optimization Techniques," International Journal of Robust and Nonlinear Control, vol 12, Issue 2-3, Feb.-Mar. 2002, p.207-242.

[63] C. Park, P. Ferguson, N. Pohlman, J. How, "Decentralized Relative Navigation for Formation Flying Spacecraft using Augmented CDGPS," *Proceedings of Institute of Navigation GPS Conference*, Salt Lake City, Utah, Sept. 2001.

[64] J. How and M. Tillerson, "Analysis of the Impact of Sensor Noise on Formation Flying Control," *Proceedings of the 2001 American Control Conference*, Arlington, VA, June 25-27, 2001, Proceedings. Vol. 5 (A01-45851 12-63), Piscataway, NJ, Institute of Electrical and Electronic Engineers, 2001, p. 3986-3991.

[65] M. Tillerson, J. How, "Advance Guidance Algorithms for Spacecraft Formation Flying," accepted for *2002 American Control Conference*, Anchorage, AK, May 8-10, 2002, Piscataway, NJ, Institute of Electrical and Electronics Engineers, 2002.